


12-2010

Speciation and spectroscopy of the uranyl and tetravalent plutonium nitrate systems: Fundamental studies and applications to used fuel reprocessing

Nicholas A. Smith
University of Nevada, Las Vegas

Follow this and additional works at: <https://digitalscholarship.unlv.edu/thesesdissertations>

 Part of the [Atomic, Molecular and Optical Physics Commons](#), [Nuclear Commons](#), and the [Radiochemistry Commons](#)

Repository Citation

Smith, Nicholas A., "Speciation and spectroscopy of the uranyl and tetravalent plutonium nitrate systems: Fundamental studies and applications to used fuel reprocessing" (2010). *UNLV Theses, Dissertations, Professional Papers, and Capstones*. 776.
<https://digitalscholarship.unlv.edu/thesesdissertations/776>

This Dissertation is protected by copyright and/or related rights. It has been brought to you by Digital Scholarship@UNLV with permission from the rights-holder(s). You are free to use this Dissertation in any way that is permitted by the copyright and related rights legislation that applies to your use. For other uses you need to obtain permission from the rights-holder(s) directly, unless additional rights are indicated by a Creative Commons license in the record and/or on the work itself.

This Dissertation has been accepted for inclusion in UNLV Theses, Dissertations, Professional Papers, and Capstones by an authorized administrator of Digital Scholarship@UNLV. For more information, please contact digitalscholarship@unlv.edu.

SPECIATION AND SPECTROSCOPY OF THE URANYL AND TETRAVALENT
PLUTONIUM NITRATE SYSTEMS: FUNDAMENTAL
STUDIES AND APPLICATIONS TO USED
FUEL REPROCESSING

by

Nicholas Alexander Smith

Bachelor of Science
Lake Superior State University
2005

A dissertation submitted in partial fulfillment of
the requirements for the

**Doctor of Philosophy Degree in Radiochemistry
Department of Chemistry
College of Sciences**

**Graduate College
University of Nevada, Las Vegas
December 2010**

Copyright by Nicholas Alexander Smith 2011
All Rights Reserved



THE GRADUATE COLLEGE

We recommend the dissertation prepared under our supervision by

Nicholas Alexander Smith

entitled

Speciation and Spectroscopy of the Uranyl and Tetravalent Plutonium Nitrate Systems: Fundamental Studies and Applications to Used Fuel Reprocessing

be accepted in partial fulfillment of the requirements for the degree of

Doctor of Philosophy in Radiochemistry

Department of Chemistry

Kenneth Czerwinski, Committee Chair

Alfred Sattelberger, Committee Member

Gary Cerefice, Committee Member

Ralf Sudowe, Graduate Faculty Representative

Ronald Smith, Ph. D., Vice President for Research and Graduate Studies
and Dean of the Graduate College

December 2010

ABSTRACT

**Speciation and Spectroscopy of the Uranyl and Tetravalent
Plutonium Nitrate systems: Fundamental Studies and
Applications to Used Fuel Reprocessing**

by

Nicholas Alexander Smith

Dr. Kenneth R. Czerwinski, Examination Committee Chair
Professor of Chemistry
Chair of the Department of Radiochemistry
University of Nevada, Las Vegas

This dissertation explores the use of UV-Visible spectroscopy and Time Resolved Laser Induced Fluorescence spectroscopy as near real time process monitors of uranium and plutonium concentrations in aqueous reprocessing trains. The molar absorptivities and linear ranges of these metals were investigated under total nitrate and acid concentrations similar to those found in current reprocessing systems. Concurrent to this, a new multiple wavelength monitor was derived that is capable of determining the total nitrate concentration spectroscopically. This method uses the uranium absorbance spectrum to calculate the nitrate concentration in solution. When used as part of an Advanced Safeguard suite, this technique can provide information on the process chemistry in use.

The fundamental chemistry of the uranyl nitrate system was investigated to add to the thermodynamic data set. A combination of spectroscopic measurements, Density Functional Theory calculations, Extended X-ray Absorption Fine Structure spectroscopy, and observations of solvent extraction studies were used to theorize a new model of uranyl-nitrate speciation. In this model, the dominant species at low nitrate

concentrations is $\text{UO}_2(\text{NO}_3)_2$ and the UO_2NO_3^+ species is de-emphasized. Spectrophotometric titrations of the uranyl system were used to determine the $\log \beta_{2,1}$ values for this system at multiple ionic strengths and the zero ionic strength stability constants were calculated using the Specific Ion Interaction Theory.

The UV-Visible spectroscopy of the tetravalent plutonium nitrate system was investigated as a function of nitric acid concentration. Two pseudo-isobestic points were identified in the spectra which can be used to determine the total Pu^{IV} concentration. Factor analysis was then used to investigate the speciation of the system; a total of 5 species exist between 2 and 10 M HNO_3 . This information can be used to focus future studies.

ACKNOWLEDGMENTS

There is a long list of people that I would like to thank as the process of completing a doctoral degree is so overwhelming that without support anyone would crack under the pressure long before the defense. I want to thank my wife, Heather, first and foremost; she has put up with more than anyone else during this long ordeal and I can only hope that I can repay her for all of the time and energy she has expended to support me. Next, I would like to thank my dissertation committee, Drs. Ken Czerwinski, Gary Cerefice, Al Sattelberger, and Ralf Sudowe. They were instrumental in shaping both my research and my theories throughout my time at UNLV. My family deserves to be mentioned as they all have followed my academic career closely and have always been both interested in my work and encouraging of my endeavors. I would like to thank Tom O'Dou, Trevor Low and Julie Bertoia for maintaining and managing the group laboratories; these individuals make possible the work that all of us do and we would be lost without them. Thanks are in order for Drs. Patricia Paviet-Hartmann and Thomas Hartmann who provided unique viewpoints and welcomed suggestions due to their experiences outside of academia. Finally, I would like to thank my cadre-mates: Craig Bias, Rich & Julie Gostic, Kiel Holliday, Chinthaka Silva, and Amber Wright: without other students to guide us we guided ourselves through this ordeal and I thank you all.

TABLE OF CONTENTS

ABSTRACT	iii
ACKNOWLEDGEMENTS	v
LIST OF TABLES	viii
LIST OF FIGURES	ix
CHAPTER 1 INTRODUCTION	1
1.1 Dissertation Overview	2
1.2 Motivation for Research	2
1.3 Project Goals	5
CHAPTER 2 BACKGROUND	6
2.1 Definitions and Formulae	6
2.2 Review of the Uranyl Nitrate Literature	13
2.3 Review of the Plutonium(IV) Nitrate Literature	28
2.4 Ionic Strength Effects	34
2.5 Theoretical Modeling of Thermodynamic Quantities	36
2.6 Solvent Extraction of Actinides	36
2.7 Process Monitoring and IAEA/DOE Safeguards	39
CHAPTER 3 ANALYTICAL	44
3.1 Titrations	44
3.2 Ultraviolet-Visible Spectroscopy	51
3.3 Time Resolved Laser Induced Fluorescence Spectroscopy (TRLFS)	57
3.4 Inductively Coupled Plasma – Atomic Emission Spectroscopy	63
3.5 X-Ray Absorption Fine Structure Spectroscopy	66
3.6 Radiometric Techniques	69
CHAPTER 4 EXPERIMENTAL	73
4.1 UV-Visible Spectroscopy Batch Experiments	73
4.2 TRLFS Batch Experiments	88
4.3 Potentiometric Titrations	90
4.4 Spectrophotometric Titrations	92
4.5 EXAFS Spectroscopy	95
CHAPTER 5 MODELING	98
5.1 Hyperquad & HypSpec	98
5.2 Specific Ion Interaction Theory	103
5.3 Density Functional Theory	106
CHAPTER 6 DISCUSSION AND CONCLUSIONS	102
6.1 Direct Measurement Techniques	108

6.2	Indirect Techniques	117
6.3	Thermodynamics.....	126
6.4	Conclusions.....	146
REFERENCES.....		149
VITA.....		160

LIST OF TABLES

Table 1	Selected uranyl nitrate formation constants. From [66].	14
Table 2	Selected tetravalent plutonium nitrate stability constants. From [69].	29
Table 3	Response of electrode to buffer solutions with 3 M KCl and saturated NaCl fill solutions. Results are the average of three measurements	45
Table 4	Stern-Volmer relationships governing quenched systems	63
Table 5	Uranium Line Emissions and possible interferences ($\geq 40\%$ of U relative intensity, ± 0.1 nm) – from iTeva software.	66
Table 6	Composition of sample series used in the Multivariate Analysis project	75
Table 7	Chemical characteristics of simulated reprocessing streams	77
Table 8	Composition of samples for the first multiple wavelength monitor study (Peak Ratios Study 1).	81
Table 9	Composition of samples for the second multiple wavelength monitor study (Peak Ratio Study 2)	82
Table 10	Composition of uranyl-AHA series. Each series was composed of 10 samples. Acid concentration was controlled with addition of nitric acid.	84
Table 11	Potentiometric titration sample compositions.	92
Table 12	Spectrophotometric titrations, initial sample composition. All concentrations are in molality (m). All titrants were prepared at the same molal concentration as the sample ionic strength, I_m . For each titration, 15-18 data points were collected.	94
Table 13	Nitric acid and metal concentrations for EXAFS Samples	97
Table 14	Molar absorptivities, limits of linearity, and detection limits for selected simulated process stream chemistries	110
Table 15	Calibration equation and limits of linearity for TRLFS of uranyl under relevant, simulated reprocessing conditions	113
Table 16	Results of LSC and Alpha spectrometry for final Pu concentration.	115
Table 17	Spectroscopic characteristics of the plutonium(IV) spectrum at various nitrate concentrations. Error is extrapolated from Pu(IV) concentration.	115
Table 18	Comparison of the first three uranyl acetate stability constants. Errors represent 3σ .	127
Table 19	DFT Calculated bond distances and HOMO-LUMO gaps. ^a Data from [95]	132
Table 20	Refined stability constants for the uranyl dinitrate stability constant, $\log \beta_{2,1}$, at multiple ionic strengths, refinement scenarios. Error is propagated from HypSpec values.	134
Table 21	Zero Ionic Strength Stability Constants and Specific Ion Interaction parameters for the uranyl dinitrate species	140
Table 22	Number of significant factors in the plutonium nitrate system in the specified total nitrate ranges.	140
Table 23	Stability constants used in Figure 55 A, B, and C. Values from this work can be found in Table 20. ^a from [19]. ^b from [113].	145

LIST OF FIGURES

Figure 1	Absorption spectrum and refinement of band structure. Uranyl concentration - 9.15 mmol/L; HClO ₄ - 0.014 mol/L. Measurement made at 25°C and ionic strength of 3.00. From [24].....	18
Figure 2	Absorption spectrum of uranyl-nitrate-water system. Uranyl concentration: 3.98 x 10 ⁻² mol/L. Nitrate Concentrations in mol/L: 1 - 0.5 ; 2 - 1 ; 3 - 3.0; 4 - 5.0; 5 - 7.0; 6 - 9.0; 7 - 12.8. Sample 8 is 3.98 x 10 ⁻² UO ₂ (ClO ₄) ₂ in HClO ₄ . From [20].....	19
Figure 3	The absorbance behavior of the uranyl ion in the presence of varying amounts of nitrate. From [47].....	20
Figure 4	Uranyl nitrate in non aqueous solvents. 0.02 M uranyl nitrate hexahydrate in: -acetone; --- methyl isobutone; --.---. cyclohexane; ... acetone with 0.02 M tetrabutyl ammonium nitrate. From [26].....	23
Figure 5	Fluorescence of uranyl ion in perchloric acid showing deconvolution of the fluorescence peaks. [UO ₂ ²⁺] - 0.218 M, [HClO ₄] - 2.346 M, Ionic Strength - 3.00. From [24].....	24
Figure 6	Speciation of the uranyl nitrate system. Solid lines represent data from Wanner, et. al [66]. From [39].....	25
Figure 7	Speciation of the plutonium(IV) nitrate system from [63]. Data of Ryan can be found in [62].....	31
Figure 8	Absorption spectra of Pu(IV) at a concentration of 4.8 g/L. The spectra, obtained with 1 cm pathlength, are offset for clarity; the intensity scale is absorbance. The vertical dotted lines are at 469, 476, 483 and 491 nm. From [43].....	33
Figure 9	Extraction of actinides into TBP/dodecane as a function of nitric acid. From [67]......	38
Figure 10	Metrohm Titration system.	46
Figure 11	Spectrophotometric titration apparatus. Syringe Pump (Upper Right) delivers titrant to sample cup (foreground) on a stir plate. Peristaltic Pump (Upper Left) recirculates sample through flow through cuvette (not shown).....	50
Figure 12	a) Varian Cary 6000 [114]; b) Varian Cary 50 [115]; c) Ocean Optics USB2000+ [116]; d) Ocean Optics T300 Dip probe [117].....	53
Figure 13	Basic properties of energy transfer for fluorescent compounds. [123].....	58
Figure 14	Top) VIBRANT laser with OPO module; Bottom) Acton SP500 spectrometer and PI-MAX II CCD camera.	60
Figure 15	iCAP ICP-AES Spectrometer [71].....	64
Figure 16	Breakdown of the XAS spectrum into the EXAFS and XANES regions. The XANES region is background corrected and normalized; the EXAFS region is weighted by a factor of k ³ to produce the plot shown in the upper right. From [94].....	67
Figure 17	Tri-Carb 3110TR LSC [134].....	71
Figure 18	Traces of 95 mM uranyl, 2 M acid samples from Segments 1-5 of the Multivariate Study.....	75

Figure 19	Linear Responses of the uranyl ion under simulated reprocessing streams (Table 7). A) Response at 414 nm; B) Response at 486 nm for high uranium conditions.....	78
Figure 20	Representative spectra from each simulated reprocessing stream.....	79
Figure 21	Representative spectra from the first multiple wavelength monitor (sample PRS1 A, Table 8). Nitric acid, 4 mol/L, diluted with water, $[\text{UO}_2^{2+}] = 40.1$ mM. Total nitrate ranges from 0.15 mol/L (bottom) to 3.73 mol/L (top).....	81
Figure 22	Representative spectra from the second multiple wavelength monitor (Sample PRS2 A1, Table 9). Nitric acid, 6 mol/L, diluted with water, $[\text{UO}_2^{2+}] = 52.7$ mM.	83
Figure 23	Uranyl - AHA absorption spectrum at pH 1 and $[\text{UO}_2^{2+}] = 95$ mmol/L (Series AHA 1, Table 10).....	84
Figure 24	Initial UV-Visible spectra of Pu(IV) in 1 M HNO_3	86
Figure 25	Disproportionation of Pu(IV) into Pu(III) and Pu(VI) at low acid concentration. The small amount of Pu(III) is obscured by the larger contribution of the Pu(IV) at ~475nm. The high molar absorptivity (~150 [44]) of the Pu(VI) accounts for the large signal at 830 nm.....	86
Figure 26	Variation of plutonium absorption spectrum with varying nitric acid concentrations. $[\text{Pu(IV)}] = 1.5\text{-}1.6$ mmol/L.....	88
Figure 27	Selected uranyl fluorescence patterns in the presence of increasing nitrate concentrations.....	89
Figure 28	Linear plots of total fluorescence vs. uranyl concentration at various nitrate concentrations. Control fluorescence behavior – 0 mol/L HNO_3 ; UREX Raffinate – 2 mol/L HNO_3 ; Technetium Product – 6 mol/L HNO_3	90
Figure 29	Potentiometric titration curves, labels from Table 11. Sample composition can be found in Table 11. A) Samples containing uranyl and acetate only, 1 molal IS; B) Samples containing uranyl, acetate, and nitrate, 2 molal IS.....	93
Figure 30	Representative spectrophotometric titration (sample 008). Initial conditions: 0.049 molal uranyl, 1.95 molal perchlorate, 1.85 molal acid titrated with 2.0 molal nitric acid.	95
Figure 31	UV-Visible spectra of selected samples. $[\text{UO}_2^{2+}] = 10$ mM. The presence of sharp peaks at 423, 436, 451, and 466 are similar to peaks of known trinitrate species (Section 2.2.2.1).....	96
Figure 32	Eigenvector plots as a function of wavelength. A) Two significant eigenvector and one non-significant vector. Due to the high level of noise and low eigenvalue (0.006), the third vector is most likely noise. B) Two or three significant eigenvectors. Though the third eigenvalue is relatively low, the organized structure and low noise level suggest that a third significant, though minor, eigenvector exists.....	102
Figure 33	Increase in uranyl absorbance at 6 mol/L nitrate due to effect of lithium ion. Lithium nitrate to nitric acid ratio provided in legend, $[\text{UO}_2^{2+}] = 95$ mM. The spectral change is similar to what is observed at higher total nitrate concentrations. This spectroscopic shift is attributed in this work to the contribution of the uranyl trinitrate species similar to (Figure 4). This is supported by observations that anionic uranyl nitrates form more rapidly in nitrate salts than in nitric acid [68].....	109

Figure 34	Fluorescence spectra of the uranyl ion with varying amounts of nitric acid.	112
Figure 35	Stern-Volmer plots of lifetime and intensity quotients as a function of total nitrate concentration.	112
Figure 36	Fluorescence response as a function of uranyl concentration at 0, 2, and 6 mol/L total nitrate. Ten measurements were taken at each uranyl concentration.	114
Figure 37	Isosbestic point at 537 nm	116
Figure 38	Isosbestic point at 632 nm (2-7 mol/L nitrate only)	116
Figure 39	Deconvolution of the uranyl absorption spectrum. PRS1 A, Table 8: 40.1 mmol/L uranyl, 5 mmol/L nitrate ion.	119
Figure 40	Selected absorbance peak heights plotted against the total nitrate concentration. The 426/403 couple is easily identified in the top half of the figure. From PRS1 A.	119
Figure 41	426/403 ratio plotted against total nitrate concentration for all three PRS1 sample sets.	120
Figure 42	The 426/403 ratio plotted against total nitrate concentration. Each series started with a unique Nitric acid:Sodium Nitrate ratio and was diluted with water.	122
Figure 43	Comparison of a fixed, single wavelength monitor calibrated at 2 mol/L nitric acid vs. the peak ratio methodology.	124
Figure 44	Uranyl in the presence of AHA. $[\text{UO}_2^{2+}] = 91 \text{ mM}$, $[\text{AHA}] = 87 \text{ mM}$	125
Figure 45	Effect of increasing the first uranyl nitrate stability constant on the observable pH curve of the uranyl-acetate-nitrate system. Initial titration simulation parameters: 0.010 mol/L UO_2^{2+} , 0.03 mol/L initial acid, 1 mol/L nitrate, 25 mL initial volume. Titrant: 5 mL added, 0.5 mol/L sodium acetate, 0.5 mol/L acetic acid. Stability constants for uranyl acetate from [113]. Titration curve of uranyl-acetate system only (no NO_3^-) included for reference.	127
Figure 46	Fourier Transforms of the uranyl-nitrate EXAFS spectra. The refined bond distances from DFT modeling are listed in Table 19.	129
Figure 47	Fourier Transforms of the plutonium(IV)-nitrate EXAFS spectra.	129
Figure 48	Molecular orbital (MO) diagram of the highest-lying states of UO_2^{2+} calculated at the GGA/PW91 level of theory (left), with their corresponding graphical representation (right). Occupied valence and unoccupied (virtual) MOs are represented in red and blue, respectively.	130
Figure 49	Molecular orbital (MO) diagrams of the highest-lying states of the $\text{UO}_2(\text{H}_2\text{O})_5^{2+}$, $\text{UO}_2(\text{NO}_3)(\text{H}_2\text{O})_4^+$, $\text{UO}_2(\text{NO}_3)_2(\text{H}_2\text{O})_2$, $\text{UO}_2(\text{NO}_3)_3^-$, and $\text{UO}_2(\text{NO}_3)_4^{2-}$ lowest-energy complexes calculated using density functional theory (top), with the corresponding relaxed geometries and symmetry point groups (bottom). Occupied valence and virtual MOs are represented in red and blue, respectively.	132
Figure 50	Eigenvector plots for first three singular eigenvalues at 1, 2, 3, 4, and 6 molal ionic strength. A third species becomes more prominent above 4 molal ionic strength, though it is not a major component. This is most likely due to the higher nitrate concentrations reached in these samples.	136-137
Figure 51	Speciation diagrams for at 2 molar ionic strength; stability constants used can be found in Table 20. Solid lines represent systems including the uranyl	

	mononitrate, dashed were refined without. A) Refinement with a uranyl standard spectrum; B) free refinement of all spectra.	138
Figure 52	Linearization of the uranyl dinitrate stability constants refined with a standard uranyl spectrum included.....	138
Figure 53	Linearization of the uranyl dinitrate stability constants with free refinement of all spectra.	139
Figure 54	Graphical representation of plutonium nitrate Factor Analysis results. The number of significant factors drop at 3 and 4 mol/L total nitrate and increase at 7 mol/L nitrate. The species that adds to the system above 7 mol/L nitrate is likely the $\text{Pu}(\text{NO}_3)_6^{2-}$ species.....	141
Figure 55	Speciation diagrams for scenarios A, B, and C found in at $[\text{UO}_2^{2+}] = 50$ mmol/L. The best correlation to the experimental data is found with the data set refined including the mononitrate species. That dataset shows an excess of extractable species compared to the extraction data.	144-145

CHAPTER 1

INTRODUCTION

Reprocessing of used nuclear fuel is an option to both reduce the volume of waste that would eventually need to be disposed and also preserve a valuable energy source [1]. One drawback of most aqueous based fuel reprocessing schemes is the potential for the production, and diversion, of weapons usable material [2]. The ability to monitor these processes, in real time, for changes in metal concentration and process chemistry would increase the probability of detecting a diversion attempt. The information gained from these monitors is not only useful to inspectors as a safeguard technique but to plant operators as method to assess process performance.

This work aims to explore the applicability of optical spectroscopy, specifically Ultraviolet-Visible (UV-Vis) spectroscopy and Laser Induced Fluorescence spectroscopy, as process monitoring techniques. The limits of linearity and detection limits under reprocessing conditions will be evaluated for both systems. A novel multi-wavelength monitor to track the process chemistry in the uranyl-nitric acid system will be presented. This monitoring technique can be applied as an advanced safeguard to determine the chemistry in use at a reprocessing facility. An evaluation of the fundamental chemistry and spectroscopy of uranium and plutonium in nitric acid will be performed to add to the available data set in the literature. The changes in absorbance behavior with respect to nitrate ion concentration will be presented along with stability constants for the uranyl dinitrate species. This thermodynamic and spectroscopic information can then be incorporated into the various models used to design and predict reprocessing systems.

1.1 Dissertation Overview

Chapter 1 gives the general overview as well as the primary motivations for this work. Chapter 2 contains a review of prior work on the speciation and spectroscopy of plutonium and uranium under nitric acid reprocessing conditions, definitions and terminology, information on the effects of ionic strength, and a brief description of aqueous reprocessing techniques and safeguards goals and technologies. Chapter 3 details the various analytical techniques used throughout this work. All experimental setup and raw data are presented in Chapter 4. Titration analysis with Hyperquad and HypSpec, thermodynamic modeling with the Specific Ion Interaction Theory, and Density Functional Theory are covered in Chapter 5, while the discussion, analysis, and final conclusions are located in Chapter 6.

1.2 Motivation for Research

1.2.1 Nuclear Fuel Reprocessing

The growth of nuclear energy over the past several decades has left a large supply of used nuclear fuel waiting for a final disposition [1]. Direct geological disposal has been proposed in several countries including Canada, China, France, Germany, Russia, and the United States [3]. An alternative to direct disposal is to reprocess the used fuel to recover ^{235}U for new light water fuel fabrication and higher actinides for fast spectrum reactors. In addition to extracting these valuable materials, reprocessing also reduces the final volume of high level waste that needs to be disposed increasing the utility of a repository by reducing the heat load and total material required to be stored [4].

Aqueous reprocessing has been used in the US and abroad for more than 60 years. The original processes were developed as a part of the Manhattan Project during WWII. Since then, the US, France, the UK, Russia, India, and Japan have all operated or still operate reprocessing plants. Currently, all reprocessing plants in operation use the PUREX process which has the drawback of generating a pure plutonium product stream [3]. Several modifications, such as UREX in the US or COEX in France, have been proposed to the PUREX process to eliminate the plutonium product and increase the process' proliferation resistance [5].

1.2.2 Safeguards and Process Monitoring

While using advanced processes engineered for increased proliferation resistance is an improvement, there must also exist methods to accurately monitor the special nuclear material inventory. These methods exist to track material throughout a site, physically protect the material from theft, and monitor the chemical and physical processes in use [6]. The Department of Energy has emphasized the importance of properly safeguarding all domestic nuclear reprocessing and fabrication facilities [7].

Online process monitors have been proposed to evaluate the chemistry of the system and the material concentration therein. Process monitoring has the advantage of providing a real-time, continuous material balance for a facility, reducing the time required for the detection of any potential diversion of material. Several active and passive radiometric techniques have been proposed as well as hybrid k-edge densitometry, and optical spectroscopy [8].

Optical spectroscopic methods have several advantages over radiometric techniques for process monitoring applications. First, they are not directly affected by high radiation

environments. Second, they are able to be remotely deployed with fiber optics which keeps the instrumentation outside of the hot area. Third, they are adaptable to a wide range of analyte concentrations. While Ultraviolet-Visible and Laser Induced Fluorescence spectroscopy are well understood at the bench level [9-45] there are only a handful of references for their use as a process monitor [46,47]. Because of this, there is a need to evaluate their deployment potential for process chemistries.

1.2.3 Fundamental Chemistry

Both the uranyl and tetravalent plutonium nitrate systems have been investigated for several decades [18-22,48-65]. However, the data in the literature varies greatly and, in some cases, is directly contradictory. The value of the first uranyl nitrate stability constant, $\log \beta_{1,1}$, has been determined by many authors, although only a few have been deemed reliable [66]. Additionally, there is no consensus on the speciation of the uranyl nitrate system past the mononitrate; only a few scattered stability constants exist for the di- and tri-nitrate species [66]. This data does not correlate with physical observations of the system. The presence of the neutral species is required for certain solvent extraction systems in use [67] and the trinitrate is required for anion exchange studies [68]. These proposals, fundamentally, cannot be supported by the existing literature. Similarly, the plutonium nitrate system lacks a clear speciation model, with different authors proposing the existence of the mono-, di-, tri-, tetra-, and hexanitrate. Stability constants for the mono- through tetranitrate do exist despite any agreement on what species are found in solution [69]. The only species which is found consistently is the Pu(IV) hexanitate anion, $\text{Pu}(\text{NO}_3)_6^{2-}$, at high nitric acid concentrations [62], though no study has proposed a stability constant for this species.

1.3 Project Goals

The goal of this work is to investigate the applicability of visible spectroscopy for monitoring uranium and plutonium concentrations in aqueous reprocessing streams. This requires detailed knowledge of these elements' speciation under reprocessing conditions. Batch studies are used to examine how the absorption spectrum of the uranyl ion is affected by nitrate concentration and ionic strengths. An absorbance based multiple wavelength monitor is developed to both correct the uranyl absorbance in the presence of nitrate and to monitor the cold chemistry of the system. The effect of the complexant/reductant acetohydroxamic acid on the uranyl spectrum is also investigated. Laser Induced Fluorescence spectroscopy is used to determine uranium concentrations at the micromolar level. Spectrophotometric and potentiometric titrations are used to explore the speciation of the uranyl ion with respect to nitrate. The plutonium absorption behavior with respect to nitrate is also investigated. Factor analysis is used to determine the number of significant spectroscopic parameters with respect to nitrate.

CHAPTER 2

BACKGROUND

This chapter will provide an abbreviated background of the various theoretical concepts and experimental techniques used in this dissertation. Section 2.1 will define and discuss the various formulae and concepts relating to speciation and spectroscopy. Sections 2.2 and 2.3 will discuss the available literature relating to the speciation and aqueous spectroscopy of uranyl nitrate and plutonium nitrate, respectively. Section 2.4 will review the effects of ionic strength effects while Section 2.5 will cover thermodynamic modeling with the Specific Ion Interaction Theory. Section 2.6 discusses the current state of solvent extraction processes currently under development for use in aqueous spent fuel recycling while Section 2.7 reviews modern safeguards and the methods incorporated into fuel recycling facilities to detect material diversions.

2.1 Definitions and Formulae

There are a multitude of equations and formulae that are used to describe thermodynamic and spectroscopic systems. For the sake of clarity, the relevant formulae will be defined and explained using the standard terminology.

2.1.1 Chemical Activity

The activity of a chemical species is directly related to the species' chemical potential. Therefore, factors such as temperature, pressure, ionic strength, and solution composition will all affect the chemical potential of the species and thus its availability to participate in bonding [70]. This then changes the "effective concentration" of the

species. To correct for these factors, the activity coefficient was introduced. The activity of a species is related to its concentration and is defined in Equation 1:

$$\begin{aligned} &\text{Equation 1} \\ &\{A\} = \gamma_A [A] \end{aligned}$$

where $\{A\}$ is the activity, $[A]$ is the chemical concentration, and γ is the activity coefficient for component A . The temperature and ionic strength of the solution should be included for reference [71].

Much effort has been devoted to finding ways to determine and model the change in the activity coefficient of various species. For many simple systems, this has been investigated and can be readily determined [70]. Osmotic pressures, vapor pressure measurements, and other colligative property measurements are often used to determine activity coefficients [72-74]. The modeling of these activity coefficients is covered in more detail in the Section 2.5 and Chapter 5.

2.1.2 Ionic Strength

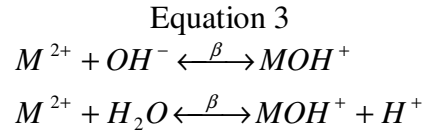
The ionic strength of a solution with N ions is defined as follows:

$$\begin{aligned} &\text{Equation 2} \\ &I = \frac{1}{2} \sum_{i=1}^N z_i^2 c_i \end{aligned}$$

where z is the absolute value of the ion's charge and c is the concentration of the ion [71]. The equation holds true for both molar and molal concentrations; ionic strengths on the molar scale will generally be referred to as I , while those on the molal scale will be denoted I_m .

2.1.3 Thermodynamic Constants

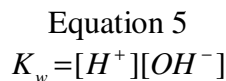
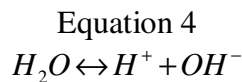
There are several ways to define the relationship between multiple species in solution. In general, the constant is dependent on the way the reaction is written and how the reactants are defined. For example, the two equilibria in Equation 3 will have different stability constants despite describing the same reaction.



While there are several correct ways to write these equations, this work will adhere to the guidelines set down in the Chemical Thermodynamics Series [66]. In all cases, the constants can be expressed in either the molar (M , mol/L) or molal (m , mol/kg solvent) scale. The ionic strength should be stated for all constants, except in the case where they have been extrapolated to zero ionic strength (Section 2.5). Constants evaluated at zero ionic strength will be denoted by the inclusion of a superscript degree sign ($^{\circ}$).

2.1.3.1 Ion Product of Water

Water is an autoprotolytic compound and its dissociation is governed by an equilibrium constant known as the ion product and commonly referred to as K_w [71]. The equilibrium concentrations of H^{+} and OH^{-} ions are described by this quantity according to Equation 5.

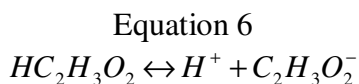


This quantity, like other thermodynamic parameters, is affected by the ionic strength of the system. A review by Fanghänel, Neck, and Kim [75] provides an overview of

prior experimental work as well as parameters for both the Specific Ion Interaction Theory (SIT) and Pitzer models (see Section 2.5). When necessary, K_w will be given along with the ionic strength of the determination.

2.1.3.2 Protonation Constants

The degree to which a weak acid has dissociated in solution is described by the acid's protonation constant [71]. For example, in the dissociation of acetic acid (Equation 6), the protonation constant gives the equilibrium concentrations of free acetate and hydrogen concentrations as well as remaining acetic acid (Equation 7). Commonly, these constants are written as the negative logarithm, pK_a , for comparison.



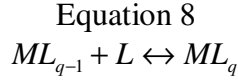
Equation 7

$$K_a = \frac{[H^+][C_2H_3O_2^-]}{[HC_2H_3O_2]_{(aq)}}$$

2.1.3.3 Formation Constants

For any reaction involving the stepwise addition of a ligand to a metal center or complex, the reaction can be described by a formation constant [66]. This constant is only valid at the stated temperature and ionic strength of the solution in which it was determined.

Equation 9 shows the general form of a formation constant for the M/L system (Equation 8) for any number, q , of ligands.



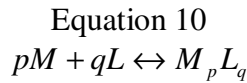
Equation 9

$$K_q = \frac{\{ML_q\}}{\{ML_{q-1}\}\{L\}} = \frac{[ML_q]}{[ML_{q-1}][L]} \cdot \frac{\gamma_{ML_q}}{\gamma_{ML_{q-1}} \cdot \gamma_L} = \frac{[ML_q]}{[ML_{q-1}][L]} \cdot \Gamma$$

In most determinations there is a negligible change in the matrix composition throughout. This allows the approximation that the ratio of the activity coefficients, Γ , is constant throughout and concentrations can be used in place of activities [76].

2.1.3.4 Stability Constants

In a situation where it is necessary to state several formation constants to describe a system with multiple ligands, it may be more convenient to describe the system with a stability constant [76]. The stability constant describes the overall reaction constant, though the governing reaction should be stated to avoid confusion. The general form of the stability constant for the reaction in Equation 10 at an ionic strength of I_M is shown in Equation 11, assuming that Γ is constant. The superscript notation for the ionic strength in Equation 11 may also be written explicitly after the constant: $\beta_{q,p}(I_m)$.



Equation 11

$$\beta_{q,p}^{I_m} = \frac{[M_p L_q]}{[M]^p [L]^q}$$

It should be noted that in the case of weakly complexing ligands, a large change in the matrix usually must occur in order to see an appreciable result. This significantly alters the activity of any species present and negates the assumption that Γ is constant [77]. The ability to correct for this variation is limited, usually by utilizing a thermodynamic model such as SIT. However, the interaction coefficients of species with

respect to the matrix may not be well established and therefore must be estimated from available data (Section 2.5).

2.1.3.5 Adjustment of Constants

The direct comparison of thermodynamic constants requires that they were measured under identical conditions. One of the most common dissimilarities between studies is when stability constants are evaluated on different concentration scales. The general procedure is to convert constants measured on the molar scale to the molal scale according to Grenthe and Ots [78] by Equation 12

$$\text{Equation 12}$$
$$\beta_{q,m} = \beta_{q,M} (d_K)^q$$

where $\beta_{q,m}$ is the q^{th} stability constant on the molal scale while $\beta_{q,M}$ is the corresponding constant on the molar scale and d_K is the density of the solution at temperature K .

One method of comparing constants measured at different ionic strengths is to extrapolate the hypothetical Zero Ionic Strength constant. This treatment removes the effects of solution and solute non-ideality. This can be accomplished by use of either the aforementioned SIT theory or the Pitzer equations (see Section 2.5).

2.1.4 Beer's Law

The most useful relationship in visible absorption spectroscopy is the Beer-Lambert-Bouguer Law of radiation absorption [79]. It is a proportional relationship between the absorbance of a given wavelength of light (A), the concentration of the analyte (c) in mol/L, and the pathlength of the absorption (l) in centimeters (Equation 13). The constant of proportionality, ϵ in L/mol·cm, is the molar absorptivity constant which varies with wavelength.

Equation 13

$$A_{\lambda} = cl\epsilon_{\lambda}$$

The absorbance is defined as the inverse logarithm of the transmittance of the cell, which is defined in Equation 14.

Equation 14

$$T = I/I_0$$

I_0 and I are the intensity of the light before and after passing through the sample, respectively. The relationship can be expected to be linear within a certain range which must be determined experimentally.

The basic expression of Beer's Law is valid only for a single absorbing species. Multiple species with overlapping absorbances can occur in which case the law must be rewritten as a sum. In this case, the absorbance of N species at a given wavelength is written as in Equation 15.

Equation 15

$$A = l \cdot \sum_{i=1}^N c_i \epsilon_i$$

A feature of absorbance spectroscopy that may occur when two (or more) absorbing species co-exist is the isosbestic point [80]. An isosbestic point requires that two conditions are met; the species have intersecting absorbances and the concentrations of the two species are related linearly. The point where the molar absorptivities are equal will have a constant absorbance regardless of the mole fractions of the species if the total concentration remains unchanged. The relationship for two species, X and Y , is defined in Equation 16:

Equation 16

$$A = l \cdot (\epsilon_x c_x + \epsilon_y c_y) = l \cdot \epsilon_{IB} \cdot (c_x + c_y) = l \cdot \epsilon_{IB} \cdot c_{total}$$

where ϵ_{IB} is the molar absorptivity of both species at the isosbestic wavelength. Fundamentally, the presence of an isosbestic point indicates the presence of at least two species in solution. Isosbestic points can therefore be useful in evaluating the speciation of a system. For example, if a single well defined isosbestic point exists over a range of solution conditions, there is a strong indication that only two absorbing species exist under those conditions. The caveat to this is that more species may exist in solution, though their spectra may not overlap. If they do overlap, the isosbestic point may shift position as the reaction progresses giving it a drawn out appearance. Finally, isosbestic points can allow for determination of the total concentration as the molar absorptivity of the point does not change with chemistry.

2.2 Review of the Uranyl Nitrate Literature

A large volume of published data exists on the speciation and spectroscopy of the uranyl ion in weakly complexing media. Section 2.2.1 will cover the relevant literature regarding the speciation of the uranyl ion in general and with respect to the nitrate ion. Section 2.2.2 will explore the various spectroscopic techniques used to explore the thermodynamics and electronic structure of the ion.

2.2.1 Speciation of the Uranyl Ion in Acidic Media

The behavior of the uranyl ion in aqueous solutions with multiple anions has been studied in earnest for the last sixty years. Broadly, this research has several foci, including: improving industrial processes for commercial reprocessing [81-84]; environmental behavior [9-17]; and a small fraction of studies which has attempted to

Table 1 - Selected uranyl nitrate formation constants. From [66]

Temp. (°C)	Ionic Medium	log ₁₀ K	log ⁰ ₁₀ K	Ref.
<i>UO₂²⁺ + NO₃⁻ ↔ UO₂NO₃⁺</i>				
20	1 M Na ⁺ ,H ⁺ /Cl ⁻ ,ClO ₄ ⁻	-0.3 ± 0.17	0.38 ± 0.18	19
10	2 M Na ⁺ /Cl ⁻ ,ClO ₄ ⁻	-0.52		48
25		-0.62 ± 0.09	0.01 ± 0.26	
40		-0.77		
32	1 M NaClO ₄	-1.4		49
20	8 M NaClO ₄	-0.47		50
25	1 M Na ⁺ /ClO ₄ ⁻ /NO ₃ ⁻	-0.62 ± 0.04	0.10 ± 0.07	21
40		-0.57 ± 0.06	0.18 ± 0.08	
55		-0.52 ± 0.06	0.25 ± 0.08	
70		-0.48 ± 0.05	0.32 ± 0.08	
25	Self, I < 3.12 M	0.11	-0.19 ± 0.02	22
40		0.17	-0.02 ± 0.03	
55		0.30	0.16 ± 0.03	
70		0.49	0.26 ± 0.04	
100		0.85	0.49 ± 0.04	
150		1.47	0.78 ± 0.04	
<i>UO₂²⁺ + 2NO₃⁻ ↔ UO₂(NO₃)₂(aq)</i>				
32	1 M NaClO ₄	-1.4		49
20	0.59 - 11.1 M HNO ₃	-1.66 ± 0.16		20
<i>UO₂²⁺ + 3NO₃⁻ ↔ UO₂(NO₃)₃⁻</i>				
32	1 M NaClO ₄	0.5		49
20	6M HNO ₃	-1.5		50
<i>UO₂²⁺ + 3NO₃⁻ + H⁺ ↔ HUO₂(NO₃)₃(aq)</i>				
20	0.59 - 11.1 M HNO ₃	-1.74		20

investigate the speciation of the uranyl/nitric acid/water system on a fundamental level [18-22,48-50] Formation and stability constants of consequence from these works are listed in Table 1.

A useful review of the relevant literature up to 1992 (with an update that covers through 2004) is available [66]. This compendium reviews and grades the literature available with respect to experimental stringency, recalculates error, and applies current theories to old data, which allows the experiments to be compared directly.

With respect to the uranyl/nitric acid/water system very few studies were considered reliable by the reviewers [66]. This is due in a large part to the difficulty in measuring the small complexation constants suspected to drive the uranyl nitrate system. It should also be noted that the majority of the papers on the topic were carried out using numerical methods as they predated the statistical regression programs that are common to modern researchers. However, these studies did produce some relevant results and should be appropriately credited and explored.

The work of Day and Powers in 1954 [48] is given prominence in the review, mainly due to their experimental setup. The experiment studied the complexation of the uranyl ion by fluoride, nitrate, chloride, and sulfates. The experiments were based on extraction of the compounds by 8-thenoyltrifluoroacetone (TTA) from acidic solutions balanced at 2.0 M NaClO₄. They determined a value of $\log_{1,1} \beta = -0.62 \pm 0.09$, though the review increased the error in the system to an absolute value of 20% from 10%.

The next study is a series of papers published in the 1950s by Ahrlund [17,19,51-53]. These examine the thermodynamics of the uranyl ion with hydroxides, acetates, sulfates, chlorides, nitrates, and bromides. The study focused on the potentiometric method to determine the complexation of the hydroxide and acetate ligands, though spectral measurements were made as well [17,52]. The later work built on this foundation by using the acetate ion as a competing ligand for the weaker nitrate, bromide, and chloride ligands [19]. The studies used an analytical methodology that was completely numeric in nature with multiple titrations required to determine a single data point.

In the case of the uranyl nitrate system, this competition method was used along with spectrophotometry to determine nitrate ion complexation. The ionic strength of the

system was balanced with sodium perchlorate or perchloric acid. However, the paper only provides data at one ionic strength, $\beta_{1,1} = 0.5 \pm 0.2$ at 1.0 M. The value is self consistent in the paper; the values obtained spectroscopically and potentiometrically agree within the error.

A discussion of a paper that was deemed inappropriate by the NEA review is warranted. The paper by Kylgin, Kolada, and Smirnova [20] was rejected by the NEA review mainly due to a lack of ionic strength control. The reviewers argued that the effects explored in the study could be due to activity factors, not necessarily speciation changes. The group investigated the uranyl ion in nitric acid up to 12.8 M spectrophotometrically. They determined that the uranyl dinitrate and the acid adduct of the trinitrate were present but found no evidence of the mononitrate in their study. It should be noted that there were no studies in this review that provided reliable data for higher nitrato complexes despite evidence of their existence via solvent extraction studies (Section 2.6) and spectroscopy in non-aqueous solvents (Section 2.2.2.1).

A 2008 paper by L. Rao explored the uranyl nitrate speciation using both spectrophotometric and calorimetric titrations [21]. The study examined multiple temperatures at a single ionic strength (1.0 mol/L) and produced stability constants with the SIT theory and enthalpies of complexation by the Van't Hoff equation. The values produced agree with the values in [66] within the error.

A similar experiment is found in the paper by Suleimenov [22] which uses a multivariate approach to refine the zero ionic strength stability constant, as well as thermodynamic constants. The approach uses a variant of factor analysis to determine the number of species in solution, 2, and assigns these as the free and mononitrate; it is

assumed that these would be the first two species in solution. It is unclear how the authors controlled ionic strength throughout the experiment and as such the zero ionic strength extrapolation should be regarded with caution.

Finally, while there are no thermodynamic studies which have produced a defensible stability constant for the uranyl trinitrate, there have been several authors who have attempted to do so [20,49,50]. In addition, there is ample evidence for their existence to be found in a review by Gindler [68]. In this there are several studies presented on the uses of anionic exchange resins in nitrate media. The adsorption of the anionic uranyl reaches a maximum distribution of ~ 10 at about 8 mol/L nitric acid. There is also an anecdotal mention in [68] that the anion forms more readily in nitrate salt solutions than in nitric acid.

2.2.2 Spectroscopy of the Uranyl Ion

The complex electronic structure of the uranyl ion gives the molecule a large number of spectroscopically active transitions. The contribution of the uranium f-orbitals gives a highly structured absorbance spectrum composed of at least a dozen separate electron transitions between the ground state and various excited states [86,87]. This electronic structure is echoed in the fluorescence spectrum of the uranyl ion. This section will explore the various spectroscopic techniques used on the uranyl ion and its complexes in nitrate based solutions.

2.2.2.1 UV-Visible Spectroscopy

A large body of work has been produced with regard to the UV-Visible spectroscopy of the uranyl ion. In most cases, the studies focus on the environmental and hydrolysis behavior of the ion [9-17]. Several studies have examined either the practical

applications of the spectroscopy or the fundamental spectroscopic features of the uranyl ion spectrum [18-25].

The basic uranyl absorbance spectrum is characterized by a series of bands starting at 495 nm and continuing well into the UV range. The band structure, in the absence of ligand effects, has three main peaks at 403, 414, and 426 nm with molar absorbances of approximately 6.27, 7.13, and 5.37 L mol⁻¹cm⁻¹, respectively [23]. The first in a series

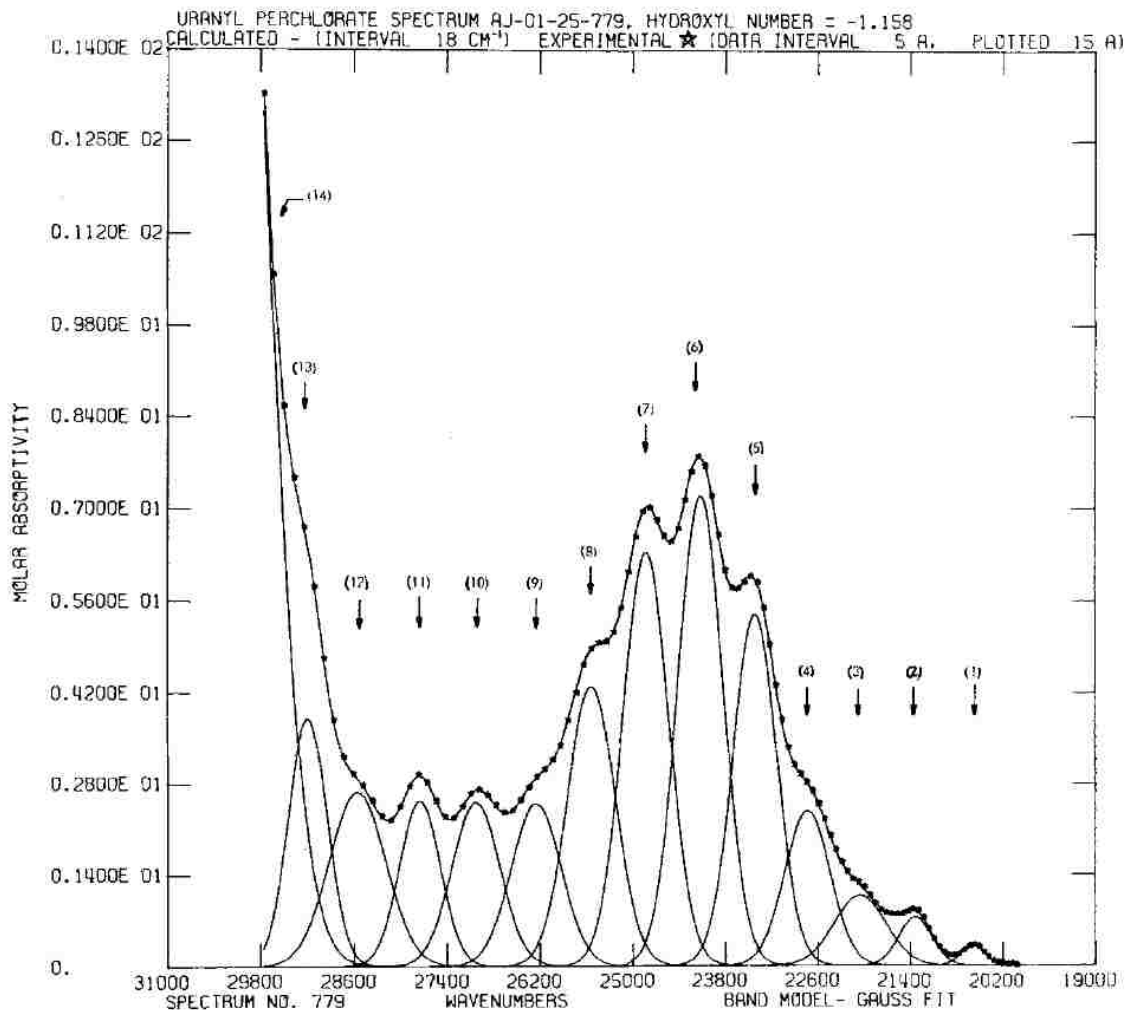


Figure 1 - Absorption spectrum and refinement of band structure. Uranyl concentration – 0.0092 mol/L; HClO₄ – 0.014 mol/L. Measurement made at 25°C and ionic strength of 3.00. From [24]

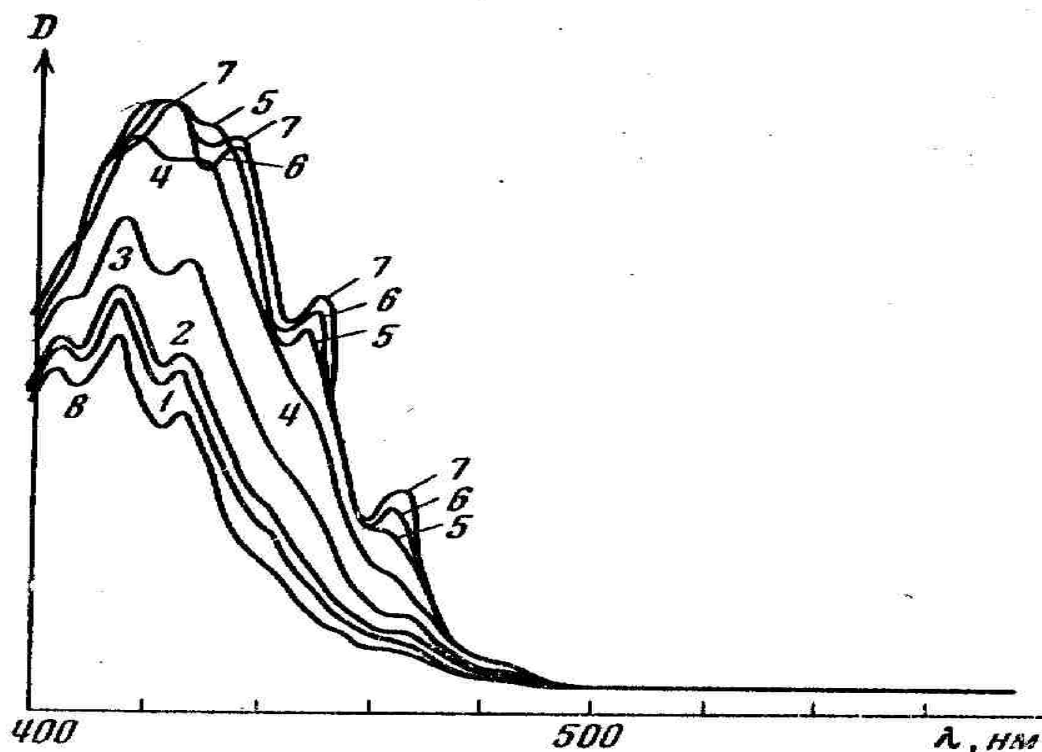


Figure 2 - Absorption spectrum of uranyl-nitrate-water system. Uranyl concentration: 3.98×10^{-2} mol/L. Nitrate Concentrations in mol/L: 1 – 0.5 ; 2 – 1 ; 3 – 3.0; 4 – 5.0; 5 – 7.0; 6 – 9.0; 7 – 12.8. Sample 8 is 3.98×10^{-2} $\text{UO}_2(\text{ClO}_4)_2$ in HClO_4 . From [20].

of papers by Bell and Biggers [23] explores this basic structure of the in perchloric acid media. The selection of perchloric acid is in keeping with the standard practice of choosing a non-complexing media as the background electrolyte [89]. The first paper mainly presents the deconvolution of the uranyl band structure. Fourteen discrete absorption bands were resolved, with peak values ranging from 486 to 332 nm, via an iterative least squares method (Figure 1). In addition to examining the hydrated uranyl ion, the absorbance of uranyl hydroxide and nitrate complexes were also investigated. All three investigations were carried out at 9 temperatures between 25 and 95°C. No thermodynamic information was extracted from this data.

Mentioned in the previous section, the paper by Kylgin, Kolada, and Smirnova [20] used a spectrophotometric method to determine stability constants. The spectra shown in this work (Figure 2) highlight very distinct shifts in the spectroscopy as the experiment is moved to higher nitrate values. This shift with respect to nitrate has been anecdotally noted elsewhere [26,27,47], though they were the only group to attempt a thermodynamic treatment of data at these high nitrate levels.

Showing similar absorbance behavior is the study by Lascola et.al. [47]. Lascola's paper detailed the efforts at the Savannah River National lab to deploy a UV-Vis based

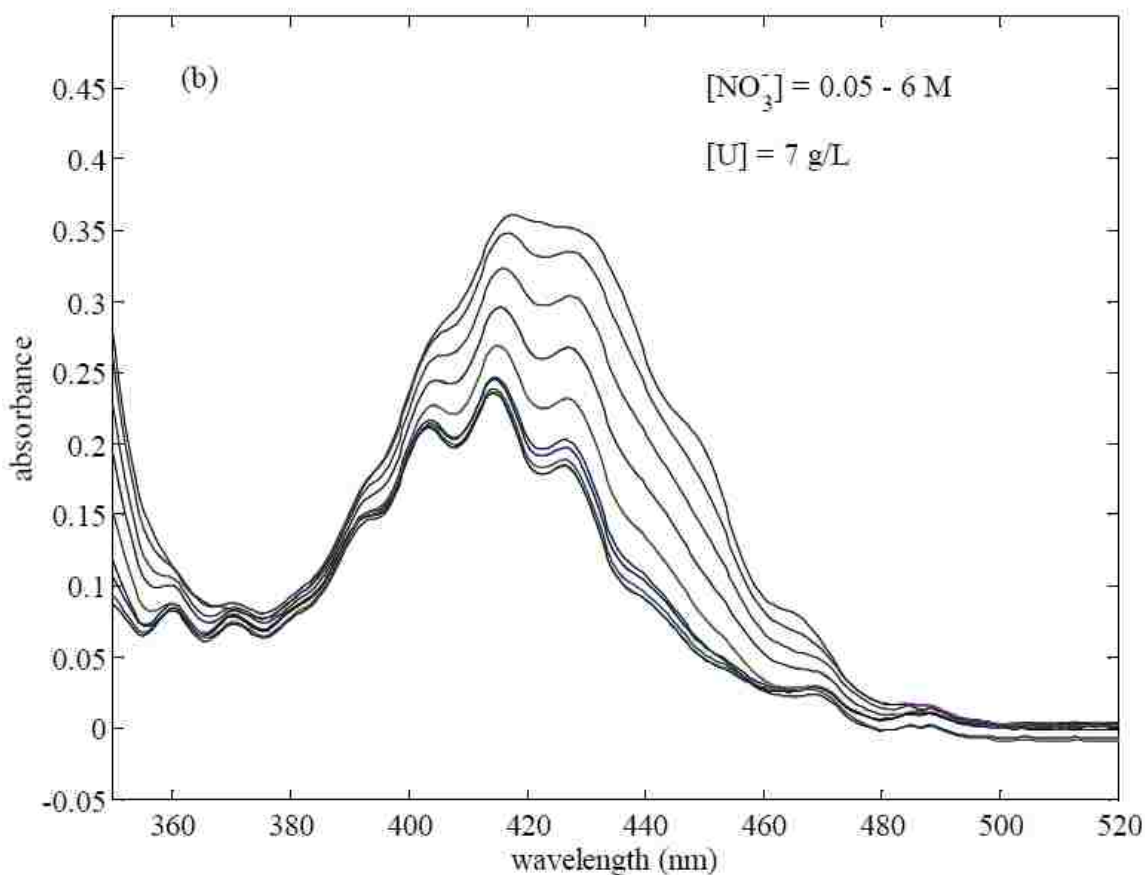


Figure 3 - The absorbance behavior of the uranyl ion in the presence of varying amounts of nitrate. From [47]

process monitor in their H Canyon reprocessing facility. The variation in the absorbance of the uranyl ion with respect to nitrate is shown in Figure 3. The stated goal was to monitor the process streams in near real time and to determine the concentrations of nitrate and uranyl ions in the system. Using a Partial Least Squares refinement, the system was able to predict the system components in a turbulent system within 5% for uranyl and 10% for nitrate. A thermodynamic refinement of the system was not pursued to improve this model.

The work done by Bostick [27] was a method to simultaneously determine the uranyl and nitrate concentrations from UV-Visible spectroscopy. The study investigated the effects of varying nitrate and metal concentration and temperature. The end result of the Bostick study was a large algebraic method that was able to determine the uranyl concentrations within 5% and nitrate concentrations within 15%. The method is based on calibration equations with the form of Equation 17 where A_λ is the absorbance at wavelength λ , M_λ and N_λ are constants of proportionality, and c_λ is a constant factor. Theoretically, this procedure is equivalent to fitting a plane through the three dimensional data set of Absorbance, $[NO_3^-]$, and $[UO_2^{2+}]$. If the calibration equations from two different wavelengths are combined, the equation can be solved explicitly for either the uranium concentration (Equation 18) or the nitrate concentration (Equation 19). The subscripts on the constants M , N , and c refer to the set of equations being used.

Equation 17

$$A_\lambda = M_\lambda [UO_2^{2+}] \cdot [NO_3^-] + N_\lambda [UO_2^{2+}] + c_\lambda$$

Equation 18

$$[UO_2^{2+}] = \frac{M_2(A_1 - c_1) - M_1(A_2 - c_2)}{M_2N_1 - M_1N_2}$$

Equation 19

$$[NO_3^-] = \frac{N_2(A_1 - c_1) - N_1(A_2 - c_2)}{M_1(A_2 - c_2) - M_2(A_1 - c_1)}$$

The method has a few drawbacks. It relies heavily on empirically derived constants and regressions. These regressions may or may not be valid between different spectroscopic systems. The method is exclusively designed for concentrations measurements and neither contributes to nor draws on information about the speciation of the uranyl nitrate system.

The study by Kaplan, et al., [26] has shown that the compound $UO_2(NO_3)_3^-$ both exists and has distinct spectroscopic features. Kaplan explored the spectroscopy of $UO_2(NO_3)_2 \cdot 2TBP$ in various non aqueous solvents as well as in the presence of tetrabutyl ammonium nitrate. The transitions of the uranyl ion become more distinct in these solvents and change dramatically when $Bu_4N(NO_3)$ was added (Figure 4). No further changes in the absorbance spectroscopy were observed at super-stoichiometric amounts of nitrate salt indicating that the reaction was complete. With this trinitrate species, absorbance bands appear between 420 and 460 nm, which is analogous to the shift in the aqueous uranyl spectrum observed in the presence of high nitrate. Additional studies have reported the similar results in other non-aqueous solvents [90,91].

2.2.2.2 Time Resolved Laser Induced Fluorescence Spectroscopy

Laser Induced Fluorescence Spectroscopy is a method for investigating the speciation of the uranyl ion or its concentration in solution by examining its fluorescence emissions and species lifetimes [28-32]. The method uses a tunable laser to excite the uranyl ion into a higher energy state. The excited molecule can then undergo several different

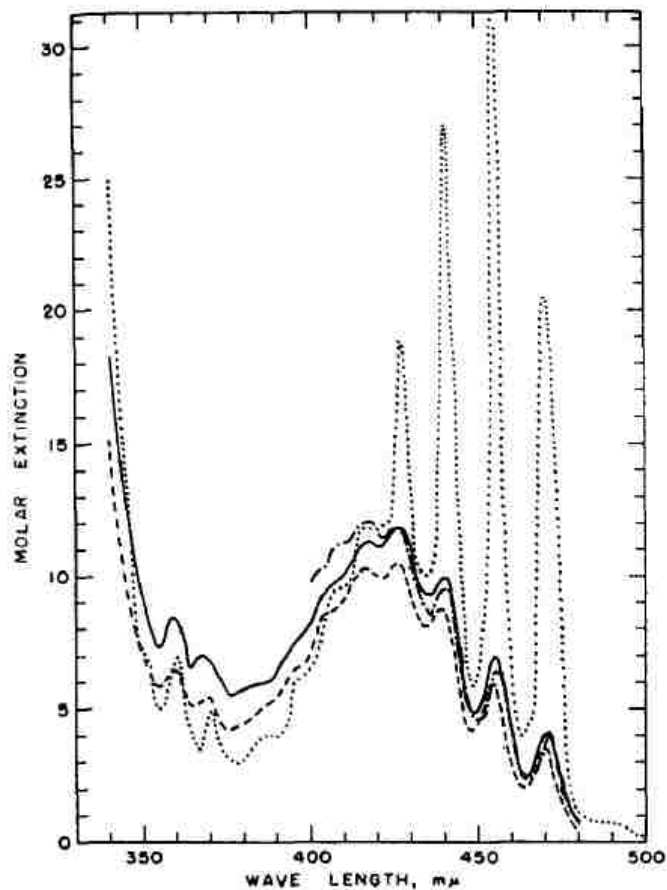


Figure 4 - Uranyl nitrate in non aqueous solvents. 0.02 M uranyl nitrate hexahydrate in: - acetone; --- methyl isobutone; --.---. cyclohexane; ... acetone with 0.02 M tetrabutyl ammonium nitrate. From [26]

relaxations in order to return to the ground state, one of these being the emission of a photon [70]. This emission can then be measured with a spectrometer and a detector. The uranyl ion has a distinctive fluorescence spectrum which can be used both to confirm its presence and concentration in a system.

The fluorescence spectrum of the uranyl ion can be found in the first paper in the series published by Bell and Biggers [23]. The structure of the fluorescence shows six large peaks at wavelengths above 470 nm (Figure 5). In addition, the rate at which the

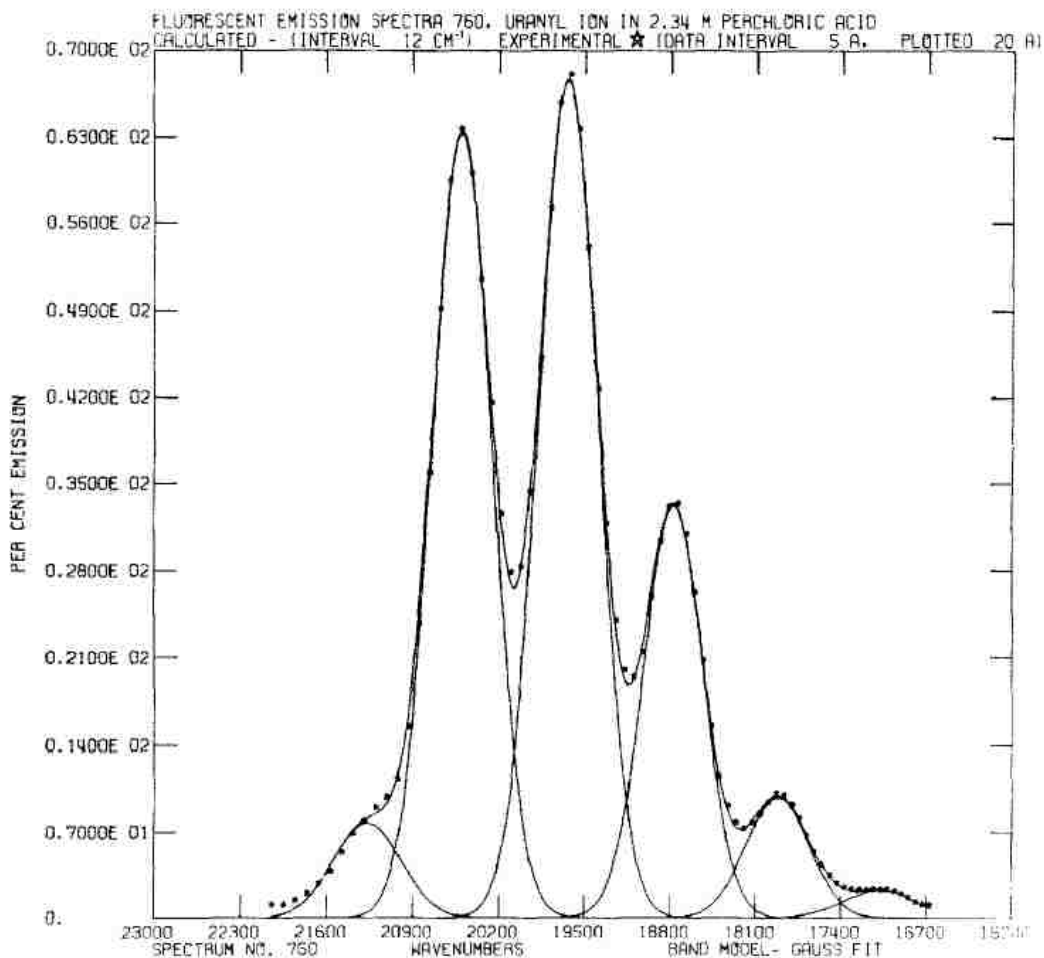


Figure 5 - Fluorescence of uranyl ion in perchloric acid showing deconvolution of the fluorescence peaks. $[UO_2^{2+}] = 0.218$ M, $[HClO_4] = 2.346$ M, Ionic Strength – 3.00. From [24]

excited state relaxes is a first order differential and is defined as the fluorescent lifetime. Since both the lifetime and the spectral shape of the system are species dependent and therefore highly coupled to the chemical environment [39]. This makes the technique not only sensitive to a particular metal ion and its oxidation state, but allows it to probe the local environment and thusly the speciation of the metal.

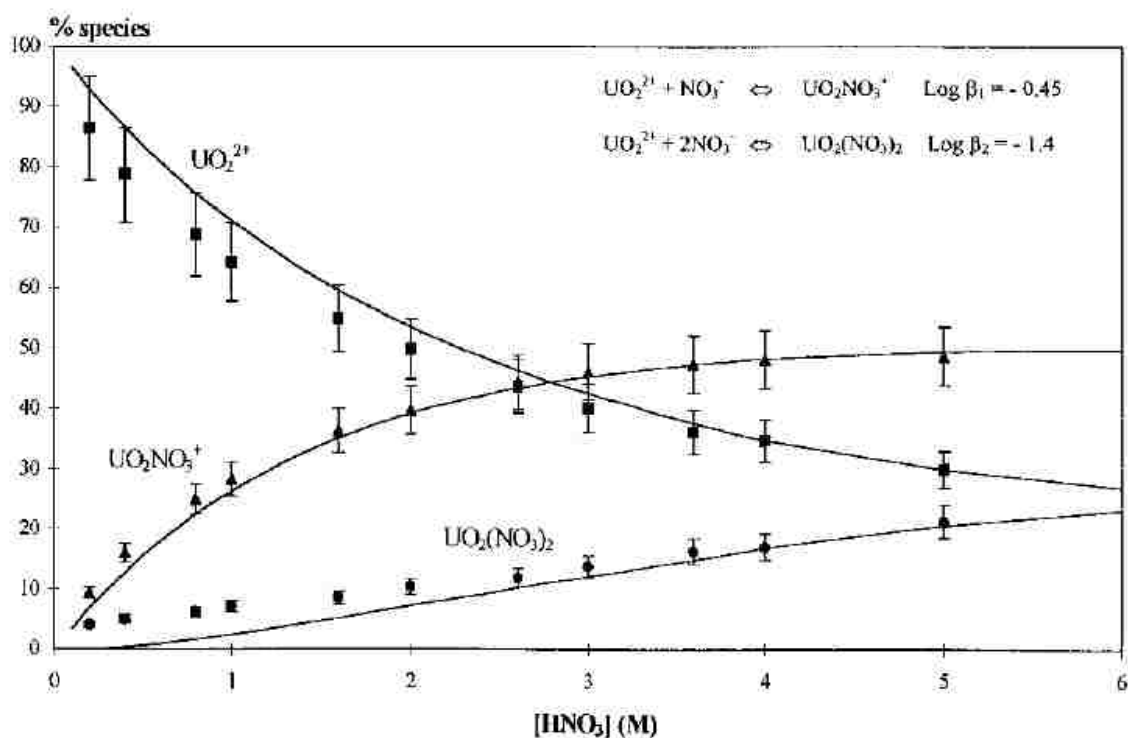


Figure 6 - Speciation of the uranyl nitrate system. Solid lines represent data from Wanner, et. al [66]. From [39]

Multiple papers from Moulin have been published examining the speciation and spectroscopy of the uranyl ion, mainly focusing on micromolar levels of uranium; these levels are consistent with and required for the sensitive TRLFS system [28,34-39,46]. In these studies, Moulin demonstrated a deconvolution based speciation refinement which appears to reproduce the stability constants found elsewhere (see Figure 6). However, it is unclear which values are being used as the mononitrate constant does not match any value from [66] and there is no agreed upon value for the dinitrate species. It appears that the value for the dinitrate species from [49] is being used. However, it must be noted that these studies are generally performed without ionic strength adjustment and at levels of uranium 4-6 orders of magnitude below reprocessing conditions (Section 2.6).

Meinrath has also produced papers examining the fluorescence behavior of the uranyl ion [10,12,40]. This work was aimed at understanding the behavior of the uranyl ion under environmental conditions and is primarily concerned with the hydroxyl species. This work is echoed by Geipel who also studied the fluorescence of hydroxyl compounds and uranyl minerals [41,42].

2.2.2.3 Extended X-ray Absorption Fine Structure Spectroscopy

X-ray Absorption Spectroscopy (XAS) is an experimental technique that measures the absorption, transmission, and scattering of photons over a specific range of energies near one of the shell edges of the target element. As the photon beam reaches the appropriate energy, it interacts with the element of interest and may then interact with other atoms in the sample. Extended X-ray Absorption Fine Structure (EXAFS) examines these features of the XAS spectrum which occurs far from the main absorption edge. EXAFS is a bulk method and can determine the average location of other atoms around the target element. Using a Fourier Transform based analysis, this scattering data can be used to recreate the local environment and produce a general structure. A review of EXAFS for actinide speciation, which gives a thorough introduction to the technique as well, can be found in the paper by Denecke (94).

In the case of the uranyl ion, EXAFS allows one to probe the number and position of the nitrates around the uranyl center. The nitrate ion only binds around the uranyl ion equatorially due to the steric interference of the axial oxygen atoms which allows the experimenter to distinguish those oxygen atoms from the ones belonging to the nitrate ion. By computing the average distance from the uranium atom to the equatorial oxygen

atoms, one can estimate of the number of nitrates around the uranium. This information can then be used in conjunction with advanced modeling techniques (Chapter 5)

Recent EXAFS studies have been performed on the uranyl nitrate system. Most notably, Ikeda-Ohno explored the visible and EXAFS spectroscopy as a function of nitrate concentration [95]. In the course of this study, they determined four uranyl species were present: the free, mononitrate, dinitrate, and trinitrate. In conjunction with their data, they refined structures for the compounds that show that the nitrates bind in a bidentate fashion. The Hennig group is also responsible for studies of the uranyl nitrate system in non-aqueous solvents [92,93]. These studies, which combine both EXAFS and UV-Visible spectroscopy, have defined the structure of the mono-, di-, and trinitrate species in both ionic liquid and acetonitrile. These measurements allow comparison of aqueous phase spectroscopy against the corresponding organic solvents to determine composition.

2.2.3 Uranium Summary

The fundamental chemistry of the uranyl nitrate system has been studied with several techniques since the 1940s. However, few of these studies have provided defensible results; high ionic strengths, variable ionic strengths, bad assumptions, and antiquated techniques have all hampered efforts to investigate this system.

The visible spectroscopy of the uranyl ion has been thoroughly investigated at the bench scale under well defined conditions. While the shift in absorbance spectra with respect to increasing nitrate concentration has been observed by multiple groups, a reasonable explanation for this behavior has yet to be proposed, nor have any single component spectra been developed.

X-ray techniques have proven to be a powerful supporting tool in investigating spectroscopic systems, though are generally not suited to primary analysis. More useful is the ability to match x-ray data to theoretical structural models.

2.3 Review of the Plutonium(IV) Nitrate Literature

Investigations into the plutonium system are even more focused than the corresponding studies of the uranyl ion. The influence of the weapons complex on plutonium research can be seen in the large number of papers dedicated to its solid state properties and purification. Few of these papers delve into the thermodynamics of the plutonium nitrate system, though several authors have attempted to investigate this system. These papers will be detailed as follows: Section 2.3.1 will look at the speciation of the plutonium nitrate system; Section 0 covers relevant redox chemistry; while Section 2.3.3 will look at Pu(IV) spectroscopy.

2.3.1 Speciation of Plutonium in Acidic Media

The speciation of Pu(IV), without considering polymerization or disproportionation, is very convoluted and can be seemingly contradictory at times. This is emphasized in the review of plutonium coordination complexes by Cleveland [96] and elsewhere [69]. Formation constants for the plutonium nitrate system are listed in Table 2. Despite the large number of studies that have produced stability constants, there is little consensus on the actual value of any of the parameters and no thermodynamic parameters exist for anionic plutonium species.

Table 2 – Selected tetravalent plutonium nitrate stability constants. From [69].

Temp. °C)	Ionic Medium	$\log_{10} K$	$\log_{10} K^\circ$	Ref.
<i>Pu</i> ⁴⁺ + <i>NO</i> ₃ ⁻ ↔ <i>PuNO</i> ₃ ³⁺				
20	2 M HClO ₄	0.46±0.1		54
25	1 M HClO ₄	0.54±0.01		55
20	4 M HClO ₄	0.74±0.02		56
25	4 M HClO ₄	0.97±0.03		57
25	0.5 M HNO ₃	0.72		58
25	1 M HNO ₃	0.75		
20	8 M HClO ₄	0.69		50
25	2 M HClO ₄	0.65±0.01		59
10	2 M HClO ₄	0.57±0.01		65
25	Various (b)	(a)	1.95±0.15	54-57,59
20	2-19 <i>m</i> HClO ₄ /HNO ₃	(a)	2.12±0.2	64
<i>Pu</i> ⁴⁺ + 2 <i>NO</i> ₃ ⁻ ↔ <i>Pu(NO</i> ₃ ⁻) ₂ ²⁺				
20	2 M HClO ₄	0.65		56
25	2 M HClO ₄	1.43±0.03		
25	2 M HClO ₄	1.43±0.03		57
20	8 M HClO ₄	0.42		50
25	2 M HClO ₄	0.65±0.01		59
10	2 M HClO ₄	0.57±0.01		65
20	2-19 <i>m</i> HClO ₄ /HNO ₃	(a)	3.66±0.4	64
<i>Pu</i> ⁴⁺ + 3 <i>NO</i> ₃ ⁻ ↔ <i>Pu(NO</i> ₃ ⁻) ₃ ⁺				
20	4 M HClO ₄	1.18±0.5		56
20	4 M HClO ₄	0.18		60
25	4 M HClO ₄	-0.39±0.5		57
25	6 M HClO ₄	-0.01±0.2		
20	8 M HClO ₄	0		50
<i>Pu</i> ⁴⁺ + 4 <i>NO</i> ₃ ⁻ ↔ <i>Pu(NO</i> ₃ ⁻) ₄ (<i>aq</i>)				
20	8 M HClO ₄	-0.72		50

(a) – Individual stability constants from each ionic strength level are not shown.
(b) – Refined by editors in [69]

From the electronic structure of plutonium, it is possible to have up to seven plutonium species in solution, from the free aquo- cation to the hexanitrate anion, inclusive. The spectrophotometric and extraction study by Brothers, Hart, and Mathers [61] started with this assumption but concluded that there are only 2-3 dominant plutonium species in solution. In solutions of sodium nitrate and perchlorate and based

on extraction studies, the authors determined that $\text{Pu}(\text{NO}_3)_4$ was the dominant species. When nitric acid above 10 M was used, they observed the hexanitrate anion, $\text{Pu}(\text{NO}_3)_6^{2-}$, which is confirmed by Ryan [62]. Another species may have been detected at high acid concentrations, a possible candidate being the acid adduct of the pentanitate species. However, there was little evidence for lower nitrate complexes.

The proposed speciation from Brothers et al. [61] is confirmed, in part, by the spectroscopic work done by Viers [63]. In a multi-technique study using EXAFS, UV-Visible spectroscopy, and NMR, they concluded that the dominant species found up to 13 M HNO_3 were the di-, tetra-, and hexa-nitrate species (Figure 7). In a separate paper by Viers [43], much of the same data was presented, though a mononitrate species at low nitrate concentrations was included. This speciation set is further bolstered by the work of Berg in 1998 [64] which details a series of spectrophotometric titrations. The study refined the mono- and dinitrate stability constants and allowed extrapolation to zero ionic strength with the SIT theory.

A review by Spahiu and Puigdomenech [97] looked at 30 different papers concerning plutonium and neptunium nitrates. In their review, it was determined that only one species, the plutonium(IV) mononitrate, was required to adequately explain the experimental literature in media below 2 M HNO_3 at ionic strengths up to $I_m=6$.

2.3.2 Plutonium Oxidation States

Plutonium has four accessible oxidation states which can coexist in solution. Due to the necessity of creating a pure plutonium(IV) stock solution, the disproportionation of Pu(IV) into Pu(III/VI) must be addressed. The governing total reaction is given in Equation 20 [98,99]. The disproportionation can be mitigated by increasing the acid

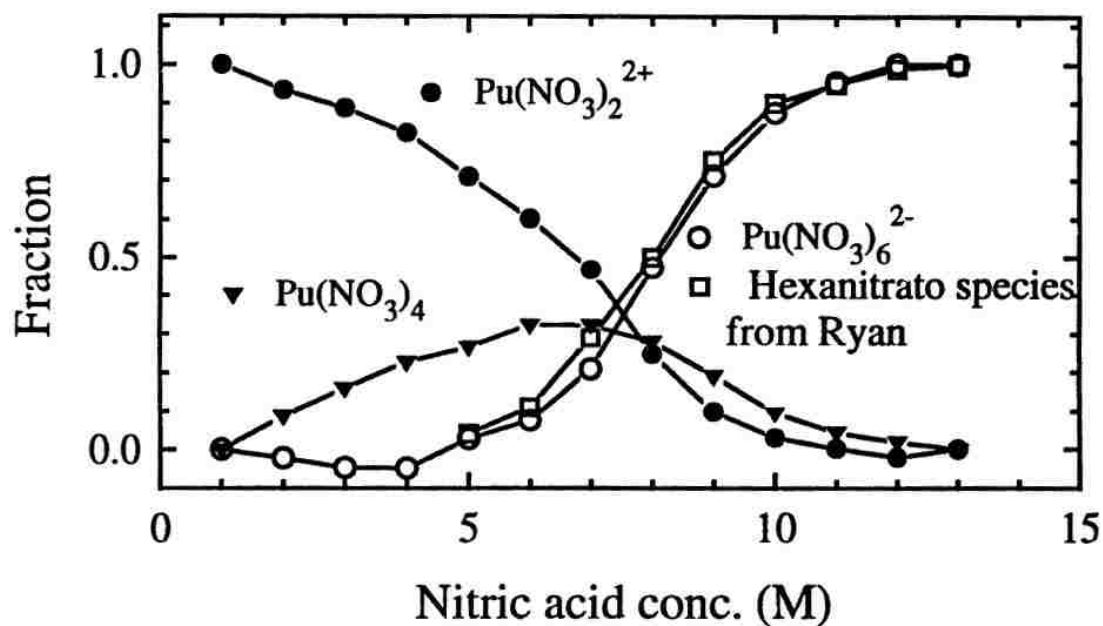
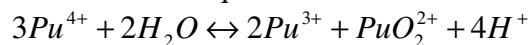


Figure 7 – Speciation of the plutonium(IV) nitrate system from [63]. Data of Ryan can be found in [62].

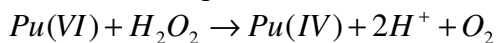
concentration per Le Chatelier’s principle.

Equation 20



The ability to produce this stock solution is vital to thermodynamic or spectroscopic work. Oxidation of Pu(III) to Pu(IV) can be accomplished by increasing the nitric acid concentration of the solution to ~8M. Reduction of the Pu(VI) to Pu(IV) is performed by the addition of a stoichiometric amount of hydrogen peroxide to the acidified solution. This proceeds according to the reaction in Equation 21 and has been used at the bench and process scale to adjust the plutonium oxidation state [99,101]. The use of peroxide to reduce Pu(VI) is preferential to other techniques as it does not leave traces of the reduced species in the solution.

Equation 21



2.3.3 Spectroscopy of Pu(IV)

As with the uranyl ion, the electronic structure of plutonium, in any of its common oxidation states, allows for several spectroscopic techniques to be used. UV-Visible spectroscopy has been used to interrogate a wide variety of plutonium containing solutions. EXAFS spectroscopy has also been used to a limited extent. The following sections will detail papers relevant to the Pu(IV)-nitrate system.

2.3.3.1 UV-Visible Spectroscopy

The UV-Visible spectroscopy of plutonium is complicated due to the fact that multiple absorbing oxidation states can coexist in solution. In addition, the oxidation states react differently to the chemical environment making systematic studies difficult to prepare and analyze [44,45]. Focusing on Pu(IV), the visible spectrum is filled with absorption bands over the entire visible spectrum (Figure 8). As the ligand concentration is varied, peaks in the spectrum can shift, increase, or decrease.

Several researchers have attempted to study the changes in the visible spectrum systematically. Most agree that the diagnostic peak for Pu(IV) occurs in the 470-490 nm region with a molar absorptivity of $\sim 55\text{-}68 \text{ L mol}^{-1}\text{cm}^{-1}$ [9,44,45]. However, this peak shifts dramatically from 469 nm to 491 nm as the nitrate concentration is varied from 1 to 13 molar (Figure 8). An unusual feature of the spectra is the distinct lack of a non-absorbing region for zeroing a spectrometer. Therefore, measuring the absorbance of these species can introduce systematic errors, such as detector drift, and must be monitored carefully.

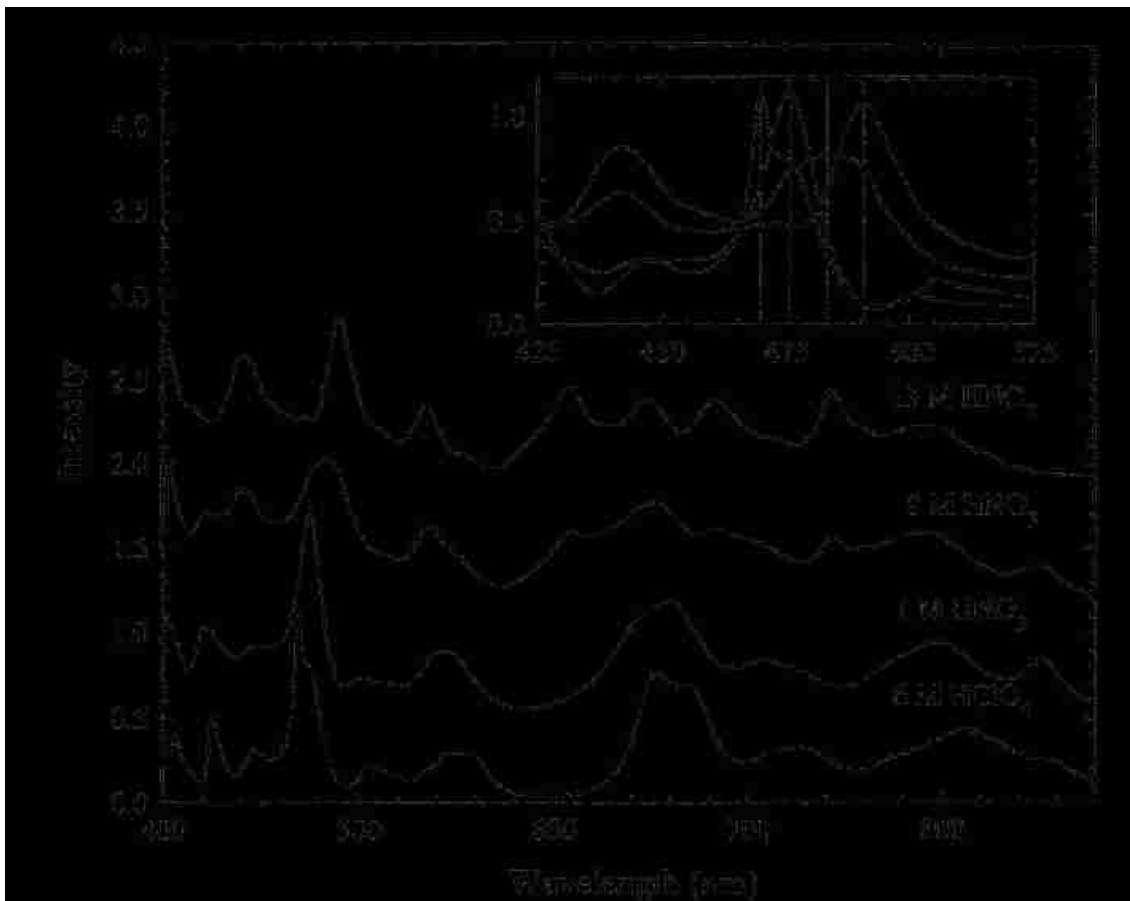


Figure 8 - Absorption spectra of Pu(IV) at a concentration of 4.8 g/L. The spectra, obtained with 1 cm pathlength, are offset for clarity; the intensity scale is absorbance. The vertical dotted lines are at 469, 476, 483 and 491 nm. From [43]

2.3.3.2 Extended X-ray Absorption Fine Structure Spectroscopy

The use of EXAFS spectroscopy on aqueous plutonium chemistry is limited to a handful of studies. One of the more comprehensive, and often cited, studies is the paper by Viers, et al., [43]. In this study, the UV-Vis, NMR, and EXAFS spectroscopy of Pu(IV) nitrate complexes was examined. The results of the work indicate the formation of three major species in solution between 1 and 13 M HNO₃: Pu(NO₃)₂²⁺, Pu(NO₃)₄, Pu(NO₃)₆²⁻. The EXAFS data was collected and a Fourier transform was performed, but

the data was not compared to theoretical models in this paper. A separate paper from Allen, et al., [102] analyzed this EXAFS data and compared the structures to available crystallographic data. They determined that the structures represented in the transforms were analogous to the solid reference materials and concluded that the nitrates coordinated to the plutonium centers in a bidentate fashion.

2.3.4 Tetravalent Plutonium Summary

In summary, the chemistry of tetravalent plutonium in nitric acid has been studied with a variety of techniques and methods. However, there is no clear consensus on the either the species present in solution or their governing thermodynamic parameters.

The visible spectroscopy is similarly unclear due to the large number of oxidation states that may or may not be present in solution. The molar absorptivities of these species change drastically with respect to nitrate making routine analysis difficult.

2.4 Ionic Strength Effects

The effect of the ionic strength of a solution on the various chemical and physical properties is a complex problem. The chemical activity of species, the solution vapor pressure, and osmotic pressure, to name a few, are all affected by ionic strength. The ability to predict and model these changes has been a goal of thermodynamic studies for many years. The effects are detailed in Sections 2.4.1 and 2.4.2 and the modeling thereof in Section 2.5.

2.4.1 Effects on Physiochemical Constants

The variation of solution properties with respect to the ionic strength can be broken into two main groups: physiochemical and thermodynamic quantities. To some extent,

they are one and the same, though they are generally treated separately. Physiochemical quantities, such as freezing point depression, boiling point elevation, or osmotic pressure changes (commonly referred to as colligative properties), have been thoroughly studied and are well understood for simple systems. Many physical chemistry texts can provide more a more in depth explanation than is warranted by this review [70].

2.4.2 Effects on Thermodynamic Quantities

Changes in the solution ionic strength alter the species activity in solution and thusly the chemical potential. Physical quantities that are derived from the chemical potential will then vary with the ionic strength [71]. This fact requires an experimenter to be exceedingly cautious when working at elevated ionic strengths as the very constants being determined can shift as basic assumptions about the system are no longer known. To combat this, a methodology has been developed to work at constant ionic strength which will keep the system static. Unfortunately, this significantly limits the scope of experiments that can be performed.

The production of solutions at desired ionic strengths also needs to be addressed. The ionic strength adjustor must be carefully chosen, not only for chemical compatibility, but also due to activity concerns as electrolytes with $z \geq 2$ may not fully dissociate [71]. The electrolyte chosen to control the ionic strength will also impact the activity coefficients, and thusly many thermodynamic quantities, of every species in the solution through the inclusion of ion interaction coefficients. This topic will be covered more thoroughly in the following section and in Chapter 5.

2.5 Theoretical Modeling of Thermodynamic Quantities

The current accepted methodology is based on extrapolation of thermodynamic quantities to zero ionic strength for direct comparison. This can be accomplished by a number of models including the Specific Ion Interaction Theory, the Pitzer Equations, the Baes and Mesmer equations, and the Davies equations. A review of these techniques can be found in the literature [103].

While each model has specific strengths, the Brønsted-Scatchard-Guggenheim theory, commonly referred to as the Specific Ion Interaction Theory, or SIT, is generally considered to be practical for ionic strengths up to $I_m=3.5$ [103]. The model uses the ionic strength and a set of empirically measured parameters to generate activity coefficients for all species in solution. These are then used to correct a measured stability constant for the effects of ionic strength. Therefore, if the stability constant for a given reaction is measured at several ionic strengths, this theory allows the extrapolation of the zero ionic strength constant, usually with a weighted Least Squares refinement. The IUPAC has released a program suite to handle the calculations of the SIT theory. The details of SIT and the IUPAC program are detailed more extensively in Chapter 5.

2.6 Solvent Extraction of Actinides

Many studies have been published on the extraction of actinides into a variety of media. Long chain or branched hydrocarbons, room temperature ionic liquids, and supercritical carbon dioxide are all popular solvents [67]. In most cases the presence of the second phase alone is not enough to reach the desired partition between the phases

and an extractant is added. The extractant tri-butyl phosphate (TBP), is of particular interest to this work due to its use in industrial reprocessing applications (see Figure 9).

The use of a two phase extraction system based on the nitric acid/tri-butyl phosphate/dodecane model is the most likely avenue for reprocessing in the United States [104]. This is what the US used for reprocessing at both federal (Hanford, WA) and civilian (West Valley, NY) sites [2]. The development of a proliferation resistant process, or suite of processes, has been and continues to be a goal of the US Department of Energy [7]. The PUREX process, widely seen as a proliferation risk, was used as the backbone for developing the UREX process, and subsequent processes downstream in the proposed reprocessing train.

2.6.1 TBP Based Extractions

The PUREX process uses TBP dissolved in an organic diluent to separate uranium and plutonium from a nitric acid feed stream [105]. PUREX was developed as an extension of the work performed as part of the Manhattan Project at the Metallurgical Laboratory of the University of Chicago [106]. PUREX, or variations of the process, have been deployed at the industrial scale for decades and remains the cornerstone of nuclear fuel reprocessing for both defense and power reactor fuels around the world [2].

Briefly, uranium and plutonium are co-extracted in the first extraction and then separated downstream. The nitric acid concentration in the process feed is adjusted to 4-6 M, which corresponds to a total nitrate concentration of 6-8 M [67]. The main drawback to PUREX is the presence of the pure plutonium product stream. This is widely seen as a proliferation risk as the material is chemically pure and the ability to measure the exact amount of material is limited [8].

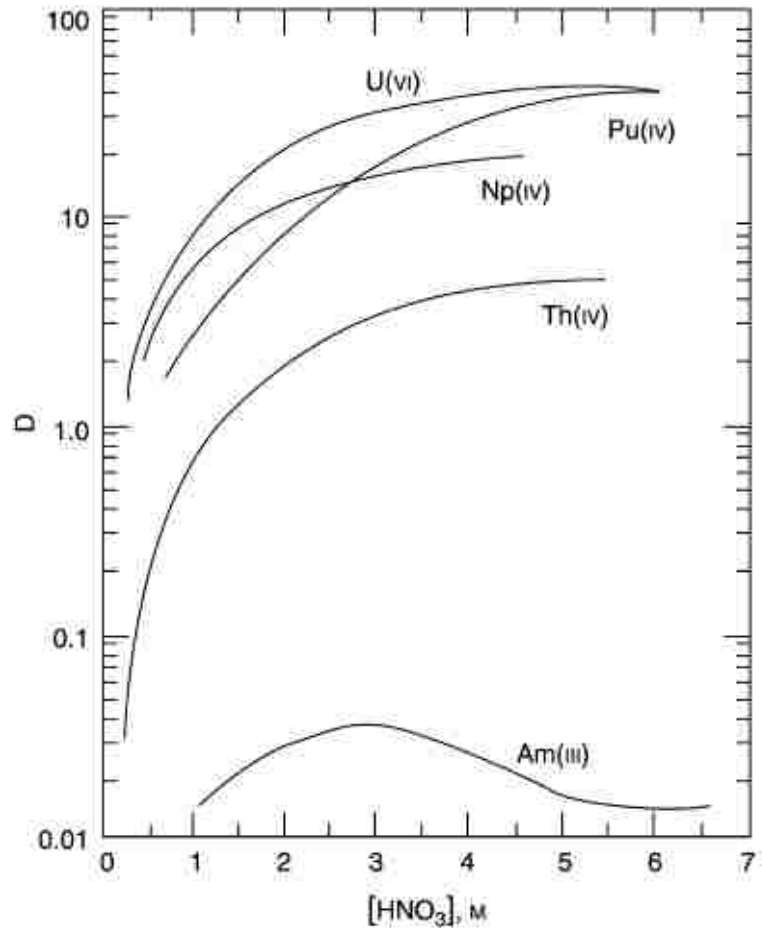


Figure 9 - Extraction of actinides into TBP/dodecane as a function of nitric acid. From [67].

The UREX process was designed as a proliferation resistant solution to fuel reprocessing [81]. It is similar to PUREX with some minor yet significant modifications. The first difference is the presence of a complexant/reductant (acetohydroxamic acid) in the feed stream to reduce the extractability of the plutonium. The feed solution nitric acid level is 1-2 M, with a total nitrate concentration of 3-4 M. As a result, the plutonium is kept mixed with other actinides to decrease the material's attractiveness.

2.7 Process Monitoring and IAEA/DOE Safeguards

In order to address the threat of nuclear weapon proliferation, a framework for the incorporation and administration of nuclear safeguards was put into place by the Treaty on the Nonproliferation of Nuclear Weapons (NPT) [107]. In addition to these international safeguards, a collection of domestic safeguards is also being pursued by the US Department of Energy. This section will detail those efforts and how they influence the application of uranyl spectroscopy to reprocessing streams.

2.7.1 NPT and International Safeguards

The Treaty on the Nonproliferation of Nuclear Weapons, of which the United States is a signatory, was ratified in 1970 and is based upon three informal “Pillars”: Nonproliferation, Disarmament, and the Peaceful Use of Nuclear Energy. These pillars are defined through the articles of the treaty.

Article III, subsections 1 and 3, define the role of safeguards for a signatory country.

From the NPT:

“III-1: Each non-nuclear-weapon State Party to the Treaty undertakes to accept safeguards, as set forth in an agreement to be negotiated and concluded with the International Atomic Energy Agency in accordance with the Statute of the International Atomic Energy Agency and the Agency’s safeguards system, for the exclusive purpose of verification of the fulfillment of its obligations assumed under this Treaty with a view to preventing diversion of nuclear energy from peaceful uses to nuclear weapons or other nuclear explosive devices. Procedures for the safeguards required by this Article shall be followed with respect to source or special

fissionable material whether it is being produced, processed or used in any principal nuclear facility or is outside any such facility. The safeguards required by this Article shall be applied on all source or special fissionable material in all peaceful nuclear activities within the territory of such State, under its jurisdiction, or carried out under its control anywhere.”

“III-3: The safeguards required by this Article shall be implemented in a manner designed to comply with Article IV of this Treaty (right to peaceful use of nuclear technology), and to avoid hampering the economic or technological development of the Parties or international co-operation in the field of peaceful nuclear activities, including the international exchange of nuclear material and equipment for the processing, use or production of nuclear material for peaceful purposes in accordance with the provisions of this Article and the principle of safeguarding set forth in the Preamble of the Treaty.”

Most of the IAEA safeguards being actively pursued fall into three main categories: nuclear material accountancy; inspection, verification, and process monitoring; and containment and surveillance [108]. The safeguards work at all levels of the fuel cycle, from the inside out. First, nuclear materials accountancy aims to track special nuclear material (i.e. ^{235}U or ^{239}Pu) from the time it enters a safeguarded area to the time it enters. This can be accomplished by any number of methods and is flexible as a system. Currently, burn-up calculations coupled with either gamma ray or neutron measurements

or both are being used [108]. Next, the plant operations need to be inspected, the processes in use must be verified through destructive or nondestructive assay, and the processes must be monitored for off-normal or suspicious events. Finally, the area is put under surveillance and physically contained on site through a combination of gates/fences and armed guards.

It is worth noting that the first sentence of Article III, section 1, states that these guidelines are only for “non-nuclear-weapons States”. This means that the United States is not obligated to submit to international safeguards monitored by the IAEA. This is because the stated intent of international safeguards is to prevent the signatory state from developing nuclear weapons; this point is moot for nuclear weapon states. Therefore, domestic safeguards are geared toward preventing proliferation by sub-national entities, such as a rogue plant operator, or acquisition of material by force.

2.7.2 Domestic Safeguards

The US has long history of domestic safeguards, some predating the NPT. These were initially put in place to prevent the loss of material. The current state of US Domestic Safeguards emphasizes physical protection of nuclear sites and a statistical monitoring program operated as the Nuclear Materials Management & Safeguards Systems [108,109]. The current policy of the Department of Energy still emphasizes safeguards as an important part of any nuclear fuel cycle. The scope has also been expanded to include advanced instrumentation for material control and accountancy in separation processes [7].

The DOE Materials Protection, Accountancy, and Control Technology (MPACT) campaign has also emphasized the importance of non-destructive assay (NDA) systems

such as optical spectroscopy, radiometric techniques, neutron spectroscopy, and densitometry [8]. The ability to monitor the process of interest without the need to take a grab sample, move that sample to a hot lab, and wait for the results has obvious appeal. These assays generally have shorter turnaround times which allows for the possibility of monitoring the relative change in a system as opposed to absolute measurements.

2.7.3 Role of Process Monitoring in Reprocessing Plants

The monitoring of the chemical reprocessing scheme is important to both the IAEA/DOE inspector and the plant operator [108]. Information on how the processes are performing allows for proper plant management as well as real time information on the material in the system. Online, near real time process monitoring is a goal of the DOE MPACT program [8]. The technologies being proposed to fill this gap are varied, ranging from stimulated neutron emission to gamma ray analysis to optical spectroscopy [108]. Ideally, the method should be able to give information on the amounts of special nuclear material in the process. If the monitor can also give information on the chemistry of the system, that would be a bonus for the plant operator. Chemical information from a monitor can also be used to detect chemistry based diversions.

One of the possible pathways for diverting special nuclear material is to change the chemistry of the fuel recycling process (Section 2.6) to one that is favorable for plutonium. For example, changing from UREX to PUREX can be accomplished by increasing the total nitrate concentration by 3-4 M and removing any complexants or reductants in the system. This change is a strictly chemical method of altering the process without any large changes in the plant infrastructure. This type of diversion can be deployed as either a prolonged, small deviation, with a large cumulative result or

quickly as a process upset. Another diversion route is to simply change the process chemistry to make the process less efficient and shunt material into a secondary stream. In this case the ability to detect the material in different streams in real time would be advantageous.

Moulin and Deniau have proposed a Time Resolved Laser Induced Fluorescence system for online process monitoring [46]. The method proposes the determination of nitrate and uranyl concentrations simultaneously with a deconvolution procedure. The method reproduces the nitrate within ~6% and the uranyl within ~15%, though the upper limit of the study was 1 mg/L, which is far below process conditions of 300g/L. Lascola et al. have also proposed an online monitoring system for uranium and nitrate concentrations which is sensitive to the chemical environment (Section 2.2.2.1) [47].

CHAPTER 3

ANALYTICAL

A variety of analytical techniques have been used to study the fundamental chemistry of the uranyl and plutonium systems. For this work, the major analytical techniques are described in detail including the theory of operation, system specifications, and sample preparation, measurement, and analysis. The methodologies pertaining to titrations (Section 3.1), UV-Visible spectroscopy (Section 3.2), Time Resolved Laser Induced Fluorescence spectroscopy (Section 3.3), Inductively Coupled Plasma, Atomic Emission Spectroscopy (Section 3.4), X-ray Absorption Fine Structure spectroscopy (Section 3.5), and radiometric techniques (Section 3.6) are covered in this chapter.

3.1 Titrations

The systematic variation of a parameter in a system can be fundamentally described as a titration. Two different types of titrations were utilized to analyze the uranyl nitrate system. The first is a potentiometric titration that competes the uranyl nitrate and acetate species against one another and measures the change in proton activity. The second is a spectrophotometric titration that varies the amount of nitrate in the system and monitors the change in the absorbance signal. This section will explore the methodologies behind both techniques.

3.1.1 Potentiometric Titrations

The general methodology was adapted from similar studies in the literature [110-112]. A potentiometric titration system from Metrohm USA which consisted of a Titrino 799, a 685 Dosimat, and an 801 Magnetic Stirrer was used (Figure 10). Both the Titrino

and the Dosimat were fitted with 5 mL displacement burettes with a volume resolution of 1 μ L. Anti-diffusion tips were used on all burette lines. Samples were analyzed in a 5 mL jacketed titration vessel which was connected to a Lauda recirculating water bath. The water bath was certified to maintain the sample temperature within 0.2°C and was monitored with a NIST traceable alcohol thermometer. The lid of the titration vessel was not jacketed, but due to the low temperature, no evaporation and subsequent condensation on the lid was expected or observed.

A Unitrode electrode (Metrohm model 6.259.100) was used in these experiments though the normal fill solution of 3 M KCl was replaced with a solution of saturated NaCl to avoid precipitation of KClO_4 in the electrode frit. The response of the electrode with the alternate fill solution was virtually identical when checked against 10 pH buffers (Table 3).

A humidified argon stream was passed through both the titrants and the sample to prevent any build up of CO_2 over time. This was done by bubbling dry argon through a

Table 3 – Response of electrode to buffer solutions with 3 M KCl and saturated NaCl fill solutions. Results are the average of three measurements

Buffer (pH)	KCl fill (mV)	NaCl fill (mV)	Difference (mV)
1	333.5	335.2	1.7
2	266.8	266.9	0.1
3	208.7	208.7	0.0
4	149.8	150.0	0.2
5	92.0	92.6	0.6
6	35.6	36.6	1.0
7	-24.9	-24.1	0.9
8	-78.5	-77.7	0.8
9	-138.8	-138.4	0.4
10	-198.9	-198.1	0.8

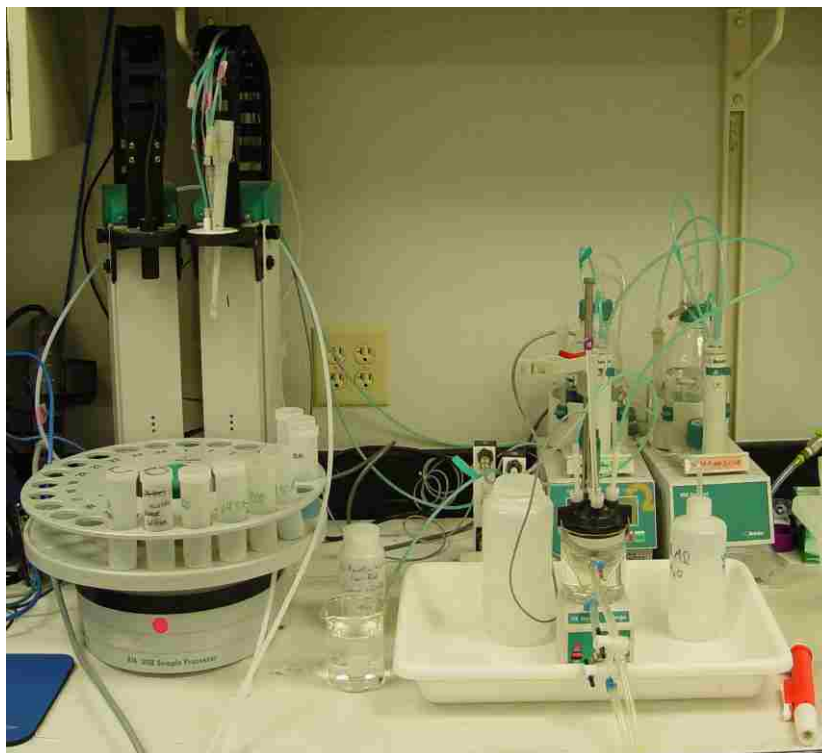


Figure 10 - Metrohm Titration system.

solution of sodium perchlorate with the same ionic strength as the titrants. This ensured that changes in the titrant or titrand concentrations over time due to evaporation would be minimized.

3.1.2 Daily System Checks and Calibration

At the beginning of each day of an experimental run, the level of fill solution in the electrode was checked and replaced if necessary. Then the response of the electrode to four standard pH buffers at 2, 5, 7, and 10 was checked. The electrode was deemed to be in good working order if the slope was $>95\%$ of the theoretical slope with less than 5% variation.

The electrode was standardized daily by titrating a known amount of standard acid, diluted into an electrolyte solution, with a NaOH solution at the same ionic strength. The

composition of the titrand was 0.25 mL of 1.0 N HClO₄ in 24.75 mL of a NaClO₄ electrolyte solution. The change in ionic strength over the course of the titration due to neutralization (0.01 M) was insignificant in comparison to the overall ionic strength. The standard potential, Nernstian slope, titrant concentration, and protolytic impurity was then refined by the GLass Electrode Evaluation (GLEE) program [113]. This allowed the system to accurately measure the pH of the system at elevated ionic strengths.

3.1.3 General Method for Competition Titrations

All titration data was collected directly in mV. Aliquots of either the acetate buffer or the sodium hydroxide solution were added to the sample cup and titrated with a standardized acid or base. The titrant was delivered in 0.050 mL increments, allowing the signal drift of the electrode to fall below 1 mV/min with a maximum waiting time of 100 seconds. Similarly, for all uranium containing titrations, the titrant was added in 0.050 mL increments and allowed to equilibrate up to 150 seconds prior to taking the measurement. Only data above pH 2.5 was used in the final analysis due to the contribution of the acid junction potential at lower pH values. This resulted in approximately 60-80 useable data points per titration.

Two titrants were used in these experiments. The first is a 0.10 N NaOH solution, at a given ionic strength, used for daily calibrations and the standardization of the acetate buffer titrant. The acetate buffer titrant was composed of 0.5 M sodium acetate, 0.5 M acetic acid, elevated to the desired ionic strength with sodium perchlorate. A 1:100 constant ionic strength dilution of the acetate titrant was used to standardize the titrant. Enough perchloric acid was added during the dilution to completely protonate the acetic acid and the sample was then titrated with a standardized base.

For each titration, the titrand was pipetted into the jacketed vessel with a volumetric pipette, the thermometer and argon was added and the sample was allowed several minutes to equilibrate. Due to the high acid concentration of the titrand, excessive buildup of carbon dioxide was not expected. The buret lines were prepared by pumping 10 mL of titrant through them to flush the lines and remove any bubbles prior to placing the buret tip in the vessel. Finally, the calibrated electrode was placed inside of the vessel, the height adjusted to ensure the frit was covered by solution, and a stir bar was added. An additional 5 minute equilibration period was allowed after the stirrer was turned on to allow the argon gas to purge the sample.

After each titration, the apparatus was rinsed repeatedly with both dilute perchloric acid and water. At the end of each day, the electrode was stored in a pH 4 buffer unless an extended period of inactivity was expected, in which case the electrode was stored dry.

Water used for all reagents was obtained from an 18.1 M Ω reverse osmosis water source (Cascadia LS Water Source, Pall Corp.). Class A volumetric pipettes and flasks (Kimax, Kimball USA via VWR) were used to create all standard solutions. A perchloric acid standard (1.0 N, VWR) was used as a primary standard. A 5.0 molar sodium nitrate (5.0 N, Ricca Chemical) solution was used to adjust the nitrate concentration in the system. Uranium trioxide (Strem Chemicals, Newburyport, MA) was dissolved in a known excess of perchloric acid prior to the addition of other components or final dilution. The total ionic strength of the solution was adjusted with sodium perchlorate. The sodium perchlorate stock solution was made by dissolving solid sodium perchlorate in water and filtering to remove impurities. The final solution was analyzed in triplicate by placing 5 mL of solution in a pre-weighed flask, recording the mass, and heating the

sample to a constant mass, usually over 2-3 days. This yielded the sample density, molarity, and molality.

3.1.4 Spectrophotometric Titrations

The methodology for the spectrophotometric titrations was loosely adapted from the work by Rao [21]. The spectrophotometric titration apparatus consisted of six parts which created a closed, recirculating system. A NE300 syringe pump (New Era Syringe Pumps) was used to deliver the titrant from a BD 20 mL Luer Lock syringe. The accuracy of the pump was determined by dispensing aliquots of water into pre-weighed vials; the pump delivered the stated volume within 0.5%. The titrant was dosed into the sample bottle via 2 mm I.D. silicone tubing (Wheaton via VWR) attached with a barbed connector embedded in the bottle lid. All tubing connectors were made from PEEK material and purchased from Bio-Chem Fluidics. The sample bottle contained a Teflon coated stir bar and was placed on a stir plate. A flow through cuvette (model 176.700, 10 mm pathlength, 1.5 mL volume, Hellma USA) was used; the inlet and outlet tubes were connected to the sample bottle and fed through a peristaltic pump (Peristar Pro 4L, World Precision Instruments) running at 15 rpm. The tubing that came with the flow cuvette required the addition of peristaltic pump tubing (PVC “white/white”, Thermo Fisher Scientific) attached to both the inlet and outlet lines. The reason for this was two-fold: first, the tubing was rigid and could not be used in a peristaltic pump; second, the total length of the tubing needed to be extended.

After an addition of titrant, the system was allowed to recirculate for at least 6 minutes to completely mix the sample. This time was determined to be sufficient by adding a small amount of copper sulfate and monitoring the 800 nm line until the signal

stabilized. After the pump was stopped, the system was allowed to rest for at least 30 seconds to ensure the solution no longer flowed. A spectrum was collected and the process was repeated.

Samples were made gravimetrically using either a Mettler-Toledo (XS205DU Dual Range) or a Sartorius (BP61S) balance. Solid uranium trioxide, concentrated perchloric acid, and concentrated nitric acid (if necessary) were added in sequence to 250 mL Nalgene HDPE bottles. The amount of water added with the concentrated acids was calculated and an appropriate mass of water was added to reach the desired molal ionic



Figure 11 - Spectrophotometric titration apparatus. Syringe Pump (Upper Right) delivers titrant to sample cup (foreground) on a stir plate. Peristaltic Pump (Upper Left) recirculates sample through flow through cuvette (not shown).

strength. After final dilution and weighing, aliquots were removed for ICP-AES analysis and the final bottle mass was recorded.

3.2 Ultraviolet-Visible Spectroscopy

This section will give a basic description of how UV-Visible spectroscopy instruments work (3.2.1) and how samples are prepared (3.2.2), measured (3.2.3), and characterized (3.2.4-3.2.6). Spectrophotometric methods were developed at UNLV and are derived from general information and practical experience [71].

3.2.1 Theory of Operation

UV-Visible spectroscopy is based on the fact that certain chemical species will absorb light of a specific frequency. In order to take advantage of this, the intensity of light before and after passing through a sample is measured and the ratio of those two measurements is taken. This ratio, expressed as the transmittance of the system, is governed by the Beer-Lambert Law (see Section 2.1.4). The way the absorbance is measured varies between different spectrometer models; since three different spectrometers were used throughout these experiments, each will be detailed separately. For the majority of experiments, the Varian Cary 6000 was used; for the initial plutonium work, a Varian Cary 50 was used; finally, an Ocean Optics USB2000 was used for fiber optic dip probe work.

3.2.1.1 Varian Cary 6000

The Cary 6000 (see Figure 12a) uses two lamps, a deuterium lamp and a tungsten halogen lamp, as light sources throughout its operations range (175-1800 nm). The light from either lamp is passed through a double Littrow monochromator and then through a

slit and into a chopping system. The chopper allows one third of the light to pass through the sample position, one third to pass through the reference position, and one third is blocked entirely. Both beams are directed through to the detector; for the UV and Visible regions this is a R928PMT Photomultiplier Tube, while for the NIR this is an InGaAs detector. Any standard cuvette (12.5 mm x 12.5 mm) is able to be used in this spectrometer.

3.2.1.2 Varian Cary 50

The Cary 50 (see Figure 12b) uses a Xenon flash lamp to illuminate the sample. This broadband light is passed through the sample and into a double monochromator system. The selected wavelength of light is then passed onto the detector. The system operates in single beam mode, and does not perform a real time correction of the lamp intensity. Fundamentally, the system is not nearly as sensitive or robust as the Cary 6000, but it is good for rapid scans and preliminary work. Any standard cuvette (12.5 mm x 12.5 mm) is able to be used in this spectrometer.

3.2.1.3 Ocean Optics USB2000 +

The Ocean Optics USB2000+ fiber optic spectrometer (see Figure 12c) was paired with a Deuterium-Tungsten Halogen broadband light source that was connected to a fiber optic dip probe (T300-RT-UV/Vis with an RT tip, Figure 12d). The collection fiber from the dip probe was then connected to the spectrometer. Inside of the spectrometer, the light reflects off a fixed diffraction grating and onto an ILX-511B Sony silicon CCD. This setup allows for fast collection times on the order of milliseconds. With appreciably long integration times, spectra collected with this device were acceptable for online

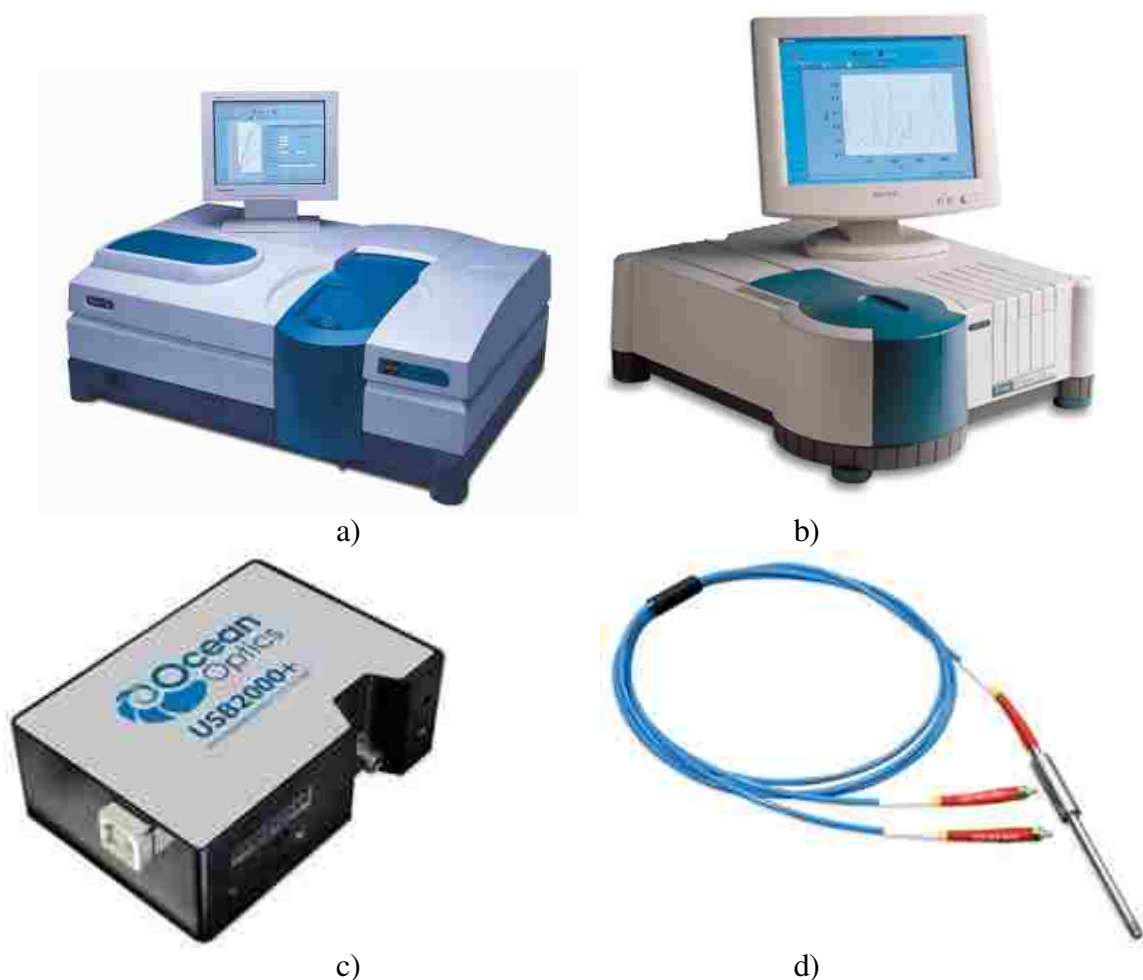


Figure 12 – a) Varian Cary 6000 [114]; b) Varian Cary 50 [115]; c) Ocean Optics USB2000+ [116]; d) Ocean Optics T300 Dip probe [117]

monitoring applications. The dip probe can utilize several different tips which vary the total pathlength.

3.2.2 Sample Preparation

General sample preparation for UV-Vis analysis is straightforward. The sample must appear in an appreciable concentration to be monitored, as determined by Beer's Law (Section 2.1.4), and must be compatible with the cuvette material. The exterior of the cuvette was cleaned with a Kimwipe prior to analysis to remove dust or absorbing

compounds. If using a cuvette is not feasible, several alternatives are available including, but not limited to: fiber optic dip probes, diffuse reflectance spheres, film holders, and capillary waveguides.

With the exception of the spectrophotometric titrations, all samples were analyzed in Polymethyl Methacrylate (PMMA) cuvettes. These cuvettes have very little absorbance in the wavelength ranges dominated by the uranyl or plutonium species. They are also inexpensive and disposable, reducing the chances of cross contamination.

3.2.3 Sample Measurement

Each UV-Vis system used has several adjustable parameters that can be used to tailor data collection. They include the wavelength range surveyed, the speed at which the monochromator scans, the data interval, and the integrations time. For the Ocean Optics solid state detector the monochromator, and thusly the wavelength range, is fixed. The most common settings in these experiments were to fix the data interval at 1 nm with an integration time of 0.1 seconds and a scan rate of 600 nm/min. Due to the high concentrations of reagent expected, these default settings where considered appropriate. For more dilute samples the integration time was increased to 0.5 seconds to improve the signal to noise ratio.

3.2.4 Background, Blank, and Zeroing Procedure

In order to accurately measure each sample, several factors need to be taken into account: the absorbance of the matrix; the absorbance of the cuvette; any clipping of the beam spot by specialty cuvettes; and drift in the detector. For every experiment, a background spectrum and a blank spectrum were recorded and the system was zeroed

prior to each sample measurement. Though several different methodologies were used throughout these experiments, the general procedure (for the Cary 6000) is outlined here.

At the beginning of each run, a background spectrum was collected with a blank solution in the sample position and the reference position, if applicable. This corrected each spectrum for the absorbance of the cuvette and the blank solution. In some cases if the matrix varied, i.e., different nitric acid concentrations, the samples were either paired so that a matrix blank was in the reference position or the background sample was left in the reference position and any changes due to the matrix were incorporated into the sample spectrum. This was acceptable during experiments that were designed to mimic an industrial process where a change in the matrix may be expected to occur.

In experiments where a specialty cuvette, such as a reduced volume or flow through cuvette, was used, it was required that an identical cuvette be placed in the reference position to correct for any beam clipping that may occur. However, some experiments were run without a reference. Since background samples were collected, it is reasonable to expect that the absorbance of the cuvette and the blank solution were corrected. Furthermore, blank samples were measured after correcting for the background absorption. Ideally, the blank sample would have no measureable absorbance and was used to ensure the system was performing within operational norms. For example, the Cary 6000 was considered to operating normally if the blank spectrum was within 0.001 absorbance units of the background spectrum over the entire measured range.

In order to correct for any drift in the detector, the system was zeroed before every sample collection. This generally requires that there exist a region where the species of interest does not absorb. Using the uranyl ion as an example, this region occurs above

~550 nm. Therefore, any scan that starts above that wavelength can be zeroed with confidence. However, for a more complex spectrum, such as that of tetravalent plutonium, there is no region in the visible or near IR that has zero absorbance. In a situation like this, the spectrometer must either only be zeroed on the blank solution and any variation in the detector zero point will be included in the variation of the samples, or the system must be given an artificial zero point and absorbance values would be relative to this point. The former method is useful for stable systems where detector drift is not an issue, while the latter should be used only when necessary.

3.2.5 Internal Calibration

The Cary 6000 has several calibration checks that it performs automatically at startup. The monochromator assembly's UV-Visible wavelength accuracy is determined from the deuterium emission lines at 656.1, 486.0 and 0.00 nm (zero order). The Near Infrared accuracy is then checked by the deuterium lines at 2624.4, 1312.2 and 0.00 nm. The system then calibrates the gain amplifiers on the photomultiplier tube. Then the system closes the shutter and checks for errors in the 0% transmission signal.

3.2.6 Comments on UV-Vis Absorbance Measurements

The results of early studies showed that the absorbance of the uranyl system was heavily dependent on the chemical environment, though the upper limit of linearity was firmly in the tens of millimolar range. At this point it was determined that the UV-Vis would not be suitable for concentration measurements without a firm understanding of the speciation. This is due to the fact that increases in either the uranyl ion or ligand concentration can produce similar spectroscopic effects.

3.3 Time Resolved Laser Induced Fluorescence Spectroscopy (TRLFS)

In the same way that certain molecules absorb visible light, other molecules fluoresce under the appropriate conditions. The ability to monitor and analyze this fluorescence gives the experimenter a large quantity of data on the electronic and vibrational structure of the molecule as well as sensitive technique for concentration measurements. TRLFS methods were derived from information in the literature and from practical experience [28,29].

3.3.1 Theory of Operation

The basic setup and theory underpinning fluorescence spectroscopy are described in the literature [122]. The premise is that certain molecules, when in an excited state, will emit photons in a characteristic pattern corresponding to the molecule's electronic structure. In order to excite the molecule, a laser is focused on the sample; the excitation wavelength used must impart enough energy into the molecule to excite it. This can be accomplished by matching the excitation wavelength to one of the fluorophore's absorbance peaks or by using a shorter wavelength in the UV region. Using the former method will yield a more specific fluorescence pattern while the latter method may excite many fluorophores if they are present in the system. The basic mechanics of energy absorption and fluorescence is shown in Figure 13 .

The fluorescence signal after the laser excitation is passed through a diffraction grating and collected on a detector. The time delay between the laser excitation and the data collection can be altered depending on the type of data being collected; a description of the timing settings can be found in Section 3.3.4.

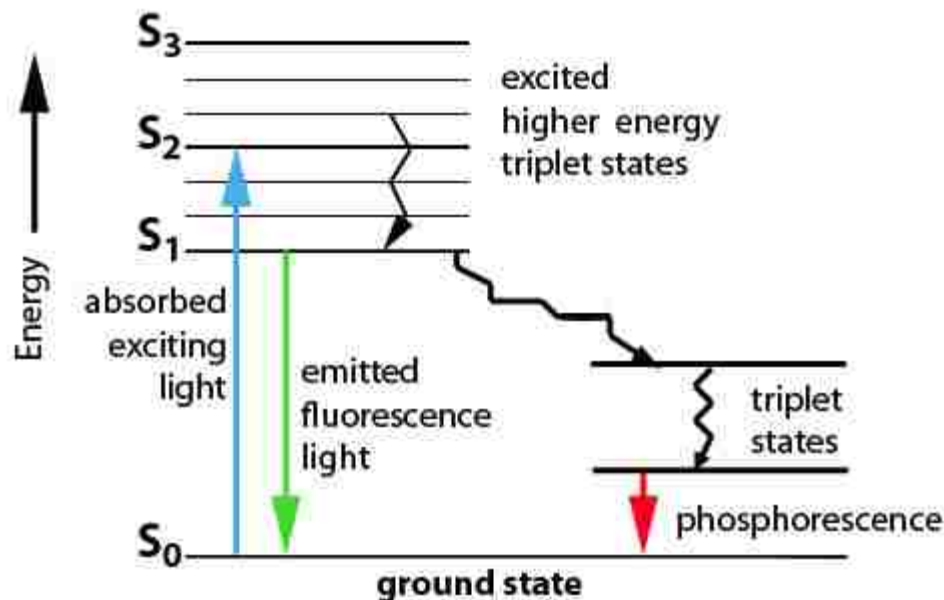


Figure 13 – Basic properties of energy transfer for fluorescent compounds. [123]

3.3.2 System Specifications

The TRLFS system was used to determine the fluorescent lifetime and fluorescent yield. The VIBRANT laser system (OPOteck, Inc., Carlsbad, CA, Figure 14a) uses the third harmonic of a Nd:YAG laser to pump an Optical Parametric Oscillator. The OPO then produces an excitation beam with wavelengths between 300 and 2400 nm. The excitation beam is then focused through a periscope assembly from Thor Labs to adjust the beam height. The beam passes through a 92/8 pellicle beam splitter; the lesser split is collected on a PE25 pyroelectric power meter (Ophir Inc.). Sample fluorescence is focused onto a PI-MAX II CCD detector (Roper Scientific/Princeton Instruments, Trenton, NJ) by means of a SP500 spectrograph (Roper Scientific, Figure 14b) with an entrance slit width of 250 μm . The detector and diffraction grating are calibrated against standard Hg vapor emission lines (MS-416 Hg Lamp, Roper Scientific) using the

calibration module of the WinSpec spectroscopy package. The laser system outputs ~25 mJ/pulse at 410 nm and ranges down to less than 1 mJ/pulse in the NIR. In order to work in the UV, a frequency doubling module must be inserted which also decreases the beam energy into the low mJ/pulse range.

Measurement of fluorescent signals after the excitation pulse as well as measurement of species lifetimes was controlled by the PI-MAX Timing Generator. This unit is responsible for controlling the initial delay on the electronic shutter, the gate width of the measurement, and for incrementally changing the gate delay, width, or both throughout a determination. Every measurement is triggered by a signal sent from the laser control hardware (Q-Switch Synchro) to the timing generator indicating that the laser has fired. The initial delay time was determined by monitoring the scattering of a laser pulse on a water blank in the detector. An “Initial Delay” of 200 ns was determined, which is relative to the delay value of the Q-Switch Synchro which can be set for ± 500 ns depending on experimental demands.

3.3.3 Sample Preparation

The sample preparation for TRLFS is similar to that for UV-Vis analysis (Section 3.2.2). The fluorescent intensity of a single species is generally linear with respect to concentration [122]. In addition to chemical compatibility, ligands should be chosen so that they do not quench the fluorescent signal (see Section 3.3.5). Additionally, some ligands will enhance fluorescence and alter the lifetimes of the complexed species, sometimes quite drastically [15,29].

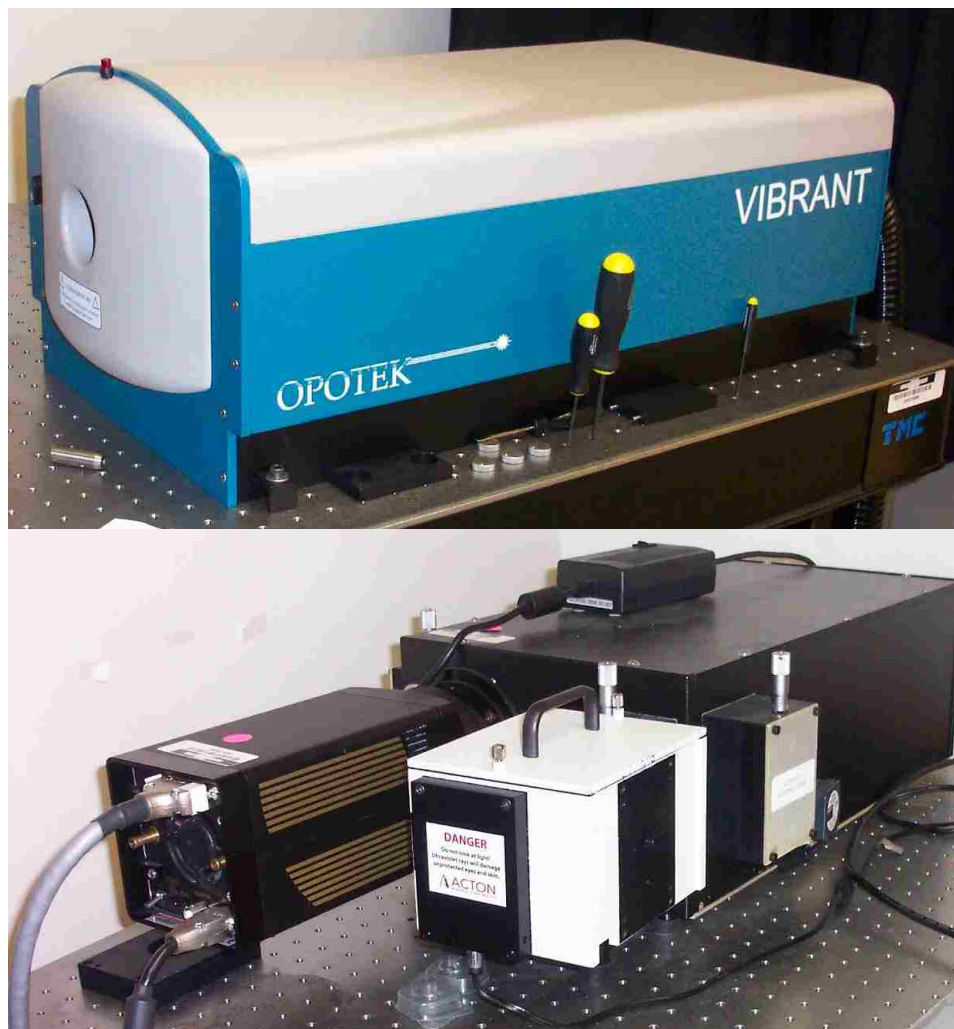


Figure 14 - Top) VIBRANT laser with OPO module; Bottom) Acton SP500 spectrometer and PI-MAX II CCD camera.

3.3.4 Sample Measurement and Analysis

Samples were passed through 0.45 μm filters to remove any particulates that may scatter the fluorescent light. Most samples were placed in 4.5 mL PMMA fluorescence cuvettes, capped, and sealed with Parafilm for the analysis. Due to the high acid nature of many samples, the samples were analyzed soon after they were made to reduce cuvette degradation. For initial samples which were involved in method development, synthetic quartz cuvettes were used (Hellma).

3.3.4.1 Concentration (Integrated Total Fluorescence) Measurements

The uranyl fluorescence was monitored between 375 and 725 nm using a 150 g/mm diffraction grating. The delay time on the CCD timing generator was set to 200 μ sec; this allowed sufficient time to account for the lag in the electronics and time for the laser to transit the physical distance. The gate width was set to 1 ms, which for most uranyl complexes was expected to be more than 10 lifetimes. At least 10 replicate measurements were recorded for each sample, with multiple laser shots accumulating on the detector for each measurement. The intensity of each shot was measured with the power meter and then summed over all accumulations in the measurement. This was then used to correct laser intensity by dividing the total integrated fluorescence (in counts) by the power (in mJ).

3.3.4.2 Lifetime Measurements

For lifetime measurements, multiple laser shots were accumulated for each sample, usually a higher number than in concentration measurements. The initial gate delay was set to 200 μ sec and the final gate delay was variable depending on the expected lifetime. The gate width was again set to 1 ms for the same reasons as above. For each sample, the integrated total fluorescence was collected and adjusted for the number of accumulations and laser intensity. The data was then fitted with an exponentially decaying function of the types in Equation 22 and Equation 23 with the graphing/fitting program Kaleidagraph (Synergy Software). The total fluorescence is described by the sum of the individual fluorescence from each species in solution plus a background intensity (I_{BG}) term to cover the detector dark current.

Equation 22

$$I = I_0 e^{-kt} + I_{BG}$$

Equation 23

$$I = I_{0,1} e^{-k_1 t} + I_{0,2} e^{-k_2 t} + I_{BG}$$

3.3.5 Comments on TRLFS

There are several factors to be taken into account when analyzing samples by TRLFS. Due to the sensitivity of the technique, very small amounts of fluorophore need to be present in the solution. This may require large dilutions and matrix adjustments to bring the sample into the appropriate concentration range. Also, the samples are subject to the phenomenon known as quenching, the process by which an excited molecule that would normally emit a photon de-excites non-radiatively. There are two types of quenching, static and dynamic [125]. Static quenching occurs when a ligand binds to a fluorophore and the complex provides an alternate route to de-excite. Dynamic quenching happens when the excited fluorophore or complex interacts with a quencher in solution. The Stern-Volmer relationship is used to define the quenching behavior via Equation 24.

Equation 24

$$I_0/I = 1 + K_{SV}[Q]$$

where I is the intensity of the fluorescence in the presence of the quencher, I_0 is the intensity of the fluorescence in the absence of quencher, $[Q]$ is the concentration of the quencher in mol/L, and K_{SV} is the Stern-Volmer constant.

If the system is quenched, either statically or dynamically, Equation 24 will produce a linear relationship. For purely dynamic (collisional) quenching, the measured lifetime of the species can be used in place of the intensity (Equation 25), where τ_0 is the lifetime of

the fluorophore in the absence of quencher, and τ is the lifetime in the presence of the quencher.

Equation 25

$$\frac{\tau_o}{\tau} = 1 + K_{sv}[Q]$$

For statically quenched systems, the Stern-Volmer constant in Equation 24, K_{sv} , is replaced by K_A , an association constant. In these systems the lifetime ratio will remain constant; the uncomplexed fluorophore will relax normally and the complexes do not fluoresce by definition. Lastly, both modes can occur simultaneously. The intensity ratio will exhibit a curved relationship, while the lifetime ratio will be linear [126]. The various fluorescence relationships are compiled in Table 4.

Table 4 - Stern-Volmer relationships governing quenched systems

	Dynamic	Static	Mixed
τ_o/τ	$\frac{\tau_o}{\tau} = 1 + K_{sv}[Q]$	$\frac{\tau_o}{\tau} = 1$	$\frac{\tau_o}{\tau} = (1 + K_{sv}[Q])(1)$
I_o/I	$\frac{I_o}{I} = 1 + K_{sv}[Q]$	$\frac{I_o}{I} = 1 + K_A[Q]$	$\frac{I_o}{I} = (1 + K_{sv}[Q])(1 + K_A[Q])$

3.4 Inductively Coupled Plasma – Atomic Emission Spectroscopy

A common laboratory instrument for determining elemental concentrations in a dilute acid matrix is the Inductively Coupled Plasma – Atomic Emission Spectrometer (ICP-AES). This instrument can analyze samples for a large number of elements with a rapid, reproducible, and sensitive technique.

3.4.1 Theory of Operation

The operating principle behind ICP-AES can be found in many instrumental analysis text books [71]. Essentially, when an atom's electrons are forced into excited states, as they fall back to the ground state they will emit photons at characteristic wavelengths. In order to excite analyte atoms, the sample solution is aspirated into an inert gas stream via a nebulizer. The carrier stream is then fed into an argon plasma. The plasma is formed by flowing argon gas through an RF coil operating in 10-50 kW range which ionizes the argon gas and reaches temperatures of 6,000-10,000 K. This extreme temperature ensures nearly total ionization of the analyte atoms.

After ionization and the subsequent relaxation, the light from the various emissions is passed through a set of optics that allows the system to monitor a specific emission line or lines corresponding to the analytes of interest. Due to this detector setup, multiple wavelengths can be monitored simultaneously allowing for rapid multi-elemental analysis. A Thermo Scientific iCAP 6500 ICP Spectrometer was used in these



Figure 15 – iCAP ICP-AES Spectrometer [71]

experiments. The instrument was set to view the uranium spectrum in axial mode monitoring the 367.007 nm emission line.

3.4.2 Sample Preparation

The sample requirements for ICP-AES analysis are three fold. First, the concentration of the analyte must be within the appropriate range, generally 1-100 ppm; for a uranyl solution this is ~400 $\mu\text{mol/L}$ at the upper limit. Second, the matrix must be adjusted to a dilute mineral acid solution; this keeps the analytes from adsorbing to the tubing or nebulizer walls and prevents hydroxide formation which may clog the system. Finally, the solution should be free of interfering species. An interfering species for AES is defined as another element that emits a photon with energy similar to that of the analyte of interest. The Thermo iTeva software automatically advises the user of potential interferences. Uranium has many available wavelengths to monitor and selecting one that is free from potential interferences can usually be accomplished (see Table 5).

3.4.3 Sample Measurement and Analysis

The system must be calibrated with a certified standard for every analyte of interest. This is done by creating a set of calibration standards over the expected range of sample concentrations and a matrix blank. The response of the instrument, in counts, is directly proportional to the analyte concentration within the limits of linearity. The system software then generates a calibration equation and the Limit of Detection (LOD) for the calibration. Each standard and sample is measured in triplicate and the average and relative standard deviation is computed. The average counts can then be used with the calibration equation to determine the analyte concentration above the LOD.

Table 5 – Uranium Line Emissions and possible interferences ($\geq 40\%$ of U relative intensity, ± 0.1 nm) – from iTeva software.

Uranium Line (nm)	Relative Intensity	State	Interferences	State	Relative Intensity
367.007	50000	II	Sc – 366.949	II	37500
			Ho – 366.952	I	70313
			Th – 366.977	I	23333
			Fe – 367.002	I	24000
			Fe – 367.009	I	30000
			Mn – 367.050	II	25926
			Sm – 367.066	II	100000
			Yb – 367.084	II	28125
385.958	30000	II	Sm – 385.874	I	19048
			Mg – 385.886	I	185185
			Fe – 385.921	I	30000
			Sc – 385.936	I	93750
			Sc – 385.938	II	93750
			Sc – 385.96	II	225000
			Sc – 385.99	II	75000
			Fe – 385.99	I	60000
263.553	25000	II	Ba – 236.478	II	10000
			Dy – 263.48	II	45000
			Al – 263.502	II	104405
			Ta – 263.558	II	350000
			Re – 263.583	II	10000
409.014	25000	II	La – 408.961	I	70000
			Yb – 408.968	I	247500
			Mn – 408.993	I	24074
			Gd – 409.041	I	44828
			Zr – 409.051	II	30000
			V – 409.058	I	10000

3.5 X-Ray Absorption Fine Structure Spectroscopy

A direct method to interrogate the local environment around an atom is X-ray Absorption Fine Structure (XAFS) spectroscopy. An explanation of how XAFS experiments and data analysis is performed can be found in the literature [94]. While the specificity of the method is directly dependent on the ability to match experimental results to a structural model, advances in modeling techniques have made XAFS very useful for solution studies. The advanced facilities required for XAFS, however, limit the availability of the technique. XAFS can be further divided into the X-ray Absorption

Near Edge Structure (XANES) region, which can determine oxidation states and coordination numbers, and the Extended X-ray Absorption Fine Structure (EXAFS) regions, which determines interatomic distances.

3.5.1 Theory of Operation

A beam of monoenergetic photons is passed through a solid or liquid sample. The photon energy is chosen so that there is a selective excitation of one element in the sample. This is accomplished by scanning the photon energy across one of the atom's ionization thresholds, thereby promoting a core electron to an excited state. Both the transmission of the photon beam as well as any fluorescence observed from de-excitation is collected by a series of detectors. A more comprehensive review of XAFS spectroscopy, specifically for actinide elements, can be found in the literature [94].

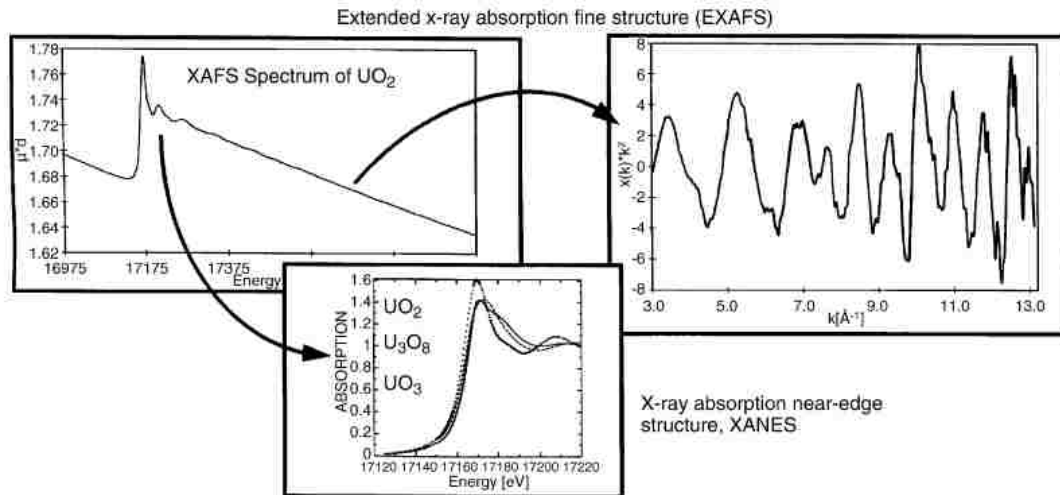


Figure 16 – Breakdown of the XAS spectrum into the EXAFS and XANES regions. The XANES region is background corrected and normalized; the EXAFS region is weighted by a factor of k^3 to produce the plot shown in the upper right. From [94]

3.5.2 System Specifications

XAFS measurements were carried out at Argonne National Laboratory's Advanced Photon Source (APS). The BESSRC-CAT 12 BM station in the XOR group was used for all experiments. Spectra were collected at and above the U-L_{III} edge at 17.166 keV and monitored the signal in fluorescence mode, at room temperature, using a bank of germanium detectors. A double crystal Si [1,1,1] monochromator was used for energy selection while the beam energy was calibrated by using an in-line zirconium foil (Zr-K edge = 17.998 keV).

3.5.3 Sample Preparation

The concentration of the sample must fall within a narrow window for liquid samples, approximately 1-10 mmol/L. Samples in this range should appear in high enough concentrations to be seen without either absorbing too much, which will obscure transmission data, or too little, which will require multiple lengthy scans. The liquid samples are placed in a specially designed sample holder composed of a Teflon block with a well cut into one side, surrounded by a gasket, and covered with a thin sheet of poly-trifluorochloroethylene (TCFE). The plastic components are situated between two aluminum plates; each filling port has a similar setup with a gasket, TCFE film, and aluminum cover.

3.5.4 Sample Measurement and Analysis

The samples are aligned in the photon beam so that the transmittance and fluorescence signals are maximized. Multiple scans are collected for each sample to improve the average spectrum; data is collected up to 14 \AA^{-1} in k space. The AutoBk program [127] was used to remove the background contribution of the scans. From there,

the program WinXAS [128] is used to analyze the data. The fitting procedure, amplitude and phase shift function were all calculated by the program Feff8.2 [129]. Input files were generated by the Atoms program [130] using available crystallographic structures or DFT models. Adjustments of the k^2 -weighted EXAFS spectra were performed under the constraints $S_0^2 = 0.9$, where S_0^2 is the amplitude reduction factor. A single value of energy shift (ΔE_0) was used for all scattering.

3.6 Radiometric Techniques

3.6.1 Scintillation counting

Liquid Scintillation Counting (LSC) is a standard method for determining the concentration of radionuclides in a solution [131]. Mixing a scintillator and the radionuclide of interest together directly and using a high efficiency detector geometry results in a very sensitive system ideally suited to detecting alpha and beta radiation.

3.6.1.1 Theory of Operation

The theory of LSC counting summarized here can be found in [131]. A scintillator, dissolved in an organic cocktail, is brought into intimate contact with a radionuclide. The radiation is absorbed by the scintillator with a high efficiency and a photon is emitted as the scintillator de-excites. This photon is usually emitted at a wavelength that is not optimal for detection with a photomultiplier tube so a wavelength shifter is added (in the cocktail) which increases detection efficiency. The intensity of light produced and the rate at which it decays during an event is proportional to the energy and type of the original interaction. This allows for alpha/beta discrimination via Pulse Decay Analysis.

A Perkin Elmer Tri-Carb 3110TR Liquid Scintillation Analyzer was used for all activity measurements [132].

3.6.1.2 Sample Preparation

The analyte must appear at a concentration suitable for scintillation counting; due to the high efficiency of this detector, this is on the order of tens to thousands of Becquerel. For high activity samples, large dilutions must be used and gravimetric dilutions are generally recommended [133]. In addition, the chemical nature of the matrix must be considered as high acid concentrations can degrade the scintillation cocktail and shift the energy spectra [131]. Chemical effects can be corrected for by using standards prepared in the same matrix or by diluting the acid concentration prior to analysis. The sample to cocktail ratio should be fixed for each experiment or group of experiments, with 5-10 mL of cocktail being used for sub mL amounts of sample. After adding the sample and cocktail to the vial, they should be mixed thoroughly to ensure the scintillator and radionuclides interact completely.

3.6.1.3 Sample Measurement and Analysis

Samples are loaded into the counter along with any standards and blanks. Samples are generally counted until the measurement error is at or below 2%, calculated as the inverse square root of the counts. This statistical cutoff technique works well with low activity samples. Samples with substantially higher activities will reach the 2% error in a matter of seconds. Such short count times produce erratic data and therefore the samples must be counted for longer times to improve the reliability of the measurement.



Figure 17 - Tri-Carb 3110TR LSC [134]

Regions of interest are defined in the detector software to discriminate the signal of interest from the extended background and low energy contributions. The specified region can then be integrated for total counts and the concentration of radionuclide can be determined.

3.6.2 Alpha Spectrometry

3.6.2.1 System Specifications

A Canberra Alpha Analyst, model 7200-04, with 12 sample chambers was used for alpha spectrometry measurements. Samples containing alpha emitting radionuclides are prepared and mounted onto a planchette. The sample was then loaded into one of the chambers and evacuated with an Edwards 2 stage vacuum pump. Passivated Implanted Planar Silicon detectors with an active volume of 450 mm^2 are used to collect the alpha decays with a resolution of 10.2 keV. GENIE 2000 software is used to run the analysis software and the system's Multichannel Analyzer.

3.6.2.2 Sample Preparation and Analysis

Samples for alpha spectrometry must be prepared so that a thin layer of material is present; thicker samples will increase the amount of self attenuation of the alpha particles which decreases the system resolution. Electrodeposition and microprecipitation are two methods used to produce alpha spectrometry samples. In this work, microprecipitation with a cerium fluoride carrier was the method of choice, following a method provided by S. Faye [136].

Samples were counted until the error in the measurement was 2% or less. Certified electroplated standards were counted to determine the detector efficiency. The peak position and total area in each peak was recorded and activity of the sample was calculated.

CHAPTER 4

EXPERIMENTAL

Many experimental techniques were used in the course of this work. This chapter will give the goal, design, and raw data for each experiment; the modeling and analysis of this data will be covered in Chapters 5 and 6, respectively. Section 4.1 will detail batch UV-Vis experiments; Section 4.2 focuses on Time Resolved Laser Induced Fluorescence of the uranyl ion; Sections 4.3 and 4.4 cover potentiometric and spectrophotometric titrations, respectively; finally, Section 4.5 will cover EXAFS spectroscopy of both uranium and plutonium samples.

4.1 UV-Visible Spectroscopy Batch Experiments

To investigate the spectroscopic behavior of uranyl and plutonium species under reprocessing conditions, it was necessary to first evaluate how they behaved in pure nitric acid. To do this, batch experiments were designed to systematically vary the nitrate and acid concentrations while maintaining constant metal ion concentrations. The goal of these experiments was two-fold: first, to develop a working model of how the spectra vary as the chemistry changes; and second, to form a basis set for future speciation experiments.

4.1.1 Uranium

4.1.1.1 Uranyl Stock Solution

To evaluate the effect of nitrate on the absorption spectrum of the uranyl ion, it was necessary to produce stock solutions of uranyl free of nitrate. Uranyl nitrate hexahydrate

was dissolved in dilute acid and precipitated from solution with concentrated sodium hydroxide. The resultant solid was washed with water, centrifuged, and decanted several times to remove excess sodium and nitrate ions. The solid was then dissolved in an excess of perchloric acid to completely solubilize the hydroxide and increase the total acid level. The sample was analyzed by ICP-AES for uranyl concentration. Stock solutions were generally made with known amounts of acid and the final acid concentration was calculated from the final uranyl concentration. If this was not done, then an aliquot was precipitated with base and the residual base was titrated with acid to determine the concentration of acid in the original sample.

4.1.1.2 Multivariate Study

Based on the methodology of Bostick (Section 2.2.2.1), a set of experiments were defined to systematically vary the nitrate, and uranyl concentrations over large ranges. Bostick defined a planar relationship between the absorbance, $[\text{NO}_3^-]$, and $[\text{UO}_2^{2+}]$ that allowed for the simultaneous determination of nitrate and uranyl concentration in an analyte solution. While the effect of acid concentration was mentioned in the Bostick work, no systematic treatment was pursued. This experiment was designed to re-evaluate the effect of these parameters on the uranyl absorption spectrum and determine if the acid concentration affected the spectrum.

The experimental parameters for this system (Table 6) are based on the previous study by Bostick and on current UREX chemistry parameters [81]. A stock solution of uranyl perchlorate was used to control the metal ion; lithium nitrate and nitric acid were used to control the nitrate concentration; and perchloric acid was used to control the

Table 6 - Composition of sample series used in the Multivariate Analysis project

Series	[UO ₂ ²⁺] (mM)	[NO ₃ ⁻] (M)	[H ⁺] (M)	No. of Samples
1	95	0.00	0.1 – 4.0	11
2	95	2.00 – 1.97	0.1 – 4.0	13
3	95	4.00 – 3.93	0.1 – 3.9	13
4	95	6.00 – 5.93	0.1 – 3.9	13
5	95	8.00 – 7.92	0.1 – 3.9	11
6	48	0.00	0.1 – 4.0	11
7	48	2.00 – 1.96	0.1 – 4.0	13
8	48	4.00 – 3.92	0.1 – 3.9	13
9	48	6.00 – 5.93	0.1 – 3.9	13
10	48	8.00 – 7.92	1.0 – 3.9	7
11	10	0.00	0.1 – 4.0	11
12	10	2.00 – 1.97	0.1 – 4.0	11
13	10	4.00 – 3.92	0.1 – 3.9	13
14	10	6.00 – 5.93	0.1 – 3.9	13
15	10	8.00 – 7.92	1.0 – 3.9	7

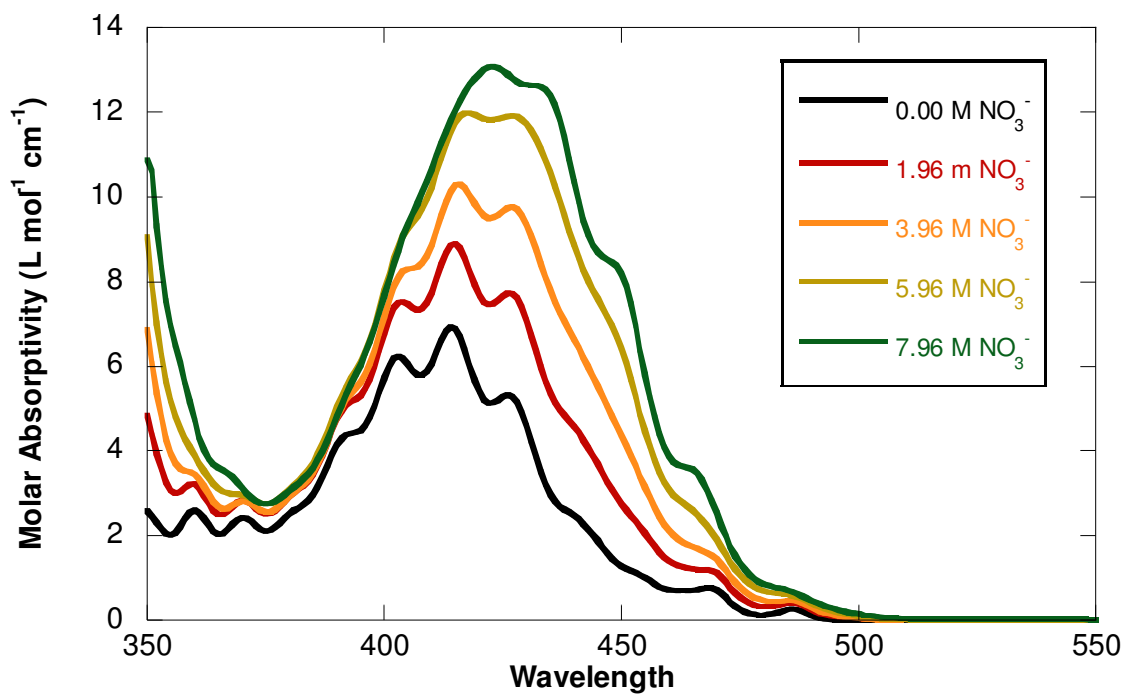


Figure 18 - Traces of 95 mM uranyl, 2 M acid samples from Segments 1-5 of the Multivariate Study

acidity of the solutions. Samples were made directly inside cuvettes by sequential addition of reagents, capped, sealed with parafilm and mixed vigorously. Several samples at higher acid or nitrate concentrations had white crystalline precipitates after the solutions settled. These samples were either omitted from the study or remade and analyzed promptly. The salt was theorized to be lithium perchlorate which has a solubility in water of 4.39 mol/L at 25° C [137].

The samples were analyzed according to the standard UV-Vis procedure (Section 3.2) on the Cary 6000i spectrometer. The samples were not temperature or atmosphere controlled. Representative spectra from this experiment can be found in Figure 18.

4.1.1.3 Linear Response Ranges under Simulated Process Chemistries

The spectroscopy of the uranyl ion was observed to shift dramatically with nitrate concentration. Therefore, the proposed use of UV-Vis spectroscopy to interrogate process streams would require a separate calibration for each process chemistry condition studied. The study looked at five different stream conditions: the UREX feed, raffinate, uranium product, technetium product, and the PUREX feed (Table 7). The goal of this experiment was to determine the linear range and molar absorptivities of the uranyl spectrum by UV-Vis spectroscopy under these varied chemistries.

A nitrate free stock solution of uranyl perchlorate was used as in previous experiments. Nitrate concentrations were controlled by addition of either nitric acid or lithium nitrate, while the acid concentration of the system was controlled by addition of perchloric acid. Uranium concentrations were varied over three orders of magnitude to

Table 7 - Chemical characteristics of simulated reprocessing streams

Stream	[UO ₂ ²⁺] (mM)	[NO ₃ ⁻] (M)	[H ⁺] (M)
UREX Feed	20.4 – 0.95	4.0	1.5
UREX Raffinate	30.9 – 0.95	2.0	2.0
Technetium Product	20.4 – 0.95	6.0	5.5
Uranium Product	20.4 – 0.95	2.0	0.5
PUREX Feed	10.5 – 0.95	6.0	4.0

determine the molar absorptivity constants under the given conditions. All solutions were prepared at room temperature and without purging.

Samples were prepared directly in PMMA cuvettes as in Section 4.1.1.2. The absorbance of the uranyl ion at various concentrations was measured and the molar absorptivity was determined by plotting absorbance against the concentration and measuring the slope of the linear regression. The peak absorbance versus concentration and representative spectra of each condition are given in Figure 19 and Figure 20 respectively.

4.1.1.4 Multiple Wavelength Monitor Study

After observing the uranyl spectrum under several different nitrate concentrations, an observation was made that the molar absorptivity of the uranyl ion and the shape of the spectrum was dependent on the nitrate concentration; as the nitrate concentration increased, the maximum absorbance increased with no change in metal ion concentration. Therefore, if only a single wavelength was being monitored, any concentration measurement made without exact knowledge of the nitrate concentration would not be valid, and would bias a measurement toward higher uranyl concentrations.

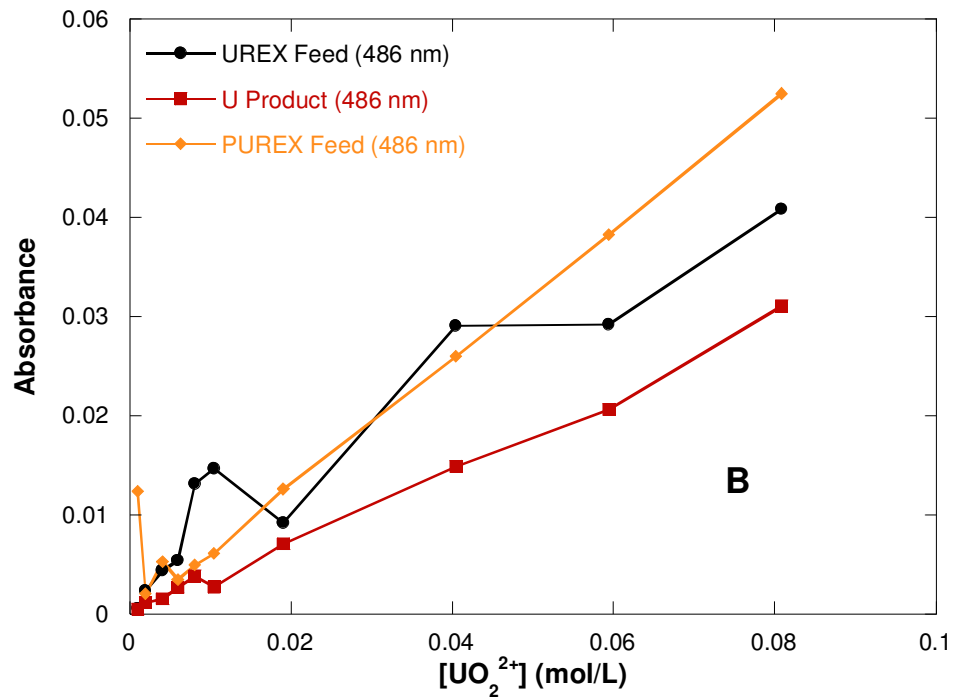
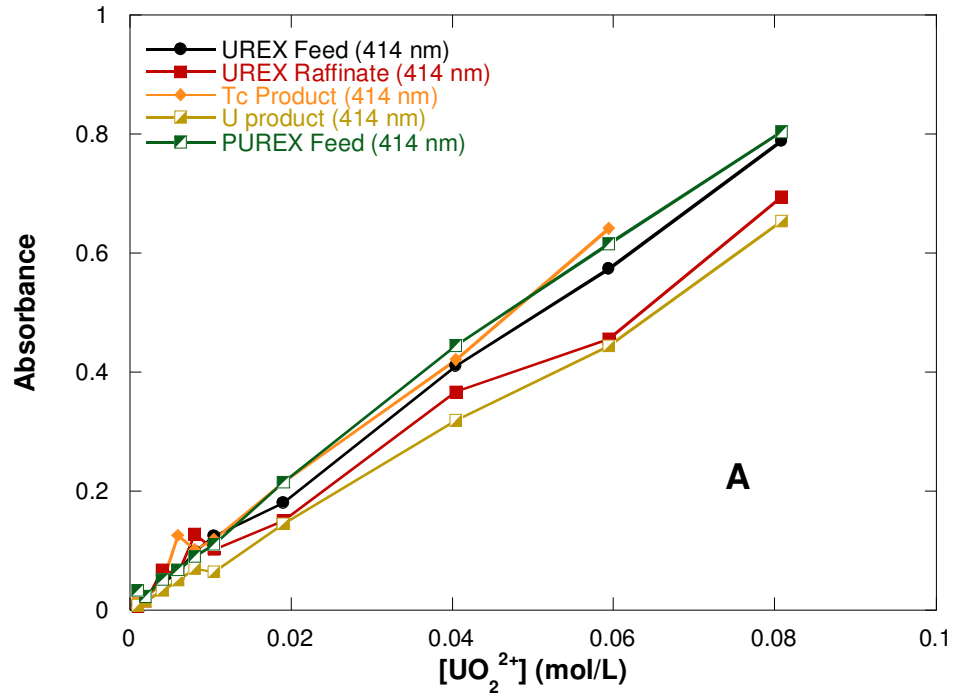


Figure 19 - Linear Responses of the uranyl ion under simulated reprocessing streams (Table 7). A) Response at 414 nm; B) Response at 486 nm for high uranium conditions.

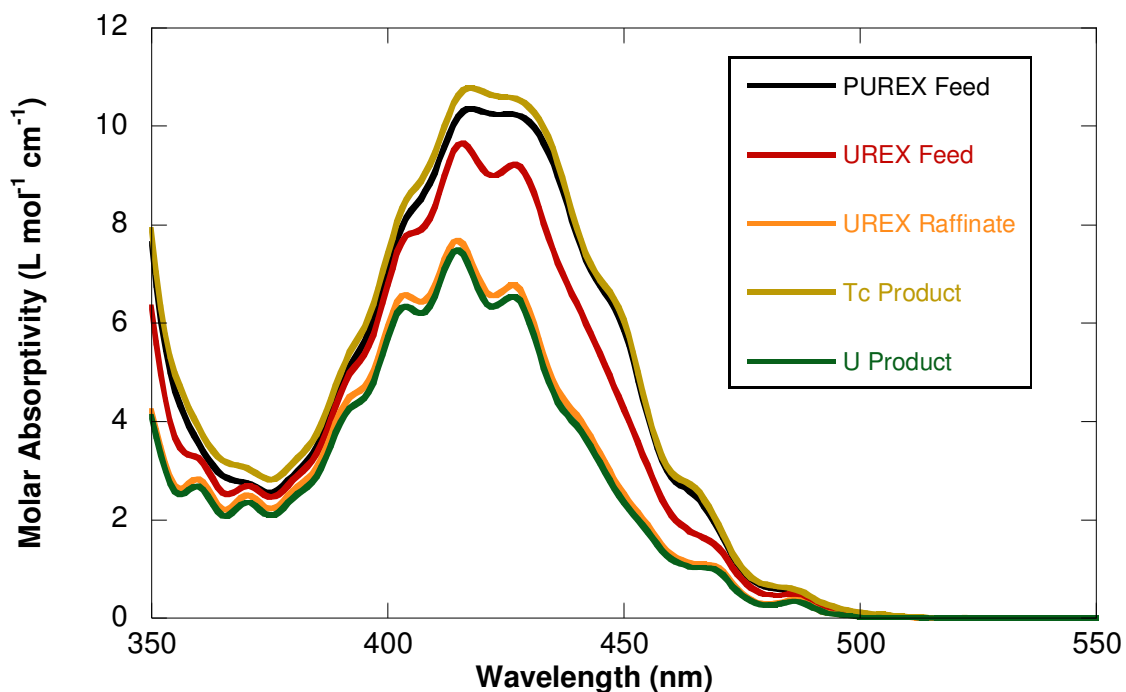


Figure 20 - Representative spectra from each simulated reprocessing stream

From this it was theorized that a quantitative measure could be developed to distinguish the system's nitrate concentration, and reduce any bias in the associated uranyl measurement, directly from the uranyl spectrum. This was accomplished by creating a set of samples with fixed uranyl concentrations and widely varying the nitrate concentration. Once the spectra were collected, they would be broken down into separate electronic transitions [23] and trends would be sought. The goal was to determine a ratio of absorbance peaks that would vary directly with the nitrate concentration and would allow for an accurate measure of the uranyl concentration.

Experience with the multivariate study (Section 4.1.1.2) showed that the ionic strength and choice of nitrate cation impacted the results. In order to determine the

magnitude of this effect on the uranyl spectrum, a stock solution of 4 mol/L nitric acid would be sequentially diluted with water, 4 mol/L sodium perchlorate, or 4 mol/L perchloric acid with an aliquot removed after each addition. The individual nitrate solutions would then be mixed with a fixed volume of the uranyl stock solution. This preparation method was designed to minimize the need for sequential, and exact, additions of reagents. Preparing all three ionic matrices in this fashion resulted in each corresponding sample having the same nitrate concentration. The composition of these samples can be found in Table 8.

A solution of uranyl perchlorate in 2.2 molar perchloric acid was used to adjust the metal ion concentration. Due to the small amount of this solution placed in each sample (1/15th of the total volume), the discrepancy between the ionic strength levels was minimized. Aliquots of the nitrate solution were pipetted into cuvettes followed by the uranyl solution. The cuvettes were capped, covered with parafilm, and mixed vigorously. All samples were analyzed on the Cary 6000i promptly; four scans of each sample were taken to improve the average absorption signal. Samples were collected at room temperature and without nitrogen purging. A sample set of spectra from these series can be found in Figure 21.

After collection, the spectrum at each nitrate concentration was deconstructed using the PeakFit software suite (SyStat Software). The peak height, area, and position were then compared to one another via a regression scheme which evaluated all possible combinations of the 12 transitions against the total nitrate concentration. A suitable

combination was defined as a ratio which was linear with respect to nitrate and one that showed a large change in value throughout the course of the experiment.

Table 8 - Composition of samples for the first multiple wavelength monitor study (Peak Ratios Study 1)

Series	Label	[UO ₂ ²⁺] (mM)	[NO ₃ ⁻] (M)	[H ⁺] (M)	Ionic Strength (M)	# Samples
H ₂ O Dilution	PRS1 A	40.1	3.73 – 0.005	3.88 – 0.15	3.89 – 0.15	25
NaClO ₄ Dilution	PRS1 B	40.1	3.73 – 0.005	3.88 – 0.15	3.88	25
HClO ₄ Dilution	PRS1 C	40.1	3.73 – 0.005	3.88	3.88	25

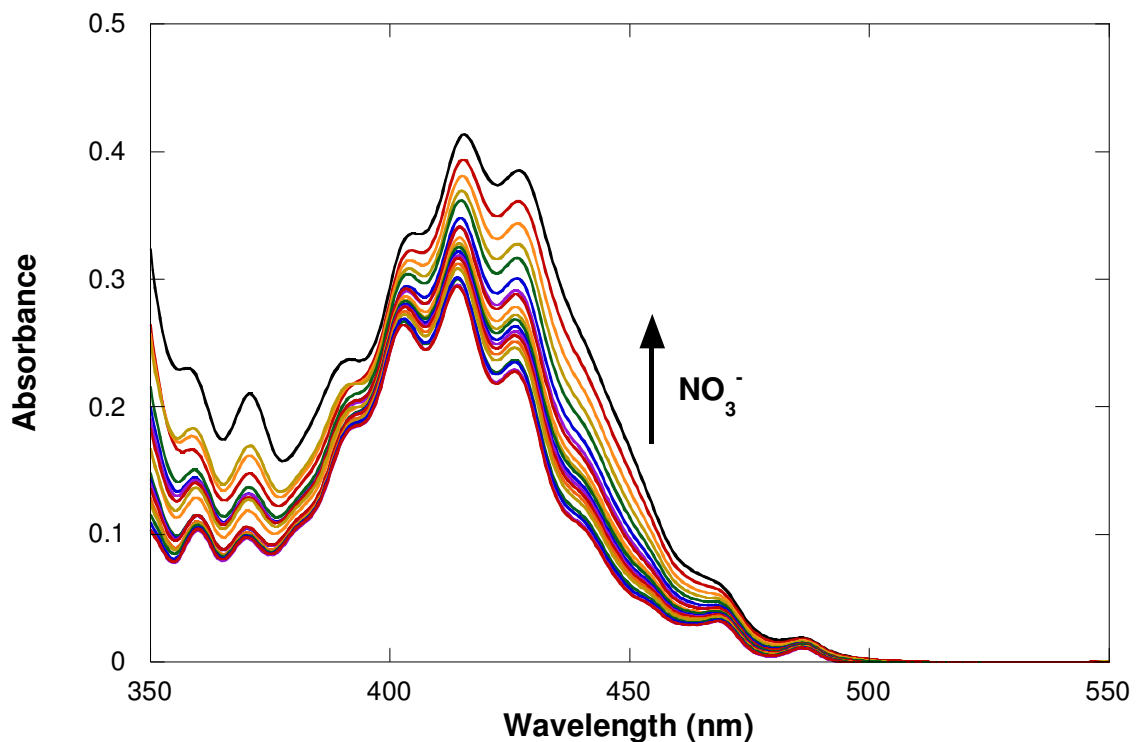


Figure 21 – Representative spectra from the first multiple wavelength monitor (sample PRS1 A, Table 8). Nitric acid, 4 mol/L, diluted with water, [UO₂²⁺] = 40.1 mM. Total nitrate ranges from 0.15 mol/L (bottom) to 3.73 mol/L (top)

A follow up set of experiments to determine the effect of acid to salt ratio on the spectra was created. A similar setup was used to create the samples in which stock solutions were serially diluted. In these experiments, three starting solutions at 6 M nitrate were produced, with one being 100% nitric acid, the second a 1:2 mixture of sodium nitrate and nitric acid, and the third a 2:1 mixture. Each individual dilution was aliquoted into three different samples to order to investigate different uranyl ion concentrations. The composition of these samples can be found in Table 9. Spectra from these studies can be found in Figure 22.

Table 9 - Composition of samples for the second multiple wavelength monitor study (Peak Ratio Study 2)

Series	Label	[UO ₂ ²⁺] mM	[NO ₃ ⁻] (M)	[H ⁺] (M)	Ionic Strength (M)
6 M HNO ₃	PRS2 A1	52.7	5.45 – 0.58	5.84 – 0.97	6.00 – 1.12
	PRS2 A2	26.4	5.45 – 0.58	5.84 – 0.97	5.92 – 1.04
	PRS2 A3	5.3	5.45 – 0.58	5.84 – 0.97	5.85 – 0.98
4 M HNO ₃ / 2 M NaNO ₃	PRS2 B1	38.7	5.60 – 0.60	4.01 – 0.68	6.00 – 0.99
	PRS2 B2	19.3	5.60 – 0.60	4.01 – 0.68	5.94 – 0.94
	PRS2 B3	3.9	5.60 – 0.60	4.01 – 0.68	5.89 – 0.89
2 M HNO ₃ / 4 M NaNO ₃	PRS2 C1	38.7	5.60 – 0.60	2.15 – 0.48	6.00 – 0.99
	PRS2 C2	19.3	5.60 – 0.60	2.15 – 0.48	5.94 – 0.94
	PRS2 C3	3.9	5.60 – 0.60	2.15 – 0.48	5.89 – 0.89

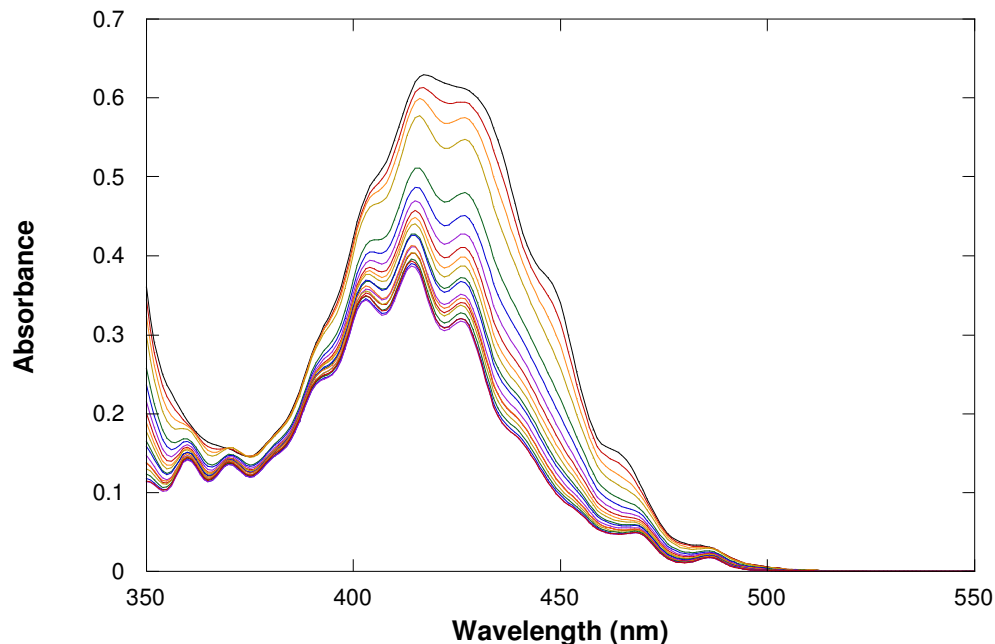


Figure 22 – Representative spectra from the second multiple wavelength monitor (Sample PRS2 A1, Table 9). Nitric acid, 6 mol/L, diluted with water, $[\text{UO}_2^{2+}] = 52.7$ mM.

4.1.1.5 Uranyl–Acetohydroxamic Acid (AHA)

The spectroscopic behavior of the uranyl-nitrate-acetohydroxamic acid system was investigated to determine the impact of the compound on the uranyl spectrum. Three series were created with increasing amounts of AHA at different pH values; in all samples, the total uranyl was kept constant at 95 mmol/L (Table 10). A representative set of spectra are shown in Figure 23.

Table 10 - Composition of uranyl-AHA series. Each series was composed of 10 samples. Acid concentration was controlled with addition of nitric acid

Series	[UO ₂ ²⁺] (mM)	[AHA] (mM)	pH
AHA 0	95	0-87	0
AHA 1	95	0-87	1
AHA 2	95	0-87	2

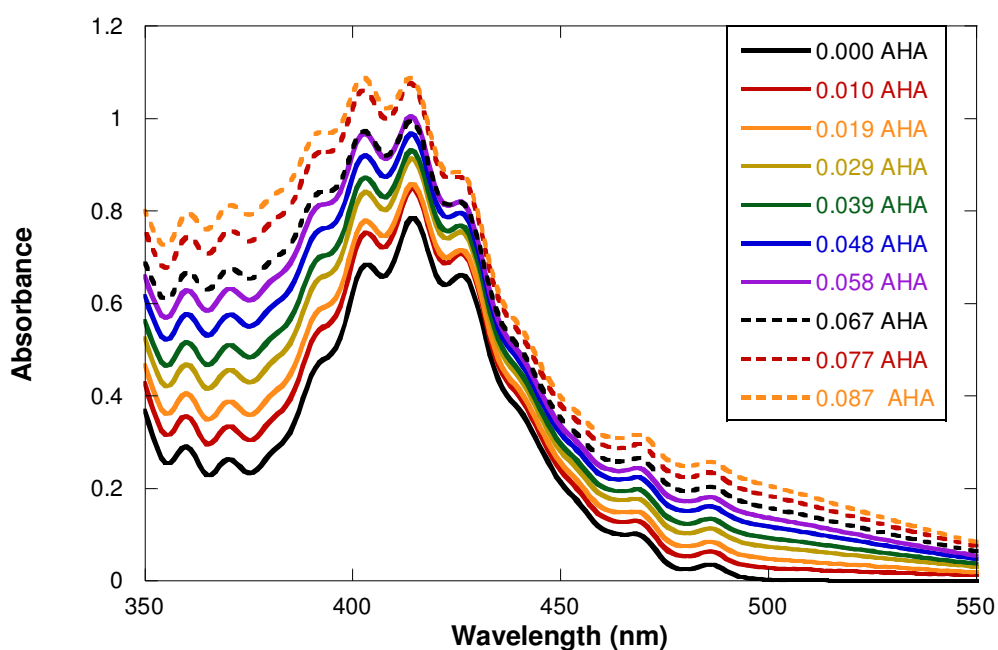


Figure 23 – Uranyl - AHA absorption spectrum at pH 1 and [UO₂²⁺] = 95 mmol/L (Series AHA 1, Table 10).

4.1.2 Plutonium

A sample of plutonium, >98% ²³⁹Pu [138], was used in these experiments. The plutonium was originally presented as less than 1 mL of a purple solution (Pu(III) [139]) with a white precipitate. The solution was diluted with nitric acid forming brown Pu(IV)

in solution, which was filtered through glass wool to remove the particulate. The solution was precipitated with sodium hydroxide, centrifuged, washed, and decanted. The remaining precipitate was dissolved in nitric acid and diluted. A sample of the stock was diluted to a nitrate concentration of approximately 1 M and analyzed immediately by UV-Vis (Figure 24). The concentration of the solution was then estimated using the molar absorptivities in [44].

The first stock solution was intentionally kept at a low acid concentration and this solution eventually disproportionated into a mixture of plutonium III, IV, and VI (Figure 25). The peak at ~830 nm was easily identified as Pu(VI) which has a molar absorptivity ~150 L mol⁻¹cm⁻¹ at 1 mol/L HNO₃ [44]. Equation 20 indicated that Pu(III) would also be produced, though its spectra would be obscured by Pu(IV). After treatment with concentrated nitric acid to oxidize any Pu(III), the solution was analyzed by UV-Vis to determine the approximate amount of Pu(VI) and treated with slightly more than a stoichiometric amount of hydrogen peroxide [99]. This procedure reduced the Pu(VI) completely and the solution remained in the tetravalent state after precipitation and dissolution in nitric acid. The solution was kept in 4M HNO₃ to reduce the rate of disproportionation.

The total nitrate concentration was determined by adding 2.592 mL of concentrated nitric acid (15.44 mol/L) into a vial containing the plutonium precipitate and the total volume was adjusted to 10 mL. The relative change in acid concentration due to the neutralization of the plutonium hydroxide was negligible compared to the overall nitric

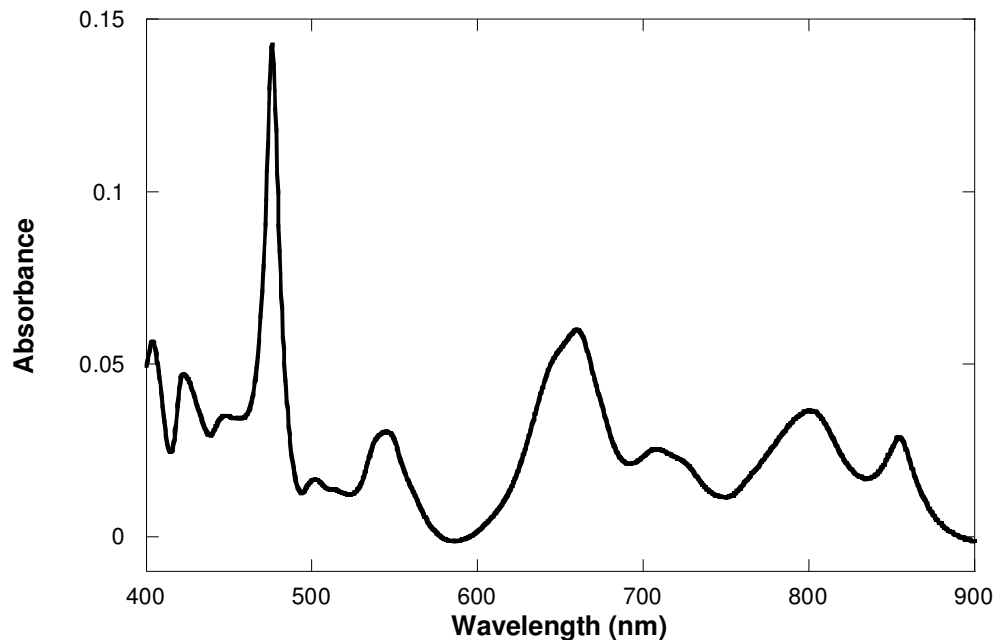


Figure 24 - Initial UV-Visible spectra of Pu(IV) in 1 M HNO₃

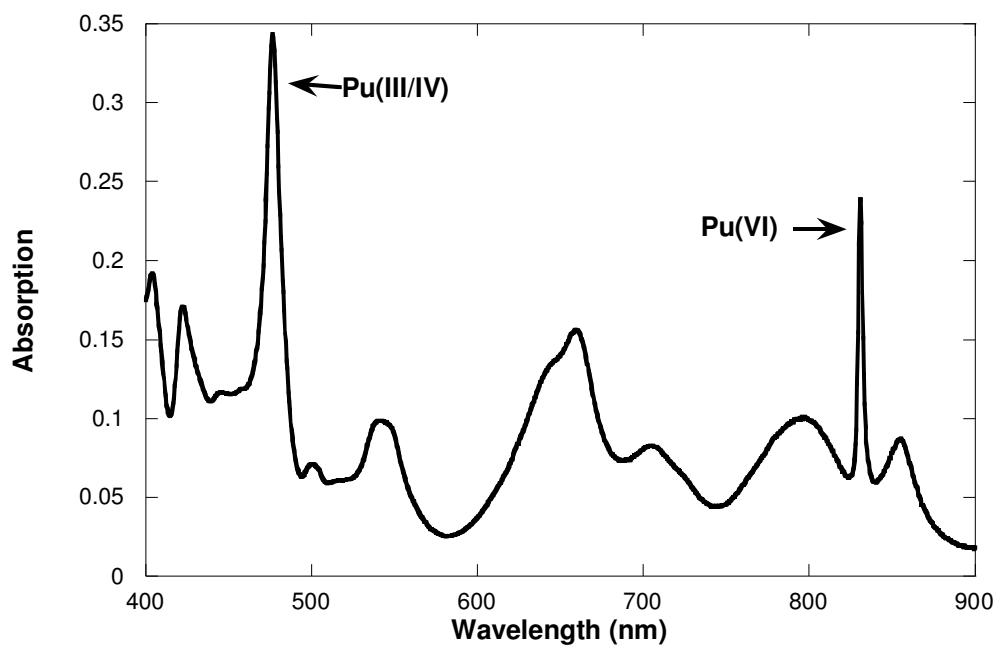


Figure 25 - Disproportionation of Pu(IV) into Pu(III) and Pu(VI) at low acid concentration. The small amount of Pu(III) is obscured by the larger contribution of the Pu(IV) at ~475nm. The high molar absorptivity (~150 [44]) of the Pu(VI) accounts for the large signal at 830 nm.

acid concentration; the Pu(IV) concentration was ≤ 10 mM, so neutralization would only consume 0.4 mmol of acid from a total of 40 mmol of acid, or ~1%. An aliquot of this solution was then prepared and analyzed by UV-Vis spectroscopy to determine the approximate plutonium concentration to facilitate dilutions for alpha spectroscopy and liquid scintillation counting.

The stock solution was then analyzed by Liquid Scintillation Counting against a NIST Standard Reference Material (SRM 4330B). Ten milliliters of UltimaGold Scintillation Cocktail was mixed with 0.1 mL of the plutonium stock solution. The solution was also analyzed by alpha spectroscopy following a cerium fluoride microprecipitation [140]. The alpha spectrum was compared to electroplated ^{241}Am and ^{239}Pu sources and the activity of the solution was calculated.

4.1.2.1 Variation of UV-Visible Spectroscopy with Nitrate Concentration

Nine samples were made for this experiment with final nitrate concentrations between 2 and 10 mol/L. An aliquot of the plutonium stock solution was then added to each vial. Once mixed, the sample was transferred to into a reduced volume PMMA cuvette and analyzed immediately on the Cary 50 UV-Visible spectrometer (Figure 26). The system had been previously blanked on a water solution and was not zeroed between samples. The system had very little detector drift in the short time frame of the experiment.

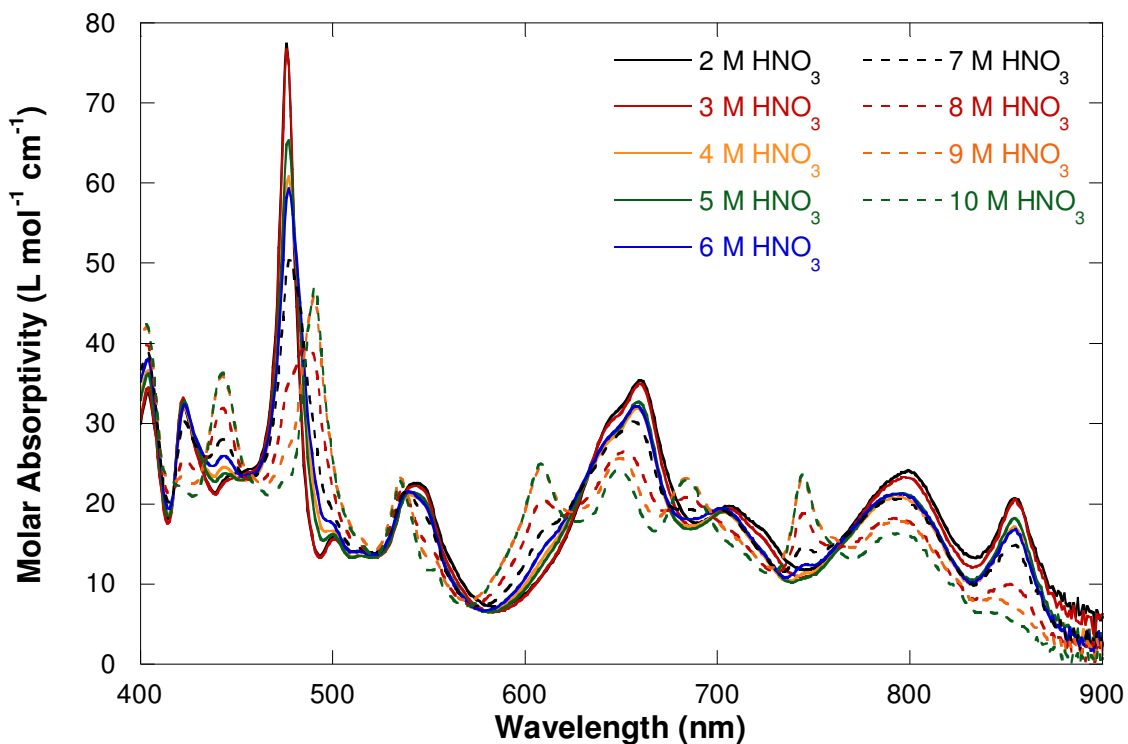


Figure 26 - Variation of plutonium absorption spectrum with varying nitric acid concentrations. [Pu(IV)] = 1.5-1.6 mmol/L.

4.2 TRLFS Batch Experiments

Due to the fact that the uranyl ion is a fluorophore, it was decided that TRLFS may be able to be used as a technique to detect low-level uranium concentrations in reprocessing streams [46]. In most aqueous recycling processes there are a few streams where low level uranium signals could be interrogated to determine process efficiency; specifically the UREX Raffinate (and areas downstream), the acid recycle, and the Technetium Product. Therefore the fundamental fluorescence behavior in nitric acid needed to be determined.

In the first experiment, 16 samples were prepared from a uranyl perchlorate stock solution in perchloric acid with a total ionic strength of 6 M and a constant 4.75 mM uranyl. The nitrate concentration was adjusted from 0 to 3 molar by adding nitric acid while the ionic strength was balanced by the addition of perchloric acid. The samples were designed to determine the effect of nitrate on the uranyl fluorescence spectrum and to determine the lifetimes of any species (Figure 27).

To use TRLFS as a technique to evaluate uranium concentration it was necessary to determine the linearity of the uranyl fluorescence signal. To do this, three sample series

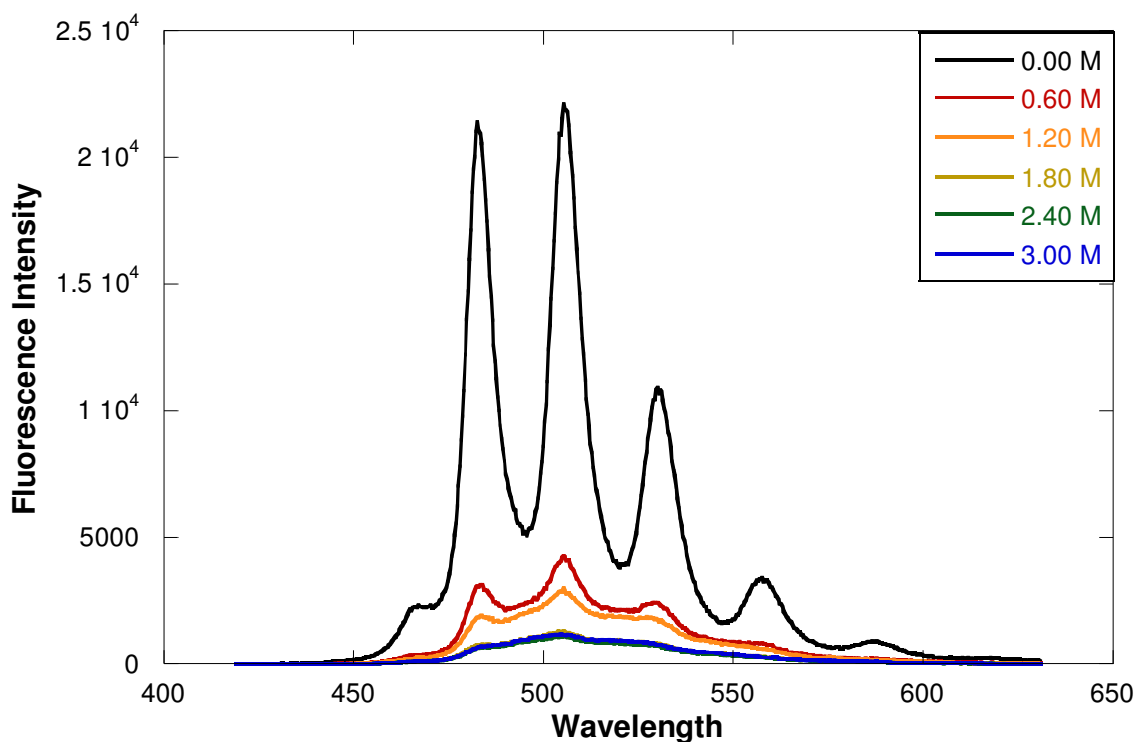


Figure 27 - Selected uranyl fluorescence patterns in the presence of increasing nitrate concentrations

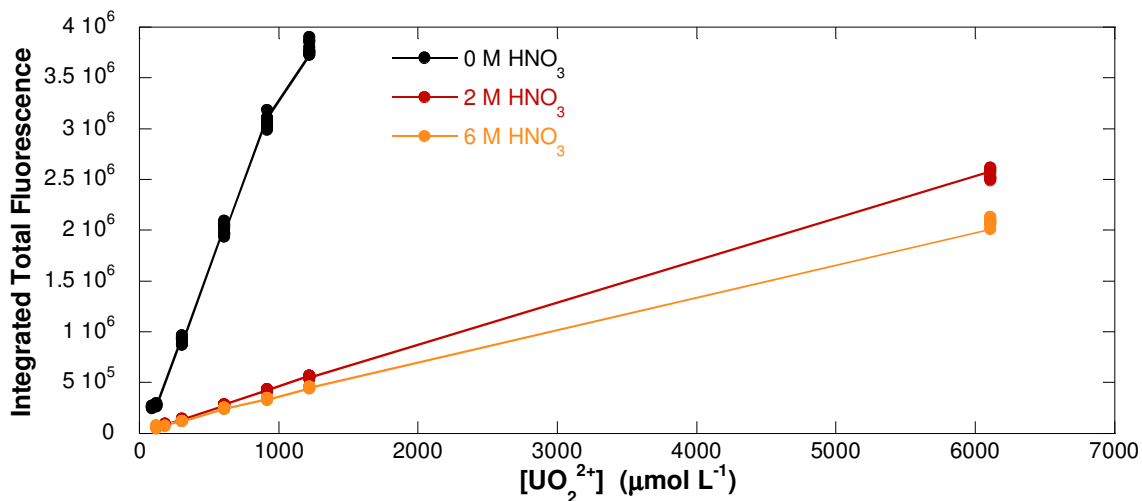


Figure 28 - Linear plots of total fluorescence vs. uranyl concentration at various nitrate concentrations. Control fluorescence behavior – 0 mol/L HNO₃; UREX Raffinate – 2 mol/L HNO₃; Technetium Product – 6 mol/L HNO₃.

were made with constant nitrate levels and varying uranyl concentrations with a total ionic strength held at 6 M. The nitrate concentrations were held at 0, 2, and 6 molar corresponding to a control, the UREX Raffinate and the Technetium Product streams, respectively. The uranyl ion was varied from 24 μM to 12 mM. The linear plots of the total fluorescence vs. uranyl concentration are shown in Figure 28.

4.3 Potentiometric Titrations

One technique considered for evaluating the uranyl nitrate stability constant was based on the methodology of Ahrland [19]. In essence, the complexity of a known uranyl-anion system is put into competition with the nitrate ion. Ahrland used the uranyl acetate species as the known ligand system. Since the work was done in the 1950's, it

was decided that the methodology could be updated with modern techniques and should produce similar results. The full general potentiometric methodology can be found in Section 3.1.1.

4.3.1 Uranyl Acetate

In order to determine the stability of any competing ligand, the complexation of the main ligand with respect to the uranyl ion must be determined. In this work acetate was selected based on the literature [19]. Samples were formed by dissolving uranium trioxide in a known excess of perchloric acid and balancing the ionic strength with sodium perchlorate. Each sample was made in a 100 mL class A volumetric flask. A saturated sodium perchlorate solution was passed through a filter to remove particulate impurities in the salt prior to use. Aliquots of the resulting solution were then pipetted into pre-weighed flasks and dried to a constant mass at high temperature. This allowed for the calculation of the molality, molarity, and density of the sodium perchlorate solution.

Sample preparation for titration is covered in Section 3.1.3. Each solution was analyzed by pipetting 25 mL of each sample into the titration cup with humidified argon purging and titrating with a standardized acetic acid buffer solution. Each titration was performed in triplicate and all data was collected directly in millivolts. The electrode was calibrated each day at the working ionic strength. Data analysis was performed with the HyperQuad program. Sample composition for the uranyl acetate system is listed in Table 11; representative titration curves are shown in Figure 29.

Table 11 - Potentiometric titration sample compositions

Sample	[UO ₂ ²⁺] (M)	[H ⁺] (M)	[NO ₃ ⁻] (M)	Ionic Strength (M)
1A	0.0095	0.0310	0.0000	0.9909
1B	0.0236	0.0528	0.0000	0.9774
1C	0.0141	0.0218	0.0000	0.9868
1D	0.0095	0.0311	0.9401	0.9911
1E	0.0234	0.0532	0.8740	0.9764
1F	0.0140	0.0220	0.9341	0.9855
2A	0.0091	0.0265	0.0000	1.8472
2B	0.0102	0.0132	0.0000	1.7983
2C	0.0092	0.0278	0.9257	1.8533
2D	0.0145	0.0187	1.8479	1.9101

4.3.2 Uranyl Nitrate

Samples were made by dissolving uranyl trioxide in a known excess of perchloric acid and balancing the ionic strength with either sodium nitrate or sodium perchlorate. All samples were made in 100 mL class A volumetric flasks.

In the same fashion as with the uranyl acetate system (previous section), the samples were titrated with a standardized acetic acid buffer solution in triplicate. The HyperQuad program, using the constants determined for the uranyl acetate system, would then be used to determine the uranyl nitrate complexity. The sample composition for these samples is shown in Table 11, while titration curves are shown in Figure 29.

4.4 Spectrophotometric Titrations

Rather than relying on a secondary phenomenon to investigate the uranyl nitrate complexity, a direct method using UV-Vis spectroscopy was proposed similar to the

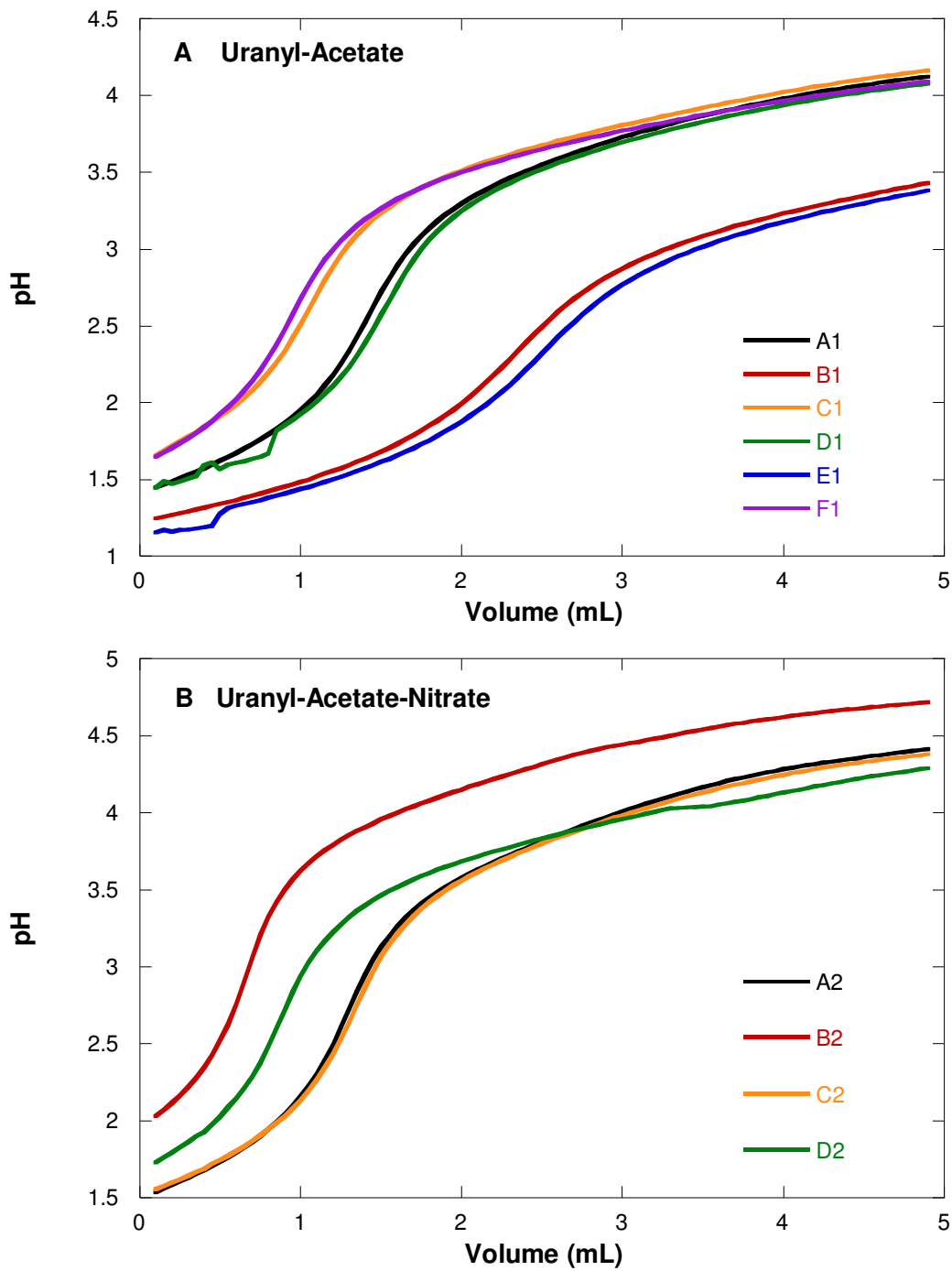


Figure 29 - Potentiometric titration curves, labels from Table 11. Sample composition can be found in Table 11. A) Samples containing uranyl and acetate only, 1 molal IS; B) Samples containing uranyl, acetate, and nitrate, 2 molal IS.

procedure used in [21]. In these experiments, an external recirculating loop (Figure 11) would be used instead of a commercial titration cell. The goal was to directly determine the uranyl nitrate stability constants at multiple ionic strengths using the HypSpec program.

Samples were made by dissolving uranium trioxide in perchloric acid, nitric acid, or an appropriate mixture of the two. The sample would then be loaded into recirculating titration system (Figure 11) and titrated with either nitric or perchloric acid. All solutions used were held at a constant molal ionic strength to facilitate analysis by SIT (Sections 2.5, 5.2). The compositions of all samples in this study are delineated in Table 12. Representative spectra for each of the titrations are shown in Figure 30.

Table 12 - Spectrophotometric titrations, initial sample composition. All concentrations are in molality (m). All titrants were prepared at the same molal concentration as the sample ionic strength, I_m . For each titration, 15-18 data points were collected

Sample	[UO₂²⁺]	[NO₃⁻]	[ClO₄⁻]	[H⁺]	Titrant	I_m	Density (g/mL)
001	0.054	0.00	0.95	0.84	HNO ₃	1.00	1.05
002	0.054	0.00	0.95	0.84	HNO ₃	1.00	1.06
003	0.046	0.55	0.40	0.86	HNO ₃	1.00	1.04
004	0.046	0.55	0.40	0.86	HNO ₃	1.00	1.04
005	0.050	0.95	0.00	0.85	HClO ₄	1.00	1.03
006	0.050	0.95	0.00	0.85	HClO ₄	1.00	1.03
008	0.049	0.00	1.95	1.85	HNO ₃	2.00	1.10
009	0.048	0.00	1.95	1.86	HNO ₃	2.00	1.10
011	0.050	0.97	0.97	1.85	HNO ₃	2.00	1.08
014	0.053	0.97	0.97	1.84	HNO ₃	2.00	1.09
012	0.053	1.95	0.00	1.84	HClO ₄	2.00	1.06
013	0.060	1.94	0.00	1.82	HClO ₄	2.00	1.07
015	0.047	0.00	2.96	2.86	HNO ₃	3.00	1.15
016	0.048	0.00	2.95	2.86	HNO ₃	3.00	1.15
017	0.049	0.00	3.95	3.85	HNO ₃	4.00	1.20
018	0.047	0.00	3.96	3.86	HNO ₃	4.00	1.20
019	0.049	0.00	5.95	5.85	HNO ₃	6.00	1.28
020	0.051	0.00	5.95	5.85	HNO ₃	6.00	1.28

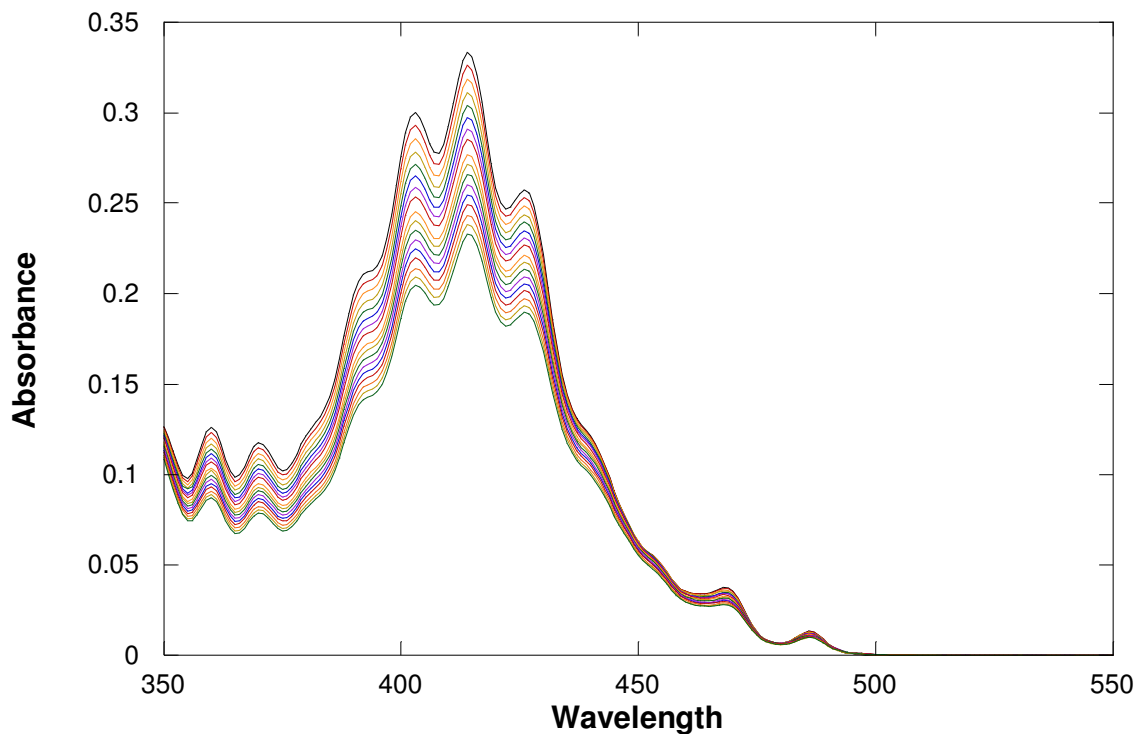


Figure 30 – Representative spectrophotometric titration (sample 008). Initial conditions: 0.049 molal uranyl, 1.95 molal perchlorate, 1.85 molal acid titrated with 2.0 molal nitric acid.

4.5 EXAFS Spectroscopy

Samples were prepared for EXAFS spectroscopy to investigate the local environment around the uranium and plutonium atoms. The goal of these experiments was to determine if the speciation of both systems could be inferred from the shifts in the k -space diagram. The Fourier Transform of this data was then used to facilitate Density Functional Theory modeling (Chapter 5).

Uranium containing samples were prepared for EXAFS spectroscopy by dissolving either uranyl nitrate hexahydrate or uranium trioxide in nitric acid. Samples were made to investigate the effect of total nitrate concentration on the uranium speciation.

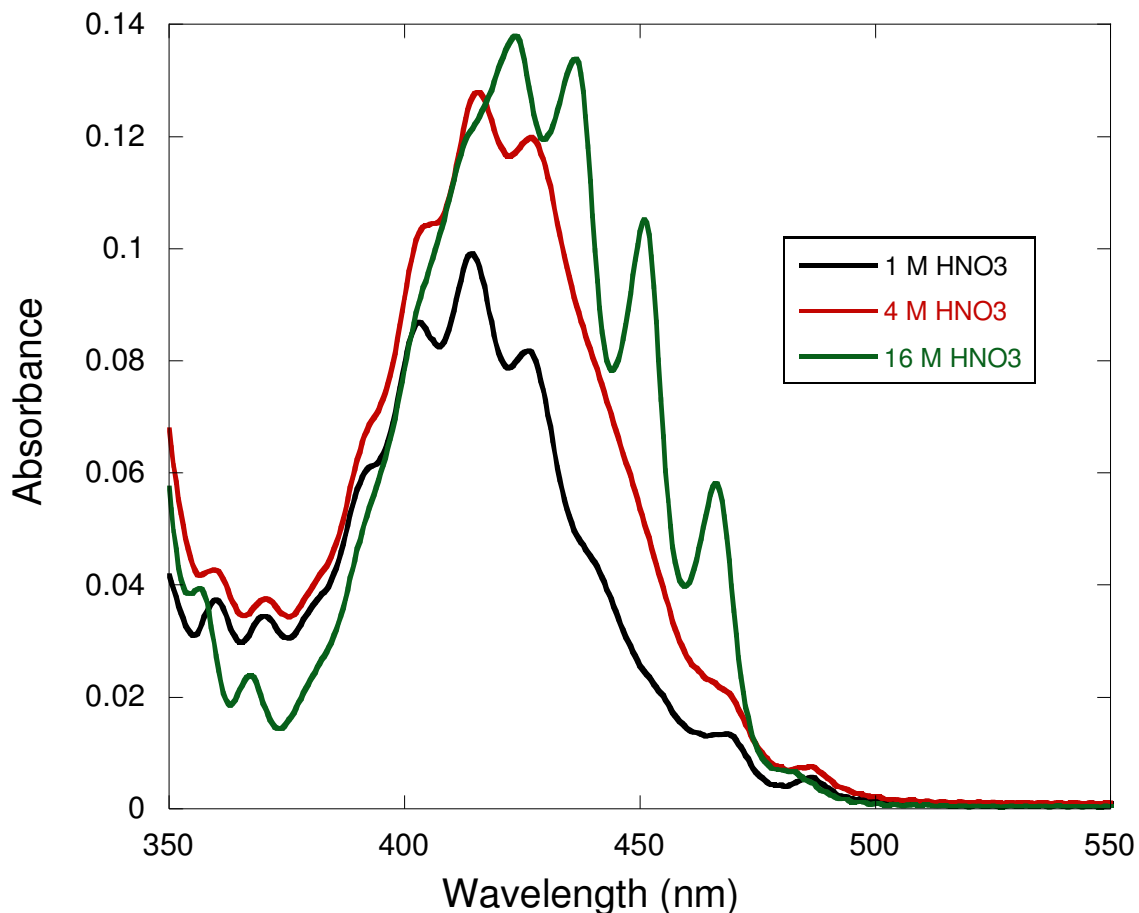


Figure 31 - UV-Visible spectra of selected samples. $[UO_2^{2+}] = 10 \text{ mM}$. The presence of sharp peaks at 423, 436, 451, and 466 are similar to peaks of known trinitrate species (Section 2.2.2.1)

Specifically, evidence for the uranyl trinitrate species was sought at higher nitric acid concentrations. There was a strong indication that the trinitrate was present at high total nitrate concentration due to the UV-Visible spectra of the samples Figure 31. The sharp peaks between 400 and 500 nm are similar to those assigned to the uranyl trinitrate in non-aqueous solvents (2.2.2.1). The plutonium nitrate samples made for UV-Visible spectroscopy were used directly to determine the general characteristics of the Pu(IV)

nitrate system. All samples were loaded, sealed, and shipped to the Advanced Photon Source at ANL for analysis.

Table 13 – Nitric acid and metal concentrations for EXAFS Samples

Metal	Metal Ion (M)	Nitric Acid (M)
UO ₂ ²⁺	10 mM	1, 2, 4, 8, 16
UO ₂ ²⁺	10 mM	4, 6, 8, 10, 12, 14, 16
Pu ⁴⁺	1.6 mM	2, 3, 4, 5, 6, 7, 8, 9

CHAPTER 5

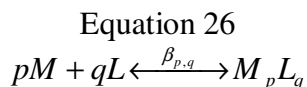
MODELING

The ability to match experimental data to fundamental models is crucial to a thorough understanding of the systems of interest. This chapter will explore the methods used to analyze and model titration data for thermodynamic parameters (Section 5.1), how this thermodynamic information is modeled with the Specific Ion Interaction Theory (Section 5.2), and how information from EXAFS is paired with structural data derived from Density Functional Theory (DFT) (Section 5.3).

5.1 Hyperquad & HypSpec

A suite of programs has been designed by Gans et al. to refine thermodynamic information from a variety of experimental systems [141]. Specifically, Hyperquad is used to analyze spectrophotometric and potentiometric titrations while HypSpec is used for spectrophotometric data only with the extra capability to analyze batch studies. Both Hyperquad and HypSpec use the same set of equations and procedures to match experimental data to thermodynamic parameters.

The refinement kernel is based on the SUPERQUAD program and uses either the Gauss Newton or the Newton-Raphson method to iteratively solve the mass balance equations present in the system [142]. For a system with multiple species, as defined in Equation 26, the mass balance equations are shown in Equation 27.



Equation 27

$$[M]_{total} = [M] + \sum_{p=1, q=1}^{P, Q} p\beta_{p,q} [M]^p [L]^q$$
$$[L]_{total} = [L] + \sum_{p=1, q=1}^{P, Q} q\beta_{p,q} [M]^p [L]^q$$

The kernel does not solve for the free ligand, L , or free metal, M , concentrations; it solves for the natural logarithm of the free concentrations of each component, $\ln[M]$ and $\ln[L]$, which constrains the concentrations to positive values; this is different from earlier programs which allowed negative concentrations to exist during refinement [141]. The kernel then uses the values of the stability constants, $\beta_{p,q}$, as adjustable parameters to improve the fit. The model fit is evaluated by calculating the residual, defined as the difference between the model and the experimental results, and then calculating the sum of the square of the residuals [142]. The residual is calculated slightly different for each program. For potentiometric titrations, the predicted pH of the system based on the refined free concentrations is compared to the experimentally determined value. Spectrophotometric systems produce (or use supplied) molar absorptivities and compare the sum of the absorbances of all species to the experimentally measured values. The evaluation proceeds iteratively until the sum of the square of the residuals fails to reduce any further.

5.1.1.1 Hyperquad Procedure

The first step in the refinement process is to specify the model and species that are to be used. Each species' composition and known or estimated stability constants are entered. Each species present has an option to be held constant, refined, or ignored. This allows known stability constants to be kept from refining.

Data sets from the Metrohm Tiamo software were stored in text files as titer-mV pairs. Each individual titration was then imported into the data editor of Hyperquad. The curve is given a label and the titrant volume and buret error is entered. The initial total concentrations of all species in the sample and the titrant are specified as well as which concentrations are held constant or refined. For each sample, the standard potential and the slope factor (Nernstian Slope/59.16 mV) from the GLEE Program (Section 3.1.2) was entered to convert the data from mV to pH. Finally, data points at pH values less than 2.5 or above 11.3 were omitted due to acid/alkaline errors [71]. The data was first fitted by hand to provide the program with best initial estimates of the stability constants prior to using the automatic refinement. This is done by manually adjusting any unknown stability constants to reduce the error in the model fit.

5.1.1.2 HypSpec Procedure

A table containing the total concentrations of each species and the absorbance values at every surveyed wavelength are compiled into a delimited text file. In HypSpec, the model file for the system is entered in the same fashion as Hyperquad. The program then allows prompts for which species are expected to absorb by denoting which “has spectrum”[sic]. Once the project has been created, pure component spectra, if available, are entered. Finally, the wavelengths to be used in the refinement are selected. Again, the data was first refined by hand with a manual adjustment of the unknown stability constants to provide the best initial estimates of the stability constants prior to using the automatic refinement.

5.1.2 Factor Analysis

Included in HypSpec is a stand alone computational module that performs Factor Analysis on any loaded spectra. The major utility of Factor Analysis is the ability to determine the number of significantly absorbing species in a set of spectrophotometric data without specifically defining either the species identity or unit spectrum. Theoretically, the module uses standard Principal Component Analysis (PCA) mathematical routines to separate the spectra into a finite number of discrete factors [143]. The program functions by determining the eigenvectors of the absorbance matrix (a $n \times m$ matrix with n = number of solutions and m = number of wavelengths) by means of a Singular Value Decomposition (SVD) [143]. For a given set of data there will be at most n non-zero eigenvectors in the SVD. Graphically, these eigenvectors are expressed as linear combinations of any unit spectra (molar absorptivities) present in the system with a corresponding set of eigenvalues. The number of non-zero eigenvalues will correspond to the number of absorbing species in the solution.

There are two caveats for determining the number of significantly absorbing species from the available eigenvalues. First, systematic errors in the absorbance system may add one or more non-zero eigenvalues to the system. Second, random errors will cause the some eigenvalues to deviate slightly from zero. Therefore, a visual inspection of the graphical eigenvectors can be done to separate those non-zero eigenvectors that correspond to species from extraneous values.

For example, in Figure 32 there are three eigenvectors in each subplot. In Figure 32A, there are two non-zero eigenvectors and one “zero” eigenvector. The third

eigenvector plot has a high degree of noise. This, coupled with the low eigenvalue suggests that the factor is not significant. In Figure 32B, there are definitely two non-zero eigenvectors and one that may or may not be a significant value. While the vector plot has a low eigenvalue, there is a marked reduction in noise in the system when compared to Figure 32A. This ambiguity requires an operator to exercise a degree of judgment as to what values can be considered significant.

5.1.3 Hyperquad Simulation Suite

The Hyperquad Simulation Suite (HySS) is a stand alone program for generating titration or speciation curves [144]. The program is setup to read Hyperquad model data files and produce results according to user supplied input. To generate a curve, the model

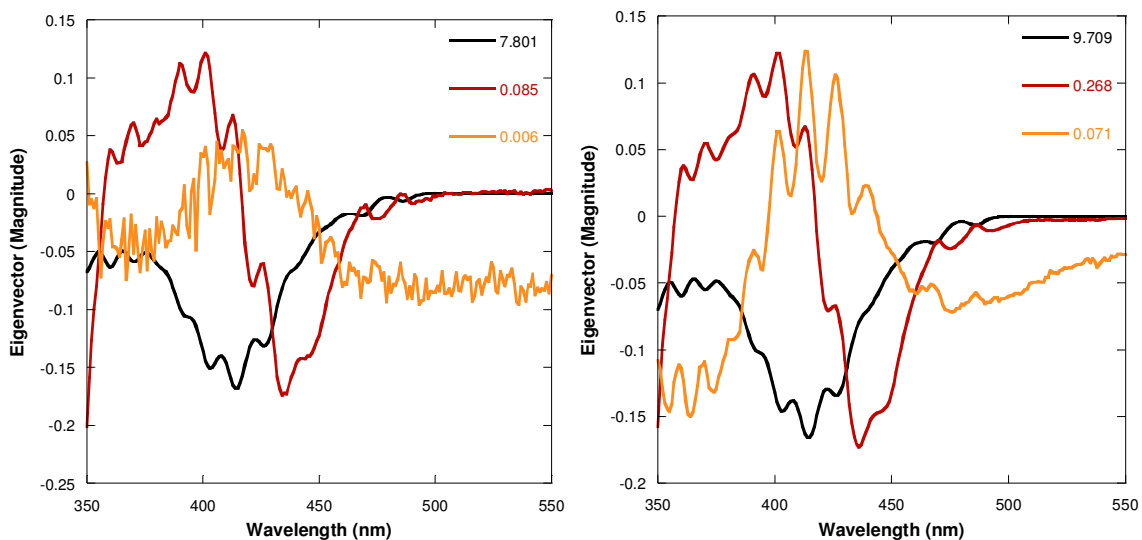


Figure 32 - Eigenvector plots as a function of wavelength. A) Two significant eigenvector and one non-significant vector. Due to the high level of noise and low eigenvalue (0.006), the third vector is most likely noise. B) Two or three significant eigenvectors. Though the third eigenvalue is relatively low, the organized structure and low noise level suggest that a third significant, though minor, eigenvector exists.

file is loaded or manually entered. This includes the species compositions and the governing stability constants. Initial concentrations of all species, titrant composition, and titration parameters are specified for a titration model; initial and final concentrations are specified for speciation curves. This program was used to generate all speciation and titration curves in this work.

5.2 Specific Ion Interaction Theory

Comparison of thermodynamic constants evaluated at different temperatures, ionic strengths, or conditions must be done by extrapolating the hypothetical zero ionic strength stability constant. Since this value presumably has no other interferences it is directly comparable to other data. The Specific Ion Interaction Theory (SIT) is one way to produce this value.

5.2.1 Ionic Strength Theory

The Brønsted-Scatchard-Guggenheim theory, commonly referred to as the Specific Ion Interaction Theory, is based on the Extended Debye-Hückel (EDH) equation (Equation 28). The EDH equation relates the activity coefficient of a species to the ionic strength of the system.

$$\text{Equation 28}$$

$$\log(\gamma_j) = -z_j^2 \cdot \frac{A\sqrt{I_m}}{1 + Ba_j\sqrt{I_m}} = -z_j^2 D$$

In this equation, z is the charge of the j^{th} species, I_m is the molal ionic strength, A and B are constants that vary with temperature, and a_j is the effective diameter of the hydrated ion. The majority of the equation, D , is the Debye-Hückel term.

Brønsted originally proposed the extension of the Debye-Hückel equation to include the effects of the media on the activity of species in solution [146,147]. This was subsequently refined by Scatchard [148] and Guggenheim [149] and is reflected in the first assumption of the SIT Theory: that the activity of the j^{th} species with charge z at an ionic strength of I_m is represented by Equation 29.

$$\text{Equation 29}$$

$$\log(\gamma_j) = -z_j^2 D + \sum_k \varepsilon(j, k, I_m) m_k$$

The summation term in Equation 29 corrects the EDH equation for short range interactions between the species of interest and the k species of opposite charge in the solution. The Ion Interaction Coefficient, ε , is the governing factor; this term is determined for each j/k pair in the system and is weighted by the molality of species k .

The second assumption of the SIT is that the Ion Interaction Coefficient is zero for uncharged species and species of the same charge. The rationale behind this assumption is that SIT corrects for short range interactions and species of the same charge will be repulsed via electrostatic interactions. Since there are no attractive or repulsive forces acting on uncharged species, the assumption that ε is zero (or arbitrarily small) is valid.

For a system that only considers a metal, M , and a ligand, L , in the ionic medium NX , the relationship between a stability constant determined at an ionic strength of I_m and the stability constant extrapolated to zero ionic strength is given in Equation 30.

$$\text{Equation 30}$$

$$\log_{10} \beta_{q,p} = \log_{10} \beta_{q,p}^\circ + p \log_{10} \gamma_M + q \log_{10} \gamma_L - \log_{10} \gamma_{q,p}$$

In instances where the ionic media is the major component of the solution, then $I_m \approx m_N = m_X$ and Equation 30 can be rearranged and simplified as follows.

Equation 31

$$\log_{10} \beta_{q,p}^{I_m} - \Delta z^2 D = \log_{10} \beta_{q,p}^\circ - \Delta \epsilon I_m$$

Equation 32

$$\Delta z^2 = z_{comp}^2 - m z_M^2 - q z_L^2$$

Equation 33

$$\Delta \epsilon = \epsilon_{(comp, N \text{ or } X)} - n \epsilon_{(N, L)} - m \epsilon_{(M, X)}$$

The Debye-Hückel term, D , is defined in Equation 28. If the stability constant for a given reaction is measured at several ionic strengths, this treatment allows the extrapolation of the zero ionic strength constant, usually with a weighted Least Squares refinement. Equation 31 is the method of choice for extrapolating zero ionic strength stability constants as put forth by the OECD-NEA as a part of the Thermodynamic Database Project [103]. In this equation, the logarithm of the stability constant at ionic strength I_m is corrected by $-\Delta z^2 D$ and plotted as a function of ionic strength. This should yield a linear relationship where the slope is the $-\Delta \epsilon$ term and the zero ionic strength stability constant is the y-intercept.

This is the method used in this work to extrapolate the zero ionic strength stability constants. The SIT module in the *Aqueous Solutions* program suite [150], which uses the NEA linearization followed by a Least Squares Refinement, was used to calculate these constants.

5.2.2 Program Specifics

The IUPAC program suite was developed to provide researchers with a standardized and simple interface for analyzing aqueous solutions, including using the SIT. The first step in the refinement process is to specify the ionic media and define the reaction under

investigation. If necessary the Ion Interaction Coefficients, ϵ or SIT parameters, can be edited if desired. Then a delimited text file of the stability constants evaluated on the molal scale, the molal ionic strength, and the error from each measurement is entered.

Data from this work is then refined using the “NEA procedure” option with a “Weighted LSM” (least squares method) [103]. The SIT parameter, ϵ , for the complex can then be adjusted to improve the fit. Additionally, a Dixon Q-test can be performed on the data to check for outliers.

5.3 Density Functional Theory

Density Functional Theory (DFT) was used to model the uranyl-nitrate-water and plutonium(IV)-nitrate-water system from first principles. This allowed analysis of how the electronic structure and point group symmetry influenced the spectra and speciation of the systems. The energy minimized structures and symmetry of a compound, the orbital hybridization, the chemical potential, μ , which can estimate the compound’s chemical “hardness”, and the relative stability of the compound can all be calculated from DFT calculations [151].

An example of the procedures used in this work is provided here for the uranyl nitric acid system [152]. The all-electron scalar relativistic calculations of the total energies and optimized geometries of uranyl complexes were performed using spin-polarized DFT as implemented in the DMol3 software [153]. The exchange correlation energy was calculated using the generalized gradient approximation (GGA) with the parametrization of Perdew and Wang (PW91) [154]. Double numerical basis sets including polarization

functions on all atoms (DNP) were used in the calculations. The DNP basis set corresponds to a double- ζ quality basis set with *d*-type polarization functions added to atoms heavier than hydrogen. The DNP basis set is comparable to 6-31G** Gaussian basis sets [155] with a better accuracy for a similar basis set size [153]. One *5f* polarization function and two diffuse *6d* and *7s* functions were included in the U basis set. In the generation of the numerical basis sets, a global orbital cutoff of 5.9 Å was used. The energy tolerance in the self-consistent field calculations was set to 10^{-6} Hartree. Optimized geometries were obtained using the direct inversion in a subspace method (DIIS) with an energy convergence tolerance of 10^{-5} Hartree and a gradient convergence of 2×10^{-3} Hartree/Å. Geometry optimization and molecular orbital analysis of the molecular complexes were performed at the Γ point. This computational approach was successfully used in previous studies of uranyl-bearing complexes [156].

CHAPTER 6

DISCUSSION AND CONCLUSIONS

6.1 Direct Measurement Techniques

6.1.1 Uranyl-Nitrate-Acid Multivariate Study

The absorbance spectra of samples in this study were analyzed according to the methodology of Bostick [27] (Section 2.2.2) without success. The addition of lithium nitrate appeared to promote the formation of uranyl trinitrate at high total nitrate concentrations (Figure 33). The spectroscopic shift is similar to that found when the total nitrate is increased (Figure 18). This effect limited the number of applicable solutions for a multivariate fit and the approach was abandoned. The experiment did yield three useful, general conclusions. First, the acid concentration does not appear to impact the uranyl spectrum greatly at $[H^+] > 0.1$ mol/L. Second, the molar absorptivities of the uranyl nitrate system shift drastically as a function of nitrate concentration. Third, the effects of cation selection, H^+ vs. Na^+ vs. Li^+ , can greatly influence results by affecting the speciation of the system. This is an effect that was not anticipated from the results of the Bostick study as sodium nitrate was used without any adverse effects. Therefore, future systems in this work will be restricted to nitric acid and sodium salts to prevent any other secondary effects from influencing the spectroscopy.

6.1.2 Uranyl Linear Response Ranges under Simulated Process Chemistries

The linearity and absorption detection limits of the uranyl system under conditions similar to those found in reprocessing streams (Section 4.1.1.2) were investigated. The limits of linearity were determined by analyzing replicate standards across a range of

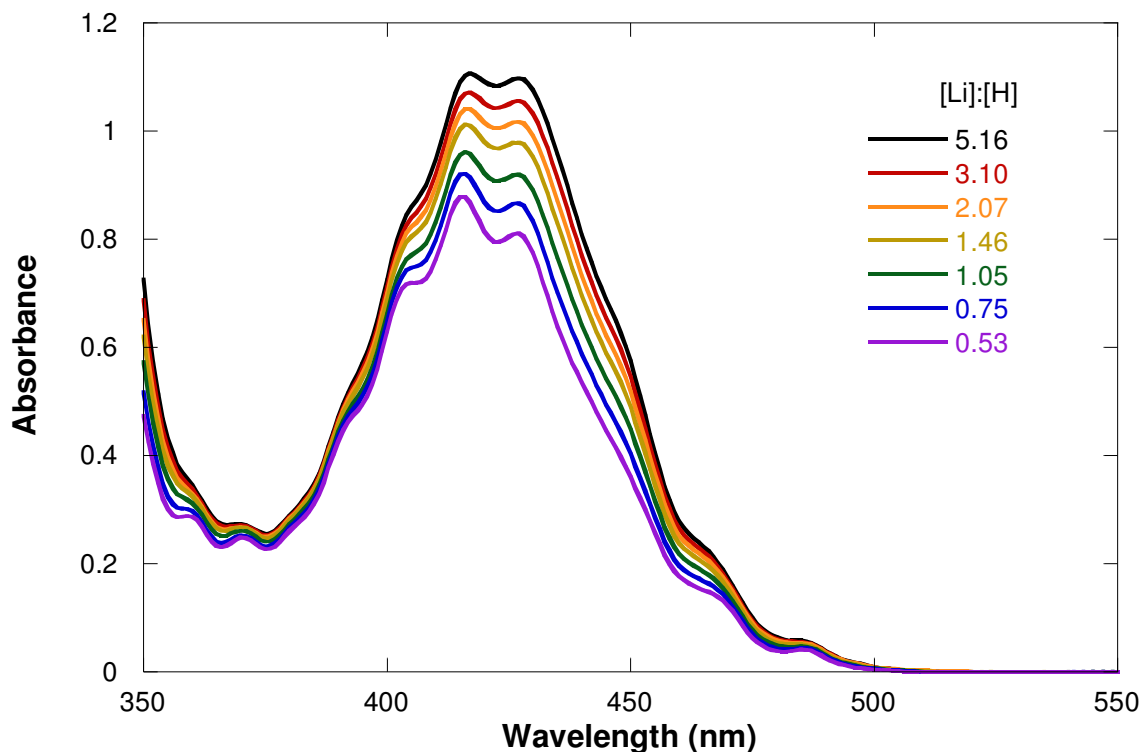


Figure 33 - Increase in uranyl absorbance at 6 mol/L nitrate due to effect of lithium ion. Lithium nitrate to nitric acid ratio provided in legend, $[\text{UO}_2^{2+}] = 95 \text{ mM}$. The spectral change is similar to what is observed at higher total nitrate concentrations. This spectroscopic shift is attributed in this work to the contribution of the uranyl trinitrate species similar to (Figure 4). This is supported by observations that anionic uranyl nitrates form more rapidly in nitrate salts than in nitric acid [68].

uranium concentrations (Table 14). The limits of linearity were first estimated visually and verified by calculating the correlation of the regression equation with different upper and lower limits. The limit of detection was determined by calculating the concentration of a blank sample plus three (3) times its standard deviation with the regression equation; this value was then compared to the lower limit of linearity. Due to the inclusion of a constant term in the regression equation and the low noise of the Cary 6000 spectrometer, the limits of detection calculated by this method were negative. Therefore, in this work

Table 14 – Molar absorptivities, limits of linearity, and detection limits for selected simulated process stream chemistries

Stream	Conditions (mol/L)		λ (nm)	$\epsilon + \Delta\epsilon$ (L/mol·cm)	Limits of Linearity (mol/L)		R^2
	[H ⁺]	[NO ₃ ⁻]			Upper Limit	Lower Limit	
UREX Feed	1.5	4	414	9.82 ± 0.11	8.1×10^{-2}	9.5×10^{-4}	0.998
			486	0.47 ± 0.02	2.0×10^{-1}	9.5×10^{-4}	0.940
Raffinate	2	2	414	8.45 ± 0.27	8.1×10^{-2}	9.5×10^{-4}	0.983
Tc Prod.	5.5	6	414	10.82 ± 0.33	5.9×10^{-2}	1.9×10^{-3}	0.986
U Prod.	0.5	2	414	7.86 ± 0.10	8.1×10^{-2}	9.5×10^{-4}	0.997
			486	0.368 ± 0.004	2.0×10^{-1}	4.0×10^{-3}	0.999
PUREX Feed	4	6	414	10.28 ± 0.15	8.1×10^{-2}	1.9×10^{-3}	0.996
			486	0.646 ± 0.003	8.1×10^{-2}	9.5×10^{-4}	0.999

the limit of detection was chosen to be the lower limit of linearity. These limits will change depending on the specific system used and therefore, the limits presented in this work should be treated as guidelines for developing a deployable system. However, the molar absorptivity constants are applicable across all systems. These can then be used to determine the required measurement pathlength based on the expected metal concentration. For streams where high uranium concentrations are expected, a second wavelength with a lower molar absorptivity was also monitored.

As expected from the multivariate study, each condition had distinct molar absorptivities for the main absorption peaks. Large enough linear ranges exist for each condition such that the uranyl concentration could be monitored in a process stream without dilution or pre-concentration due to the availability of adjustable pathlength cells and dip probes. For the UREX feed, Uranium Product, and PUREX feed streams the uranyl concentration is expected to be ~1-1.25 mol/L which is 12-15x the upper limit of linearity at 414 nm with a 1 cm cell. The same streams are only 5-6x the upper limit for

the UREX Feed and Uranium Product when measured at 486 nm with a 1 cm cell, and 12-15x the upper limit for the PUREX Feed. Therefore, the use of reduced pathlength cuvettes or dip probes allows these streams to be analyzed directly.

The UREX Raffinate is expected to have only 0.1% of the total uranium, or ~1-2 mM, and the Technetium Product is expected to have a similar uranyl concentration. Both of these ranges are near the lower limit of linearity at 414 nm and could be monitored with a standard 1 cm pathlength cell. A longer pathlength cell could be used for added sensitivity if required.

6.1.3 TRLFS of Uranyl ion in Nitric Acid

The fluorescence of the uranyl spectrum with varying amounts of nitrate was collected. The change in the fluorescence intensity (Figure 34) and the uranyl lifetime suggested that the nitrate was a quencher for the uranyl system and this was confirmed in the literature [39]. If TRLFS were to be used as a process monitor, the degree of quenching would need to be known as a function of nitrate. Therefore, Stern-Volmer plots of I/I_0 and τ/τ_0 were generated (Figure 35). The lifetime ratio shows a linear relationship with respect to the nitrate concentration and the intensity curve also shows a rough linear relationship. In this case, the total intensity of each measurement was not power corrected which led to the erratic results. However, if the lifetime of the uranyl ion is measured in process, the Stern-Volmer relationship can be used to give a rough measure of the nitrate concentration by calculating τ_0/τ and applying Equation 25. Before a practical application can be used, though, the effects of other quenching agents in the system would need to be investigated.

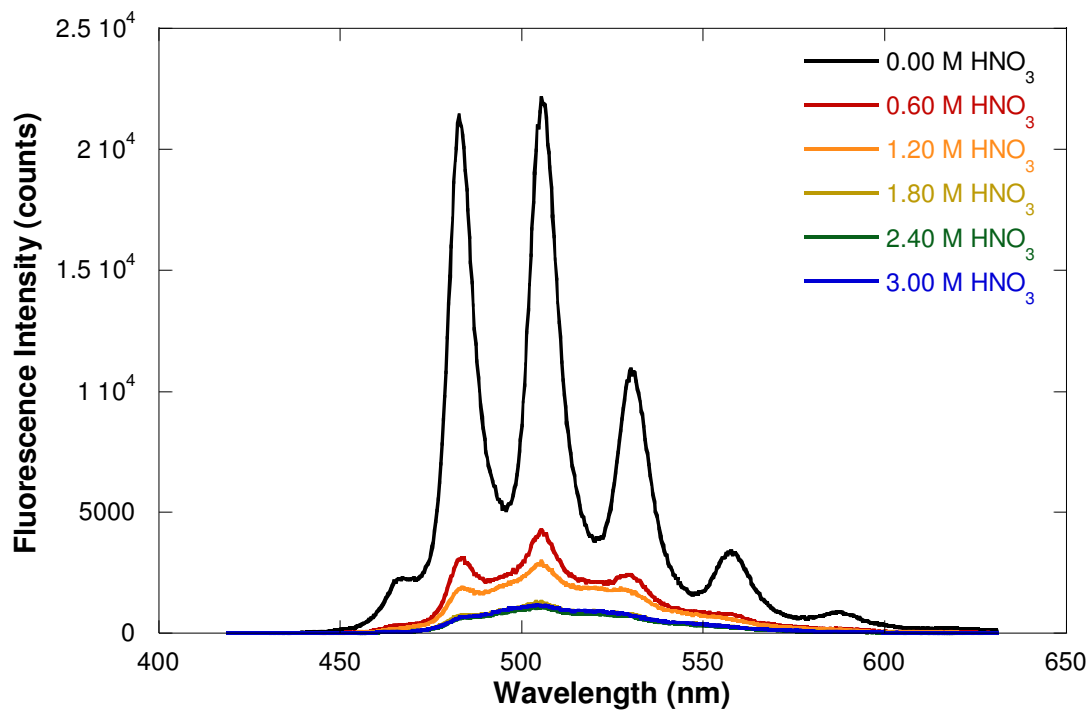


Figure 34 – Fluorescence spectra of the uranyl ion with varying amounts of nitric acid.

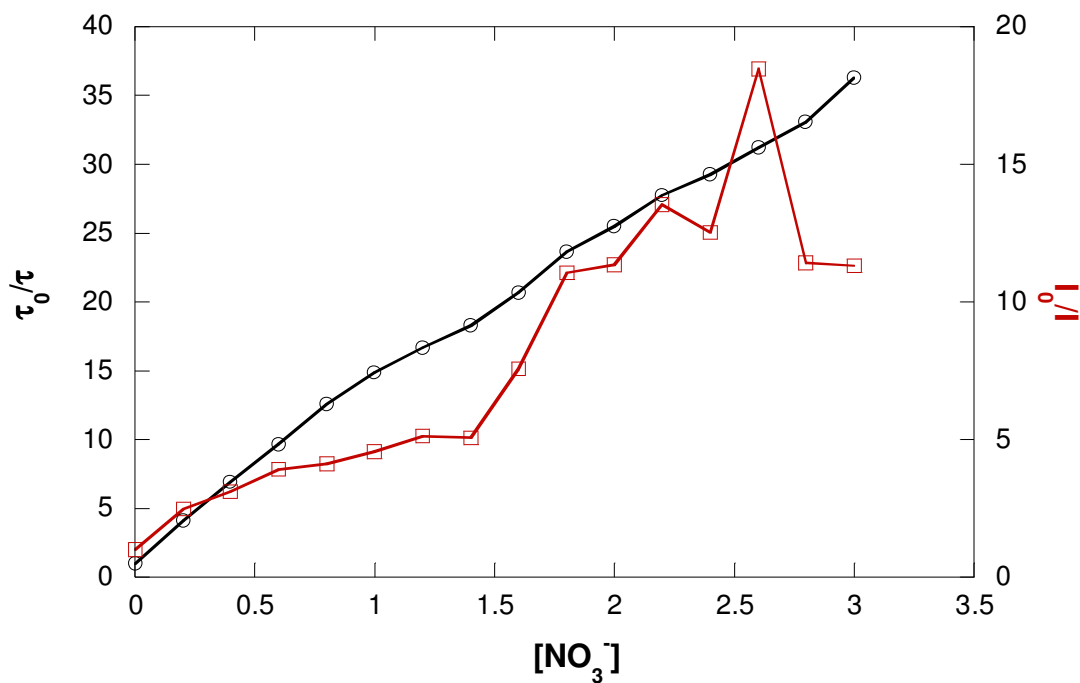


Figure 35 - Stern-Volmer plots of lifetime and intensity quotients as a function of total nitrate concentration.

The linearity of the uranyl fluorescence was not affected by the nitrate ion's quenching behavior; in fact, due to the reduction in total fluorescence, the quenched systems were able to be interrogated at higher uranyl concentrations without saturating the detector. The limits of linearity were determined and are listed in Table 15 and plots of the integrated total fluorescence as a function of nitrate concentration are shown in Figure 36.

Table 15 - Calibration equation and limits of linearity for TRLFS of uranyl under relevant, simulated reprocessing conditions

Condition	Slope	Intercept	Limits of Linearity		R ²
			Upper (μmol)	Lower (μmol)	
6 M HClO ₄	3249 ± 31	-4.80 ± 2.09 x 10 ⁴	1222	92	0.9949
2 M HNO ₃	415.2 ± 1.3	2.08 ± 0.30 x 10 ⁴	6110	122	0.9992
6 M HNO ₃	337.4 ± 1.0	2.43 ± 0.23 x 10 ⁴	6110	122	0.9993

While the total fluorescence intensity of the uranyl ion is highly dependent on the chemical composition of the system, calculation of the nitrate concentration from the Stern-Volmer relationship will allow for an appropriate calibration to be selected. Even without a quantitative calibration, the technique's ability to observe very small amounts of uranium has practical applications. Streams where a high uranyl concentration is not expected, such as the main raffinate from any nitric acid based process or the solvent recycles, can be monitored for trace levels of uranyl. From a process performance standpoint, the lower detection limit for the UREX Raffinate corresponds to less than 1% of the UREX feed, assuming a saturated uranyl nitrate feed solution.

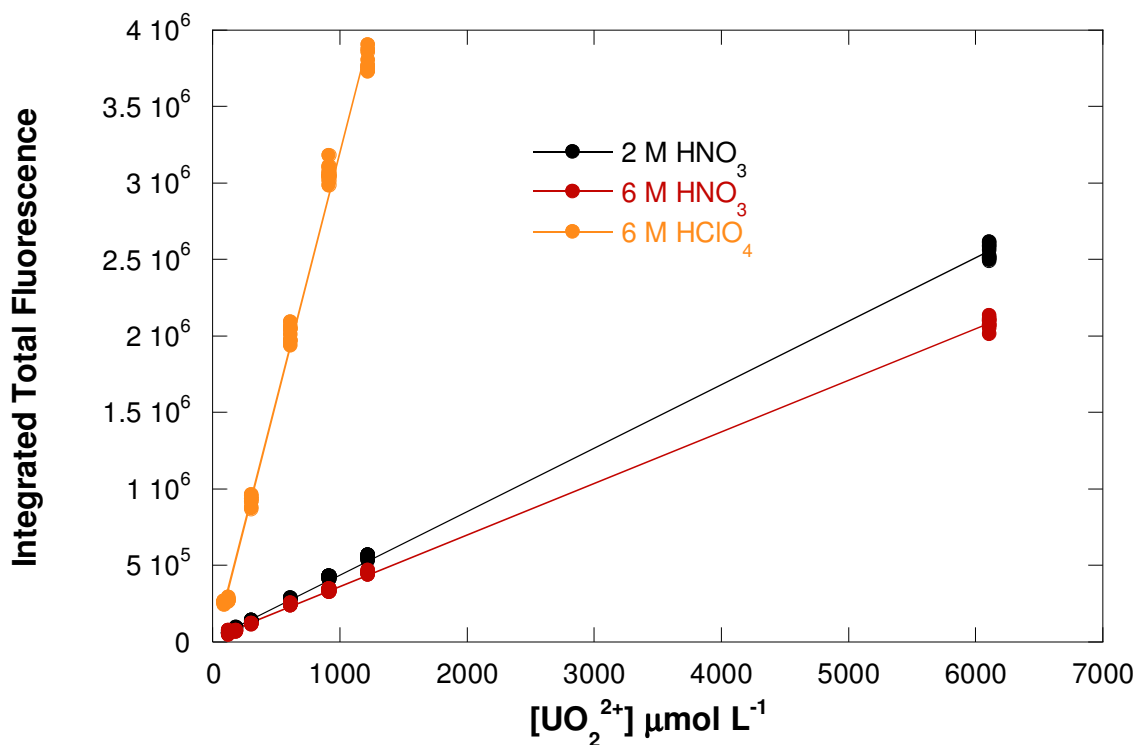


Figure 36 - Fluorescence response as a function of uranyl concentration at 0, 2, and 6 mol/L total nitrate. Ten measurements were taken at each uranyl concentration.

6.1.4 Plutonium Absorption Behavior

The plutonium stock solution was analyzed by LSC and Alpha Spectroscopy to determine the plutonium concentration prior to UV-Visible absorption studies. The LSC samples were compared to a NIST standard plutonium solution; electroplated ²³⁹Pu and ²⁴¹Am button sources were used to calibrate the alpha spectrometer. The results from the two methods (Table 16) agree and were averaged to obtain a final value of 5.55 ± 0.27 mmol/L Pu(IV). The error on the figure is propagated from the errors of the individual techniques.

The plutonium(IV) nitrate system (Section 4.1.2.1) was characterized by monitoring the absorbance spectrum from 400-900 nm, with an emphasis on the main diagnostic

bands near 480 nm. The major absorbance peak shifts from 476 to 491 nm as the nitrate concentration is from 2 to 10 mol/L. The molar absorptivity decreases from 71.8 ± 3.5 to 46.1 ± 2.2 L mol⁻¹cm⁻¹ over the same range. The peak position and molar absorptivities are listed in Table 17.

Table 16 - Results of LSC and Alpha spectrometry for final Pu concentration

Method	Result (mmol/L)
LSC	5.84, 5.63, 5.13, 5.56
Alpha Spec.	5.36, 5.80

Table 17 - Spectroscopic characteristics of the plutonium(IV) spectrum at various nitrate concentrations. Error is extrapolated from Pu(IV) concentration.

Nitrate (mol/L)	2.0	3.0	4.0	5.0	6.0	7.0	8.0	9.0	10.0
Peak (nm)	476	476	477	477	477	477.5	485	490	491
ϵ (L mol ⁻¹ cm ⁻¹)	71.8 ± 3.5	71.1 ± 3.5	58.5 ± 2.8	62.7 ± 3.0	56.8 ± 2.8	47.4 ± 2.3	37.4 ± 1.8	43.9 ± 2.1	46.1 ± 2.2

An unexpected feature in the spectra was the presence of two isosbestic points. The first point occurs at 537 nm and has an average molar absorptivity of 21.30 ± 0.50 L mol⁻¹ cm⁻¹ and the second occurs at 632 nm with an average molar absorptivity of 23.28 ± 0.22 L mol⁻¹ cm⁻¹ (Figure 37 and Figure 38). The second isosbestic point is only valid up to 7 mol/L nitrate. These points have a unique application as they allow for the determination of total plutonium(IV) concentration without an exact knowledge of the nitrate level to

within 1-3%. This is a powerful tool as the main diagnostic peak shifts in both molar absorptivity and position as the nitrate concentration is varied.

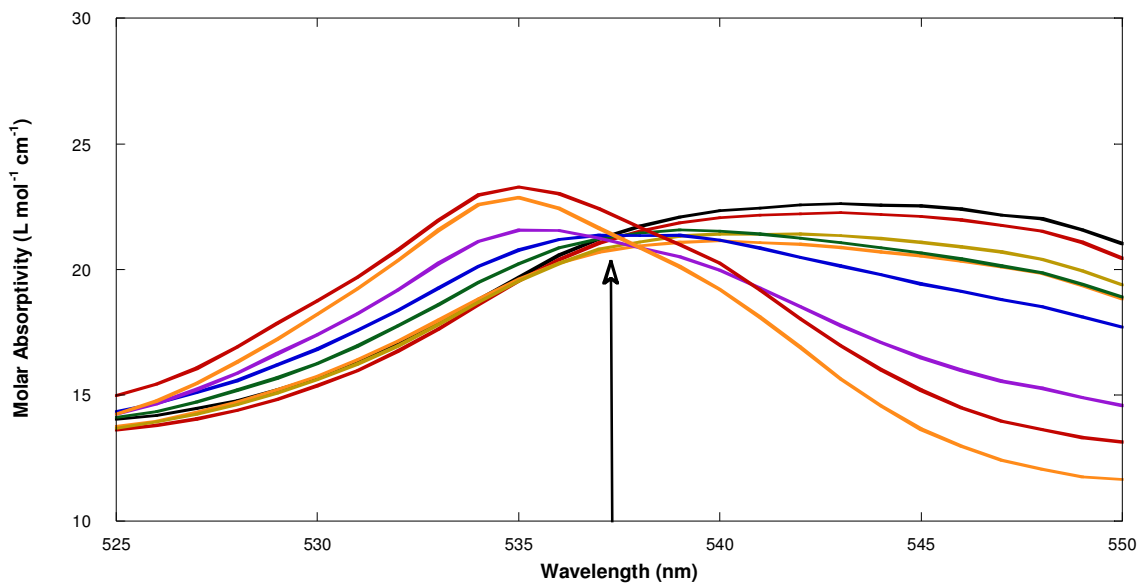


Figure 37 - Isosbestic point at 537 nm

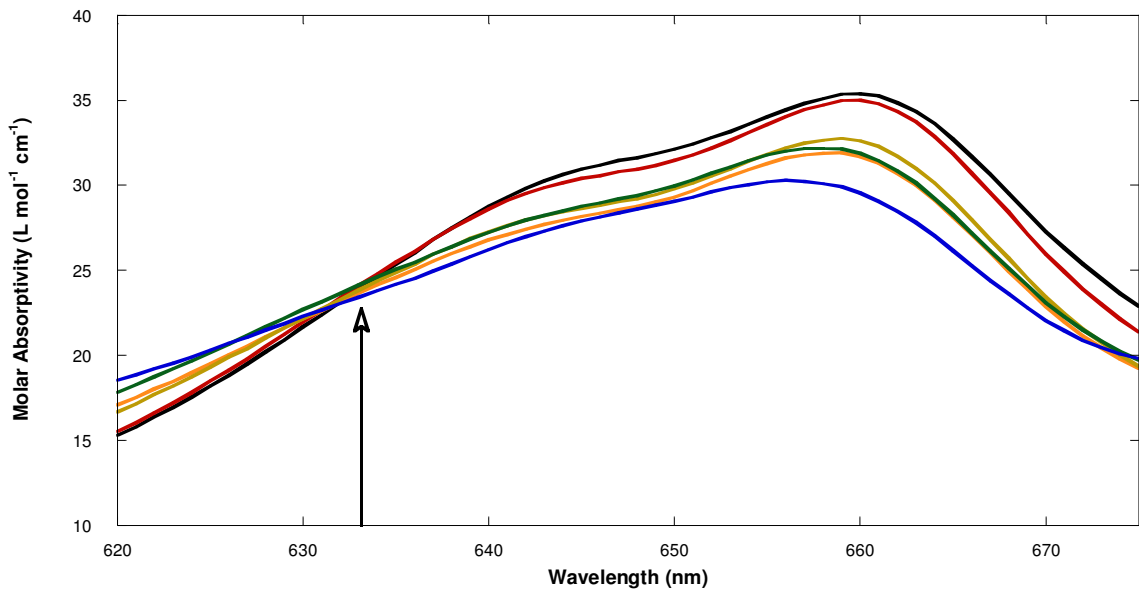


Figure 38 - Isosbestic point at 632 nm (2-7 mol/L nitrate only)

6.2 Indirect Techniques

6.2.1 Multiple Wavelength Monitor for the Uranyl System

It was hypothesized that a ratio of two absorbance peaks may be sensitive to the chemical environment. Mathematically, this multiple wavelength monitor is derived from the general Beer's Law equation for multiple absorbing species (Equation 15). This equation can be altered by factoring the total concentration of all metal species, C_T , from the sum. The resulting quotient of the individual species concentration, C_i , to the total concentration is defined as the mole fraction of the i^{th} species. This is a valid operation as in any given absorbance spectrum, the mole fractions for the system remain constant at any chosen wavelength. In this case the sum reduces to a constant factor, E_0 :

Equation 34

$$A = l \cdot c_T \cdot \sum_{i=1}^N \frac{c_i}{c_T} \epsilon_i$$

Equation 35

$$A = l \cdot c_T \cdot E_0$$

E_0 is the observed total molar absorptivity of the system, and may also be defined as the speciation weighted sum of the individual molar absorptivities and l is the pathlength of the determination. Therefore, when the ratio of the absorbance peaks at two wavelengths, λ_1 and λ_2 , is expressed in this form as a ratio, the result is:

Equation 36

$$\frac{A_{\lambda_1}}{A_{\lambda_2}} = \frac{l \cdot c_T \cdot E_{o,\lambda_1}}{l \cdot c_T \cdot E_{o,\lambda_2}} = \frac{E_{o,\lambda_1}}{E_{o,\lambda_2}}$$

This methodology of using a ratio of wavelengths is a novel technique for investigating the spectroscopy of the uranyl nitrate system. The ratio is valid at any uranyl concentration or pathlength and will produce a consistent result as long as the speciation

of the system (mole fractions) is the same. This allows the peak ratio to be used as an empirical measurement of the speciation of the system. Since the speciation is directly linked to the ligand concentration, the peak ratio should trend with the nitrate concentration.

The spectra collected for the multiple wavelength monitor, referred to as the Peak Ratio Method, were analyzed for systematic trends of absorbance band features with respect to nitrate. The first data set analyzed was composed of 4 mol/L HNO₃ diluted with water (PRS1 A, Table 8). The peak position, height, and area of each absorbance band was generated with the PeakFit program (SyStat Software) using a Gaussian fit. A representative deconvolution of the uranyl spectrum is presented in Figure 39. The fitting routine was run until a minimum correlation of 0.999 was reached. The individual pairs of peak heights or areas were examined and their linear response to nitrate was evaluated, the correlation coefficient of the linear fit was used as a metric. An acceptable trend was defined as 1) linear with respect to nitrate concentration over the expected range within reprocessing systems, ~2-6 mol/L ; and 2) varies enough that random fluctuations would not greatly influence the result. While the relationship does not have to be strictly linear, it should be reproducible. As an example, the peak heights as a function of total nitrate concentration for all 12 bands are presented in Figure 40. These values were then compared to one another to find a linear trend.

The most promising candidate was the 426/403 nm couple, using the peak height rather than the peak area. The couple provided a nearly linear relationship from 1-4 mol/L nitrate (the upper limit of this study) and uses two of the main peaks in the uranyl spectrum which will decrease the effect of random fluctuations.

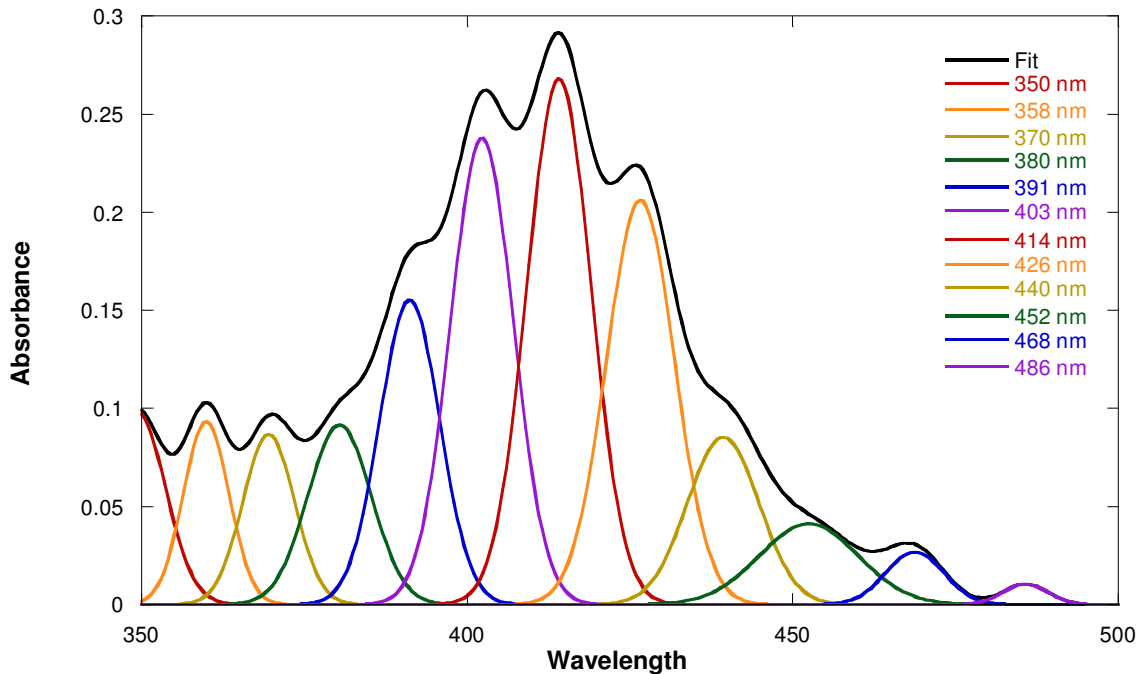


Figure 39 - Deconvolution of the uranyl absorption spectrum. PRS1 A, Table 8: 40.1 mmol/L uranyl, 5 mmol/L nitrate ion.

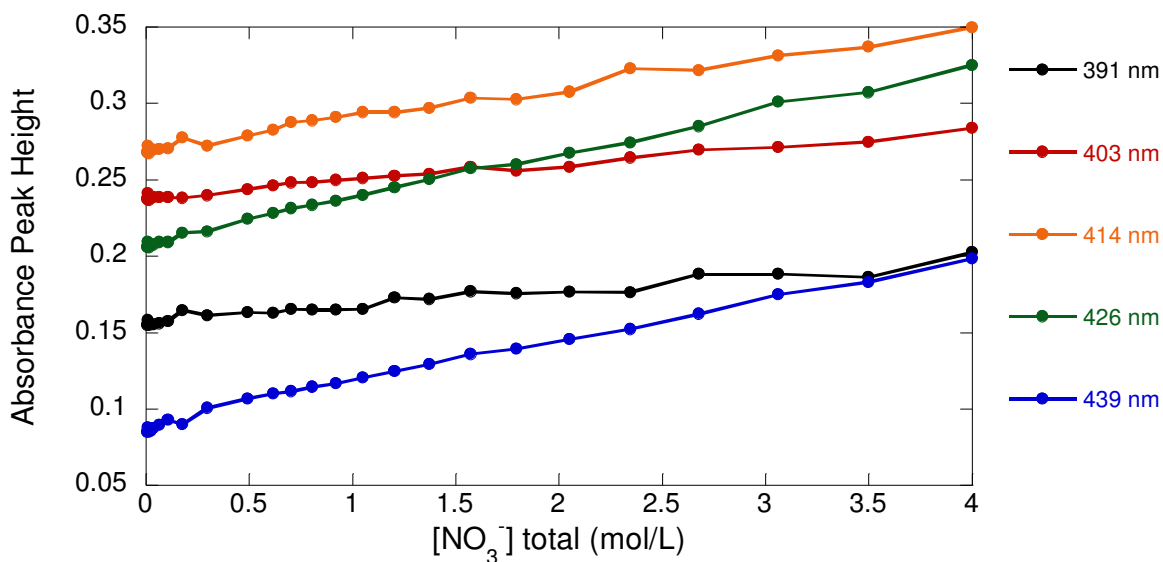


Figure 40 – Selected absorbance peak heights plotted against the total nitrate concentration. The 426/403 couple is easily identified in the top half of the figure. From PRS1 A.

The 426/403 nm ratio was then applied to the samples diluted with 4 mol/L sodium perchlorate and perchloric acid. Differences were noted between the peak ratios in the three sample sets, shown in Figure 41. The linear relationship was slightly deflected with the sodium perchlorate and perchloric acid sample sets assuming a curvilinear fit. This effect was hypothesized to be due to the influence of sodium salts or a general ionic strength effect. In the sample set diluted with perchloric acid, the ionic strength is kept constant, as is the salt counter cation, H^+ . The speciation models proposed in Section 6.3.4 show that the majority of speciation changes occur before 1 mol/L nitrate. Therefore, changes in the spectroscopy past this point are either due to the formation of a uranyl trinitrate species or from changes in the coordination environment.

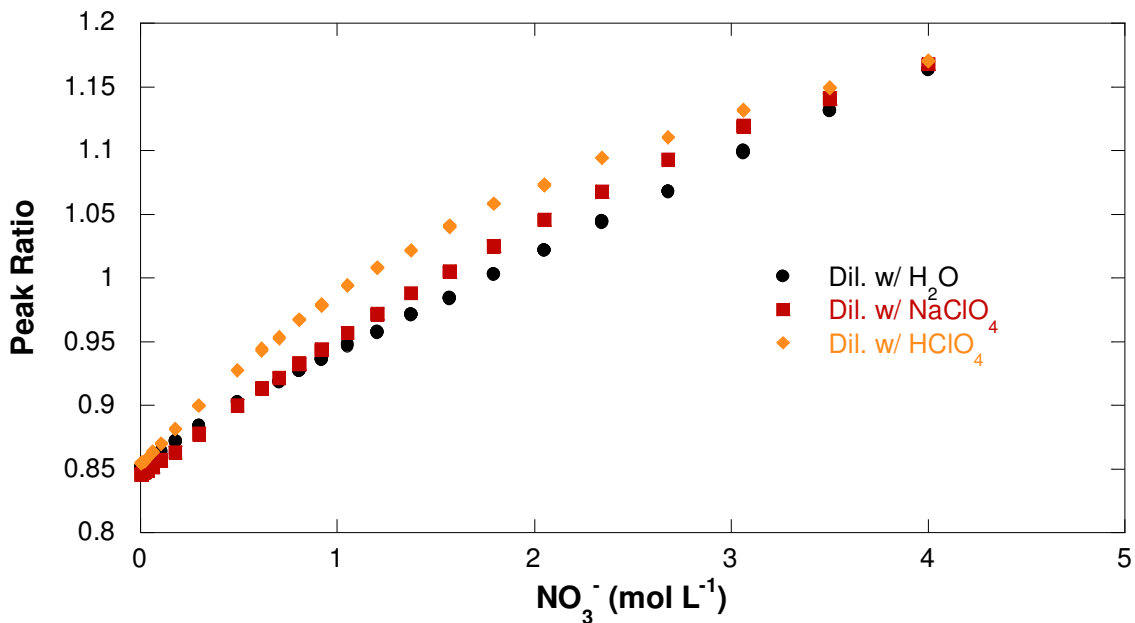


Figure 41 - 426/403 ratio plotted against total nitrate concentration for all three PRS1 sample sets.

In order to investigate the magnitude of this deflection, a second series of samples were created with varying ratios of nitric acid to sodium nitrate with a total nitrate concentration of 6 mol/L (Section 4.1.1.4). These samples were diluted with water and the peak ratio trend was applied (Figure 42). The shift in the spectrum was attributed the varying acid:salt ratio similar to what was observed in the previous study. The data was fitted to a plane with the peak ratio given as a function of the nitrate and acid concentration (Equation 37).

Equation 37

$$A_{426}/A_{403} = 0.063 \cdot [NO_3^-] + 0.020 \cdot [H^+] + 0.852$$

The constant term (0.852) is the peak ratio of the uranyl spectrum in the absence of nitrate. The nitrate coefficient (0.063) describes how much the 426 peak grows in relation to the 403 peak as a function of nitrate. The fit incorporates the acid concentration as a variable which represents the deflection of the trend from the 100% acid condition. In fact, if the acid concentration were set equal to the nitrate concentration, as it would in a 100% nitric acid system, the two terms would sum and the result would be very similar to Equation 38. However, it is not implied that the proton influences the speciation of the system directly. Instead, the cumulative effects of changing cation concentrations on the ionic strength of the system are being represented by the acid concentration.

Equation 38 is the empirical fit for samples where only nitric acid has been used in preparing the samples. The addition of salting out agents has decreased with newer processes and therefore changes in the process chemistry are expected to be based on the addition or subtraction of nitric acid.

Equation 38

$$A_{426}/A_{403} = 0.082 \cdot [NO_3^-] + 0.867$$

This method is similar in nature to the work of Bostick [27]. Both methods allow the user to predict uranyl and nitrate conditions with a single measurement. However, the Peak Ratio method only requires either Equation 37 or Equation 38 to predict the nitrate concentration of the system. If an empirically derived molar absorptivity versus nitrate relationship is produced, the uranyl concentration can be determined as well.

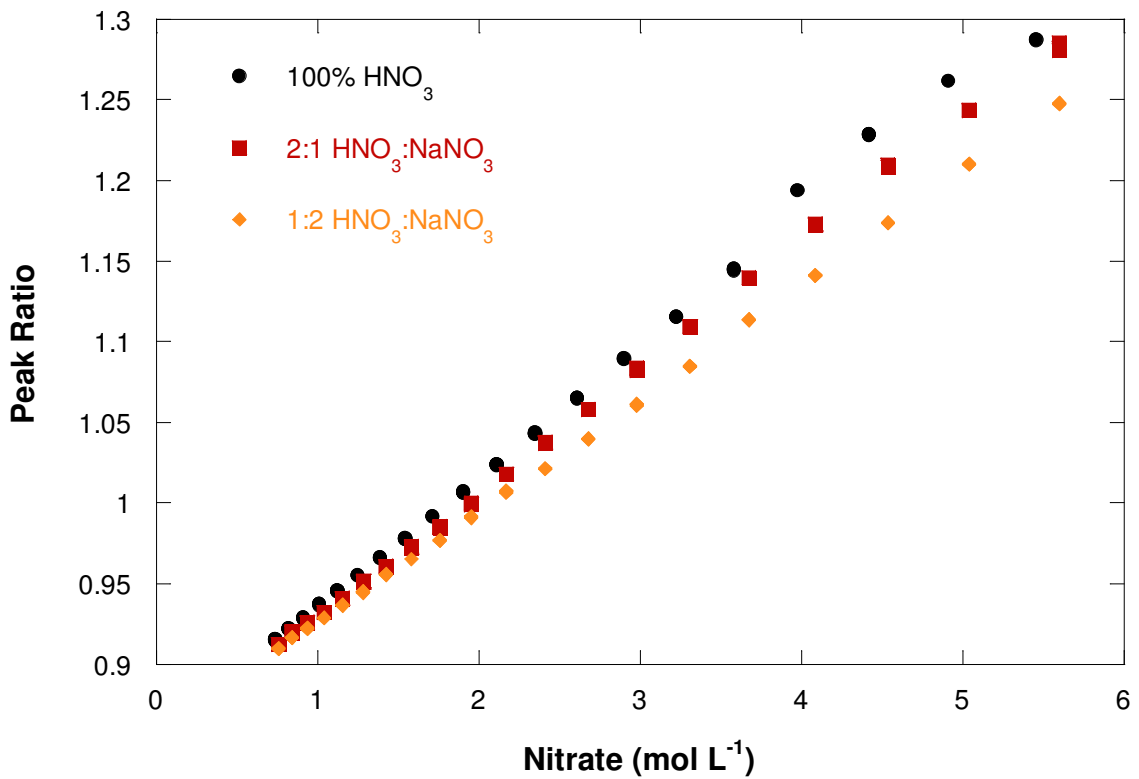


Figure 42 – The 426/403 ratio plotted against total nitrate concentration. Each series started with a unique Nitric acid:Sodium Nitrate ratio and was diluted with water.

The Peak Ratio Method has several advantages over standard, single wavelength spectrophotometric techniques. The ratio itself is independent of the metal concentration, providing that there is enough uranyl to generate a signal. It is also independent of the pathlength of the determination. These properties can be directly derived from Equation 36. The empirical fits (Equation 37 and Equation 38) are generally valid from 1-6 mol/L nitrate.

In addition to providing a monitor of the uranyl and nitrate content, the methodology can also be adapted to reduce systematic bias present in spectrophotometric measurements that only use a single wavelength for monitoring applications. Since the peak height of the uranyl spectrum is dependent on the nitrate concentration and the uranyl concentration, then an increase in either will increase the overall absorbance. Practically, without an exact knowledge of the nitrate concentration, a single wavelength method will not produce reliable results.

For example, Figure 18 shows the net molar absorptivities of the uranyl ion at different total nitrate concentrations. The molar absorptivity shifts from $\sim 9 \text{ L mol}^{-1}\text{cm}^{-1}$ at 2 mol/L nitrate to $\sim 12 \text{ L mol}^{-1}\text{cm}^{-1}$ at 6 mol/L nitrate. Without taking this shift into account, a single wavelength monitor, calibrated at 2 mol/L, would overestimate the uranyl concentration by a third. This bias can be reduced if the peak ratio of the system is used to determine the nitrate concentration first. Then an appropriate molar absorptivity can be used to determine the uranyl concentration in the system.

An analysis of one of the Peak Ratio data sets, shown in Figure 43, demonstrates the error in the uranyl concentration as a function of total nitrate concentration. In this example, the Standard Method represents a fixed, single wavelength monitor calibrated at

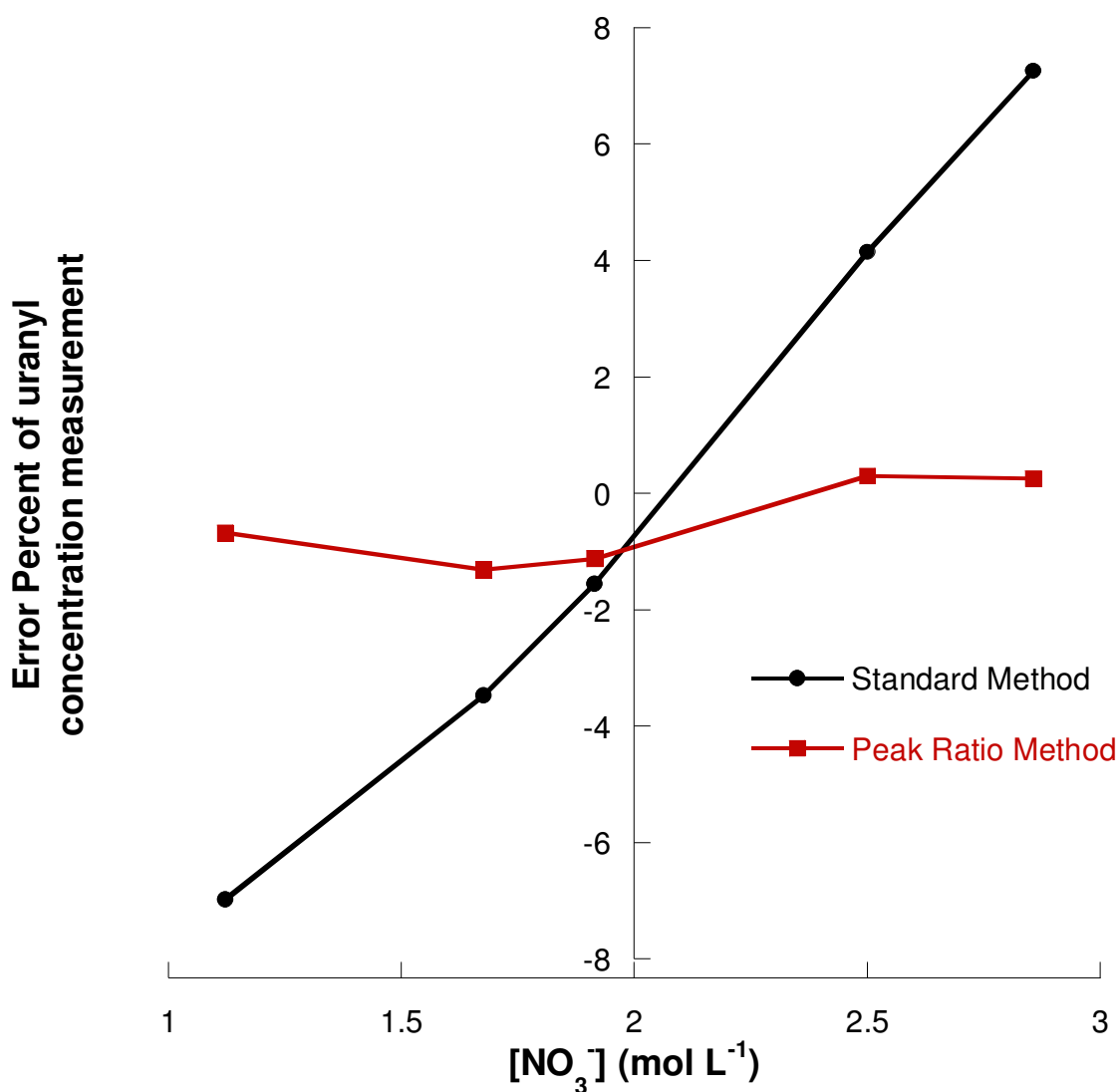


Figure 43 – Comparison of a fixed, single wavelength monitor calibrated at 2 mol/L nitric acid vs. the peak ratio methodology.

2 mol/L nitrate and the Peak Ratio Method uses an empirical molar absorptivity versus nitrate curve to generate a uranyl concentration from the nitrate level. The error in the uranyl measurement for the Standard Method is driven directly by the variation in the total molar absorptivity of the uranyl ion. While a deviation of 4 mol/L total nitrate may not occur during normal operation, it will occur if the process chemistry is altered

intentionally for a diversion attempt or unintentionally during a process upset. With the Peak Ratio method, the total uranium concentration measurement will correctly adapt to the changing chemistry allowing for an accurate accounting of material. It will also provide information on how the process was altered, e.g. if the amount of metal has increased/decreased or if the chemistry itself was changed.

Finally, the method can be used as a near real time process monitor to look for changes in the process chemistry. The peak ratio can be calculated quickly and is only limited by the ability of the spectrometer to collect the spectrum. For monochromator systems, this can be on the order of minutes, while solid state detectors can collect entire spectra multiple times per second. The latter is favorable for single wavelength monitors which provide continuous absorbance readout.

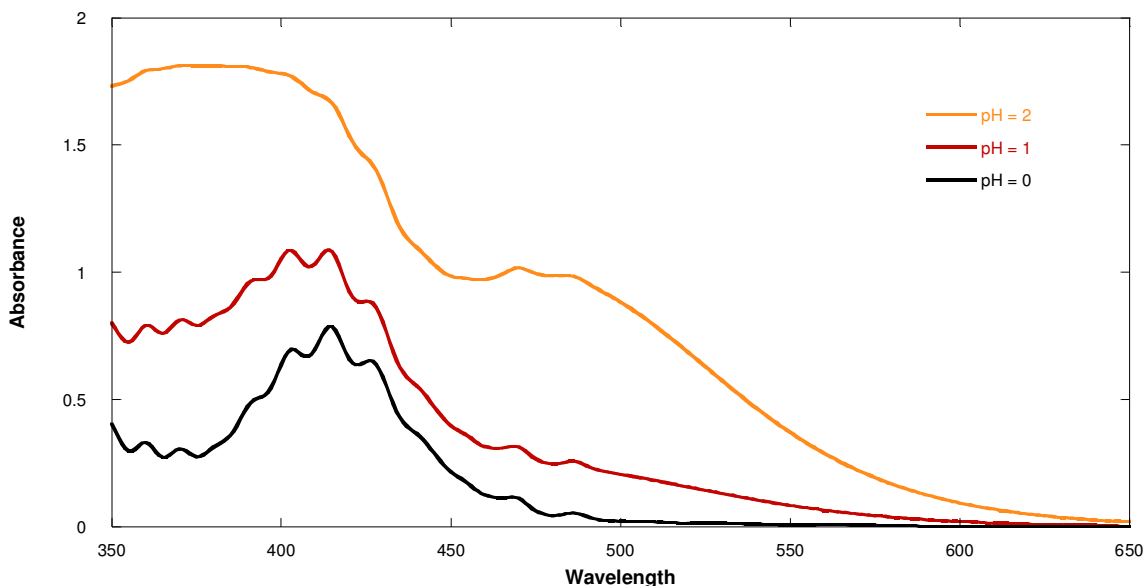


Figure 44 - Uranyl in the presence of AHA. $[\text{UO}_2^{2+}] = 91 \text{ mM}$, $[\text{AHA}] = 87 \text{ mM}$

6.2.2 Acetohydroxamic Acid Detection

The contribution of Acetohydroxamic Acid (AHA) to the feed stream is evident by the effect it has on the uranyl spectrum at elevated pH. The uranyl-AHA complex is distinguished by absorption bands at 470 and 372 nm. Figure 44 shows the effect of increasing pH on the absorption spectrum of uranium in the presence of AHA. Since AHA has been proposed as an additive to only proliferation resistant processes, titration of an aliquot of the process stream would demonstrate the presence of AHA very rapidly and thus confirm the stated process chemistry.

6.3 Thermodynamics

6.3.1 Potentiometric Titrations of Uranyl Nitrate

The potentiometric titrations of the uranyl acetate nitrate system were analyzed with the Hyperquad program. The first part of this methodology involved determining the uranyl acetate stability constants at the ionic strengths involved in this work. These values would serve as a check to ensure that the methodology is producing consistent and realistic results. The appropriate titrations data sets were loaded into Hyperquad as well as literature values for the uranyl mono-, di-, and triacetate as a starting point for the refinement [112] and applicable hydroxide species [66]. The program was allowed to free refine all three uranyl acetate constants. The K_w for each system was interpolated from literature values [75]. The results from these titrations and literature values are shown in Table 18. There is a reasonable agreement between this experimental data and the literature values which demonstrates that the method was working as expected.

Table 18 - Comparison of the first three uranyl acetate stability constants. Errors represent 3σ .

	$\log \beta_{1,1}$	$\log \beta_{1,2}$	$\log \beta_{1,3}$
Jiang et al. [112]	2.58 ± 0.03	4.37 ± 0.14	6.86 ± 0.04
Ahrland [19]	2.4 ± 0.1	4.4 ± 0.4	6.3 ± 0.9
This work	2.09 ± 0.04	4.50 ± 0.03	6.25 ± 0.03

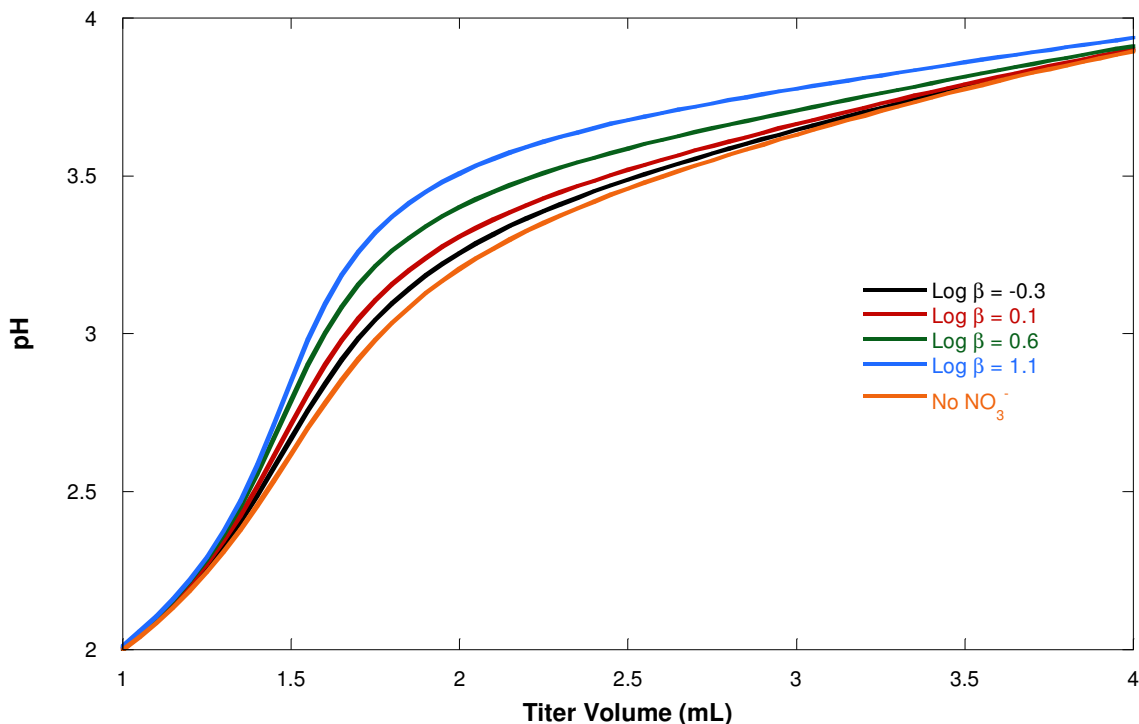


Figure 45 - Effect of increasing the first uranyl nitrate stability constant on the observable pH curve of the uranyl-acetate-nitrate system. Initial titration simulation parameters: $0.010 \text{ mol/L UO}_2^{2+}$, 0.03 mol/L initial acid, 1 mol/L nitrate, 25 mL initial volume. Titrant: 5 mL added, 0.5 mol/L sodium acetate, 0.5 mol/L acetic acid. Stability constants for uranyl acetate from [112]. Titration curve of uranyl-acetate system only (no NO_3^-) included for reference.

Data files for nitrate containing samples were loaded into the Hyperquad program along with the previously determined uranyl acetate values. The system was allowed to free refine the uranyl mononitrate species. The system would not refine to produce a

defensible result with the values entered. Figure 45 demonstrates the relative sensitivity of the uranyl-acetate-nitrate system by simulating titration curves with increasing $\log \beta_{1,1}$ values. The system, as outlined above, does not appear to possess enough sensitivity to the nitrate ion, especially at the low expected value of the mononitrate stability constant, to affect perturb the uranyl acetate speciation greatly. This modeling result and the failure to refine a $\log \beta_{1,1}$ value using a comparable potentiometric methodology casts doubt on the results of Ahrlund.

6.3.2 EXAFS Spectroscopy

The Fourier Transforms of the uranyl and plutonium(IV) systems were used to determine interatomic bond distances and supply information for DFT modeling of solution structures. The Fourier Transform diagrams for the two systems are shown in Figure 46 and Figure 47. Table 19 lists the DFT refined bond distances for the uranyl system; refinement of the plutonium system was not pursued at this time. Samples with a higher total Pu(IV) concentration need to be prepared and analyzed to provide a better data set for DFT refinement.

6.3.3 DFT Modeling

DFT modeling of the uranyl system was pursued to determine the energy levels and geometries of the system to support spectroscopic measurements. Specifically, DFT was employed to further evaluate structural data from EXAFS spectroscopy. However, the information gathered was useful in supporting hypotheses concerning uranyl complexation with nitrate and the UV-Visible spectroscopy of this system.

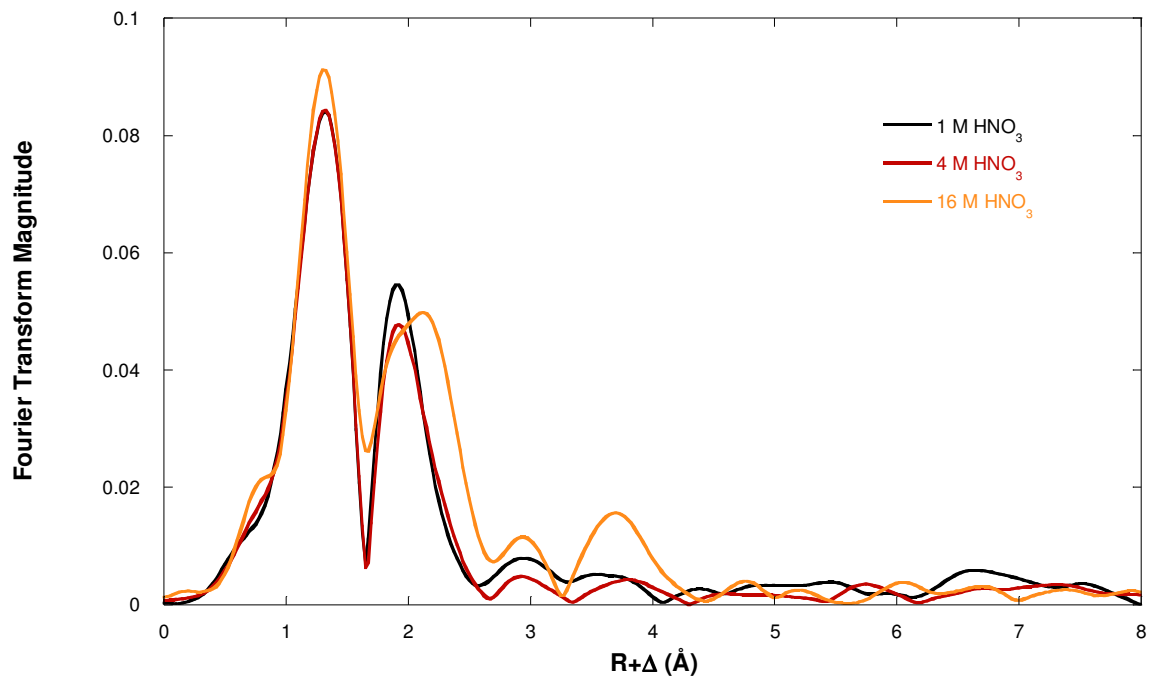


Figure 46 – Fourier Transforms of the uranyl-nitrate EXAFS spectra. The refined bond distances from DFT modeling are listed in Table 19.

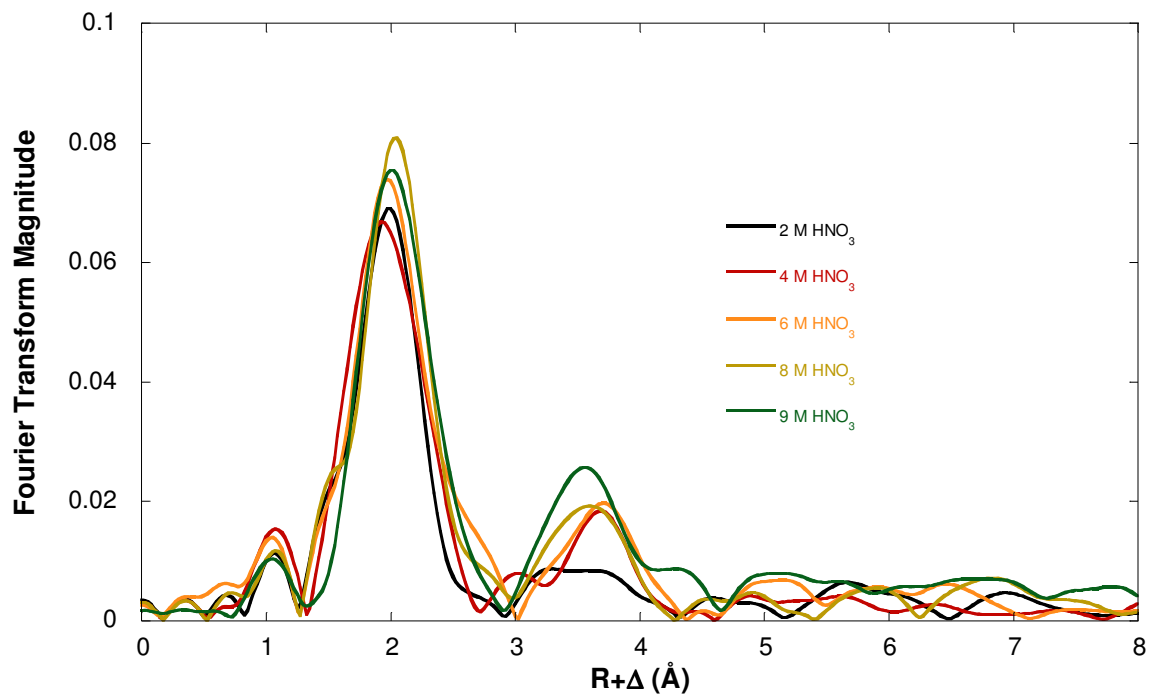


Figure 47 – Fourier Transforms of the plutonium(IV)-nitrate EXAFS spectra.

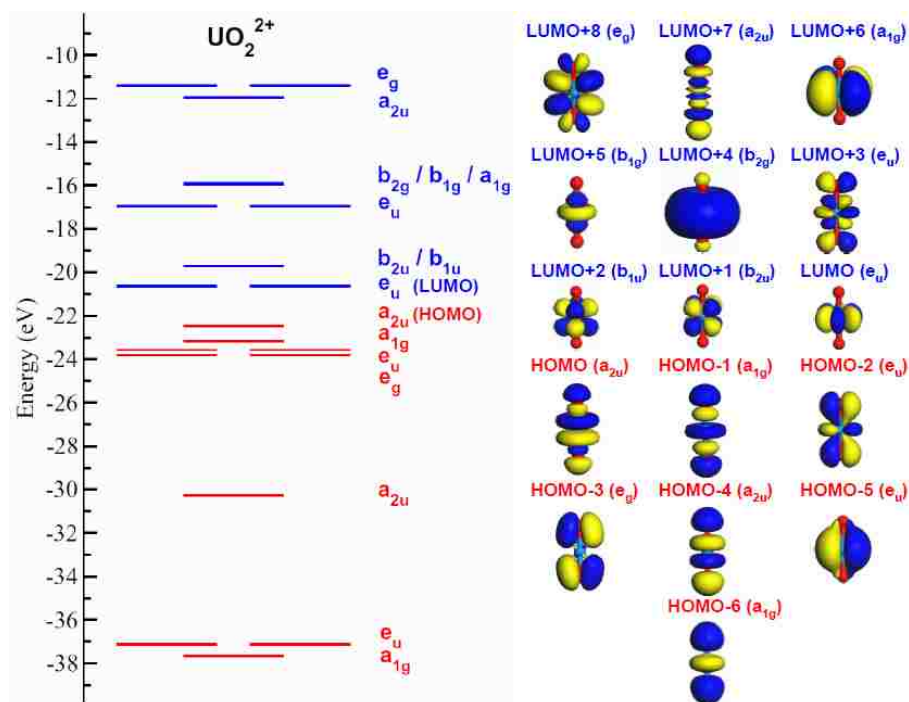


Figure 48 - Molecular orbital (MO) diagram of the highest-lying states of UO_2^{2+} calculated at the GGA/PW91 level of theory (left), with their corresponding graphical representation (right). Occupied valence and unoccupied (virtual) MOs are represented in red and blue, respectively.

Optimized geometries and molecular orbital (MO) diagrams of the highest-lying states of the stable UO_2^{2+} , $\text{UO}_2(\text{H}_2\text{O})_5^{2+}$, $\text{UO}_2(\text{NO}_3)(\text{H}_2\text{O})_4^+$, $\text{UO}_2(\text{NO}_3)_2(\text{H}_2\text{O})_2$, $\text{UO}_2(\text{NO}_3)_3^-$, and $\text{UO}_2(\text{NO}_3)_4^{2-}$ complexes computed using spin-polarized density functional theory (DFT) are represented in Figure 48 and Figure 49 and calculated bond distances are shown in Table 19. The calculated U–O distance in UO_2^{2+} is 1.72 Å, in close agreement with previous fully relativistic results [157] and experimental data [95]. As shown in the corresponding MO diagram in Figure 48, the highest occupied MOs are formed predominantly from the mixing of O 2*p* and U 5*f* orbitals (e.g., the a_{2u} HOMO of UO_2^{2+} is the result of O 2*p_z* and U 5*f_z³* hybridization), while the lowest unoccupied MOs tend to be mostly composed of U 5*f* orbitals (e.g., U 5*f_{xyz}* for the b_{2u} LUMO+1 and U

$5f_{z(x^2-y^2)}$ for b_{2u} LUMO+2). For reference, the calculated energy gap between frontier orbitals for the free, gaseous phase molecule is 1.84 eV for UO_2^{2+} .

As depicted in Figure 49, the equilibrium structure of the pure hydrate complex adopts the C_2 point-group symmetry, while the stable mono-, di-, tri-, and tetranitrato conformers possess C_1 , C_{2h} , D_{3h} , and C_{2h} symmetries, respectively. With the exception of the tetranitrato complex where both η^1 - and η^2 -binding modes are present, the lowest-energy structures of U(VI) nitrate complexes tend to favor the η^2 coordination for the nitrate chelating ligands. This result is consistent with previous DFT calculations performed at the GGA/B3LYP level of theory with the use of effective core potentials (ECP) [95].

The kinetic stability and chemical hardness of these stable structures of uranyl(VI) nitrate complexes have also been assessed in terms of energy separation between the highest occupied and the lowest unoccupied molecular orbitals (HOMO-LUMO energy gap), a larger energy gap translating in an increased stability of the molecular complex. The calculated HOMO-LUMO gaps are shown in Table 19.

Therefore, $\text{UO}_2(\text{H}_2\text{O})_5^{2+}$ is expected to be the most stable complex, while nitrate complexes are found to increase their stability by successive addition of one to three NO_3^- ligands. Consistent with the experimental findings reported in this study – which do not show a spectral signature of $\text{UO}_2(\text{NO}_3)_4^{2-}$ at room temperature – and previous *ab initio* Car-Parrinello molecular dynamics studies [158], the $\text{UO}_2(\text{NO}_3)_4^{2-}$ is predicted to be the least stable uranyl nitrate complex.

According to the DFT calculations, the uranyl mononitrate species is the least stable of all the uranyl nitrate species with the exception of the tetranitrate which is not

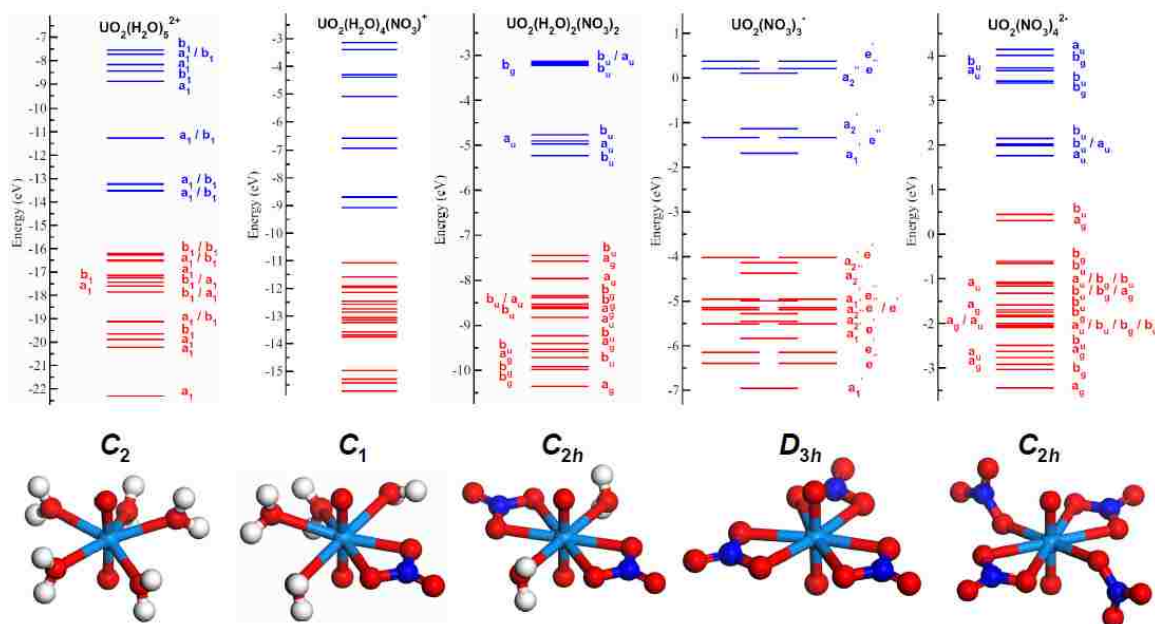


Figure 49 - Molecular orbital (MO) diagrams of the highest-lying states of the $\text{UO}_2(\text{H}_2\text{O})_5^{2+}$, $\text{UO}_2(\text{NO}_3)(\text{H}_2\text{O})_4^+$, $\text{UO}_2(\text{NO}_3)_2(\text{H}_2\text{O})_2$, $\text{UO}_2(\text{NO}_3)_3^-$, and $\text{UO}_2(\text{NO}_3)_4^{2-}$ lowest-energy complexes calculated using density functional theory (top), with the corresponding relaxed geometries and symmetry point groups (bottom). Occupied valence and virtual MOs are represented in red and blue, respectively.

Table 19 – DFT Calculated bond distances and HOMO-LUMO gaps. ^aData from [95]

Species	U-O _{ax}	U-O _{eq} (H ₂ O)	U-O _{eq} (NO ₃)	HOMO-LUMO gap (eV)
$\text{UO}_2(\text{H}_2\text{O})_5^{2+}$	1.77 1.76 ^a	2.48-2.52 2.44 ^a	-	2.68
$\text{UO}_2(\text{NO}_3)(\text{H}_2\text{O})_4^+$	1.79-1.80 1.76 ^a	2.56-2.64 2.41 ^a	2.44 2.49 ^a	2.00
$\text{UO}_2(\text{NO}_3)_2(\text{H}_2\text{O})_2$	1.79-1.80 1.76 ^a	2.61 2.49 ^a	2.50 2.51 ^a	2.22
$\text{UO}_2(\text{NO}_3)_3^-$	1.79-1.80 1.76 ^a	-	2.51 2.50 ^a	2.33
$\text{UO}_2(\text{NO}_3)_4^{2-}$	1.79-1.80 1.76 ^a	-	2.45 (uni)/2.60 (bi) 2.43 (uni)/2.56 (bi) ^a	1.31

expected to exist in solution. Therefore, if the stability constant is low enough the species may not exist in appreciable amounts in solution. This brings about an interesting observation: If the mononitrate is not present in high enough amounts to contribute

spectroscopically, then the changes observed at low nitrate concentrations could be attributed to the uranyl dinitrate. Therefore, if the dinitrate exists in appreciable concentrations at these low nitrate concentrations, then the stability constant of the dinitrate would necessarily be much higher than previously thought.

6.3.4 Uranyl Spectrophotometric titrations

Initial attempts to determine the uranyl nitrate stability constants using values similar to those in the literature failed to refine. This result combined with the DFT calculations and solvent extraction data suggested that the uranyl mononitrate might contribute very little to the absorption spectrum due to its low concentration. Therefore, the major absorbing species in solution would then be the uranyl dinitrate. This assumption was held throughout this set of experiments.

Each spectrophotometric titration was analyzed with the factor analysis module included in the HypSpec program (Section 5.1.2). At most, 2 absorbing species were found in each series, though a minor component may be present in the 4 and 6 molal samples due to the presence of a more highly structured eigenvector plot (Figure 50). The eigenvectors are a graphical representation of the spectroscopic factors in the systems. Each eigenvector plot is associated with a given eigenvalue from the refinement. Each eigenvector has to be evaluated individually based on the eigenvalue and the noise in the system. The lower the eigenvalue and the higher the noise the less significant the factor will be. Each eigenvector plot will resemble an absorption spectrum but it is not directly relatable to any one species as each is a linear combinations of the single component spectra in the solution [161].

Unlike previous studies [18,19,21,22,48], the model used in this work includes only the dinitrate as a refinable species. The system was refined with several different sets of model parameters. First, the use of a standard uranyl spectrum, at the desired ionic strength, was included or the system was allowed to free refine all spectra. Second, the system was refined both with and without the uranyl mononitrate species. In cases where the mononitrate was included, the stability constant was extrapolated to the ionic strength of the titration using SIT and literature values for $\log \beta_{1,1}^0$ and $\epsilon_{\text{UO}_2/\text{ClO}_4}$ and $\epsilon_{\text{UO}_2/\text{NO}_3}$ [66]. The stability constant was then varied ± 0.1 log units to determine how sensitive the dinitrate value was to the mononitrate value. The $\log \beta$ values for the various refinement scenarios are listed in Table 20.

Table 20 - Refined stability constants for the uranyl dinitrate stability constant, $\log \beta_{2,1}$, at multiple ionic strengths, refinement scenarios. Error is propagated from HypSpec values.

Refinement Scenario		Ionic Strength (molal)				
$\Delta(\log \beta_{1,1})$		1.0	2.0	3.0	4.0	6.0
$\log \beta_{1,1}$		-0.315	-0.223	-0.080	0.082	0.433
Uranyl Standard Spectrum	-0.1	2.55 ± 0.01	2.07 ± 0.01	2.18 ± 0.01	2.12 ± 0.01	3.24 ± 0.02
	0.0	2.68 ± 0.01	2.21 ± 0.01	2.33 ± 0.01	2.26 ± 0.01	3.45 ± 0.02
	0.1	2.82 ± 0.01	2.36 ± 0.01	2.48 ± 0.01	2.41 ± 0.01	3.69 ± 0.02
	Not Used	1.81 ± 0.01	1.16 ± 0.01	1.24 ± 0.01	0.80 ± 0.01	1.41 ± 0.01
Free Refine	-0.1	2.03 ± 0.01	1.61 ± 0.01	1.53 ± 0.01	1.43 ± 0.01	2.53 ± 0.01
	0.0	2.26 ± 0.01	1.73 ± 0.01	1.66 ± 0.01	1.57 ± 0.01	3.73 ± 0.02
	0.1	2.26 ± 0.01	1.87 ± 0.01	1.81 ± 0.01	1.72 ± 0.01	2.93 ± 0.01
	Not Used	1.35 ± 0.01	0.81 ± 0.01	0.60 ± 0.01	0.49 ± 0.02	0.90 ± 0.01

Speciation diagrams were generated using the HySS program for select refinement scenarios. Due to the increased strength of the dinitrate stability constant, most of the variation occurs below 1 mol/L nitrate. Scenarios at 2 molar ionic strength both with and

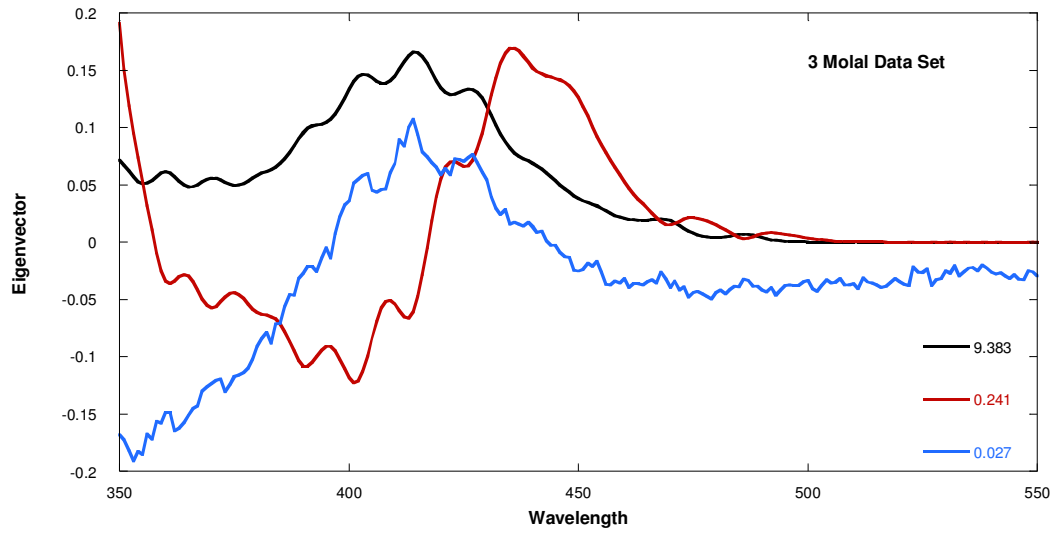
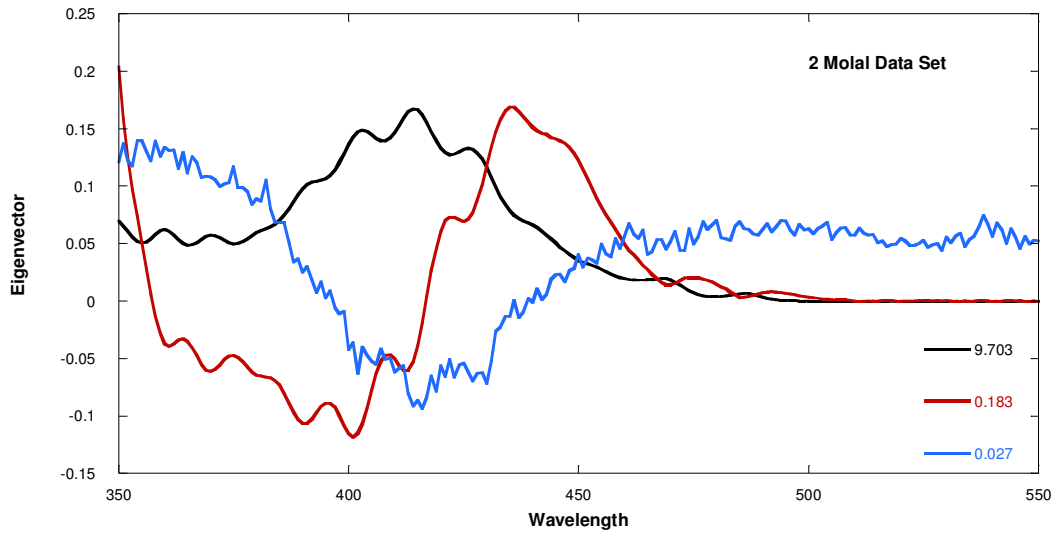
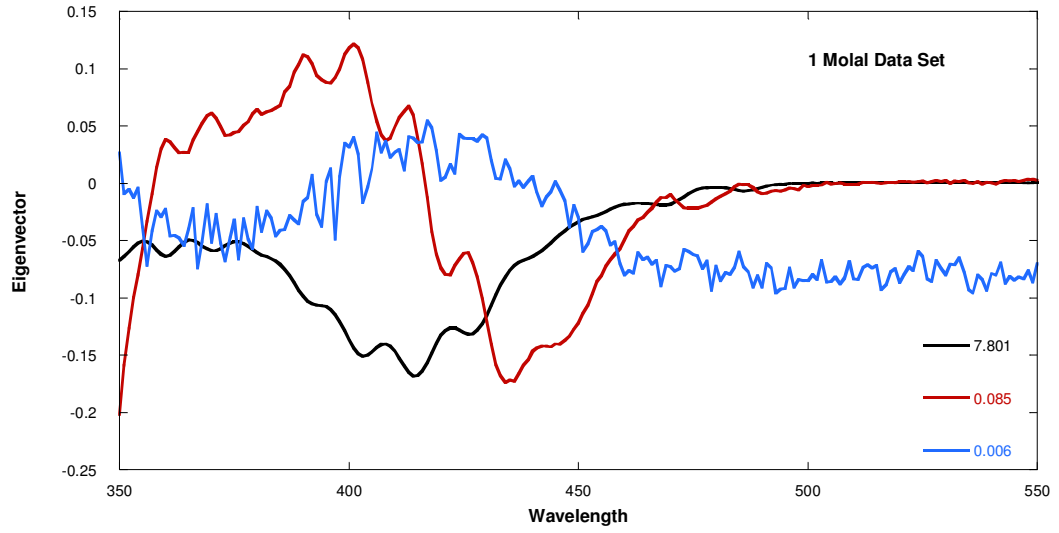
without the mononitrate species and refined with a standard uranyl spectrum are shown in Figure 51 A. The same scenarios with a free refinement of all spectra are shown in Figure 51 B. The simulations use fixed values for the stability constants at 2 molal ionic strength throughout.

6.3.5 SIT refinement

The stability constants determined in the previous section were extrapolated to zero ionic strength using the “Ionic Strength Corrections for Stability Constants” module of the *Aqueous Solutions* program suite (Section 5.2.2). The zero ionic strength stability constants and the complex ion interaction coefficients for the various refinement scenarios are listed in Table 21. The program was set to follow the NEA method for extrapolation of the zero ionic strength stability constant with a weighted Least Squares Method. The stability constants from Table 20 were adjusted according to Equation 31 (Figure 52 and Figure 53). This linearization is the basis for extrapolation of the zero ionic strength stability constant.

Ideally, the data points would form a linear relationship where the intercept corresponds to the zero ionic strength stability constant and the slope is the net change in ion interaction coefficients, $\Delta\epsilon$ (Equation 33). One caveat is that the method is generally only applicable up to an ionic strength of 3.5 molal; therefore the data collected at 6 molal ionic strength has been excluded though the choice was made to include the 4 molal data points. The data sets which show the greatest degree of linearity are the sets refined without including standard spectra for the uranyl ion.

Two different models have been proposed here for the uranyl-nitrate system. The first is the standard model which includes the mononitrate (using the values in the



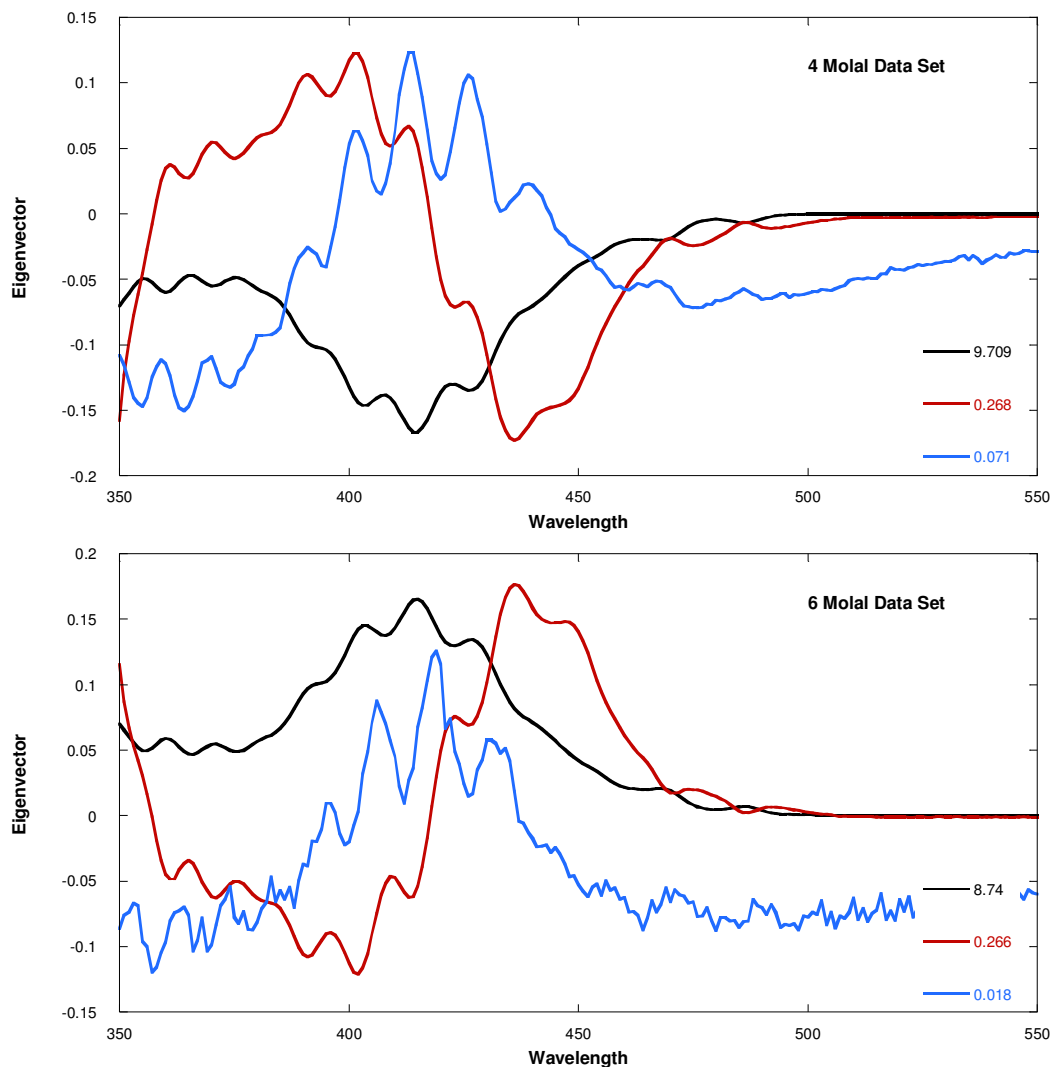


Figure 50 - Eigenvector plots for first three singular eigenvalues at 1, 2, 3, 4, and 6 molal ionic strength. A third species becomes more prominent above 4 molal ionic strength, though it is not a major component. This is most likely due to the higher nitrate concentrations reached in these samples.

literature). This is in keeping with the assumption that the nitrates add successively to the uranyl ion. The second model excludes the mononitrate completely which assumes that either the stability constant is significantly lower than it is currently presumed or that the species does not form in solution at all. This can be seen in the small influence of the mononitrate on the speciation of the uranyl-nitrate system in Figure 51. This second

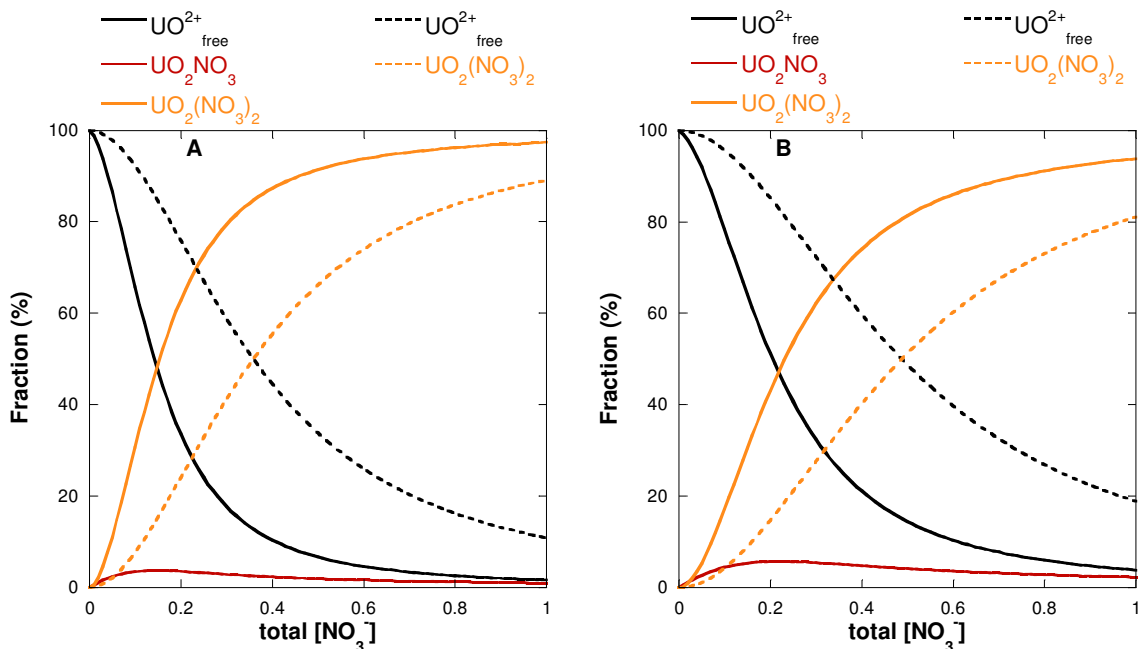


Figure 51 - Speciation diagrams for at 2 molar ionic strength; stability constants used can be found in Table 20. Solid lines represent systems including the uranyl mononitrate, dashed were refined without. A) Refinement with a uranyl standard spectrum; B) free refinement of all spectra.

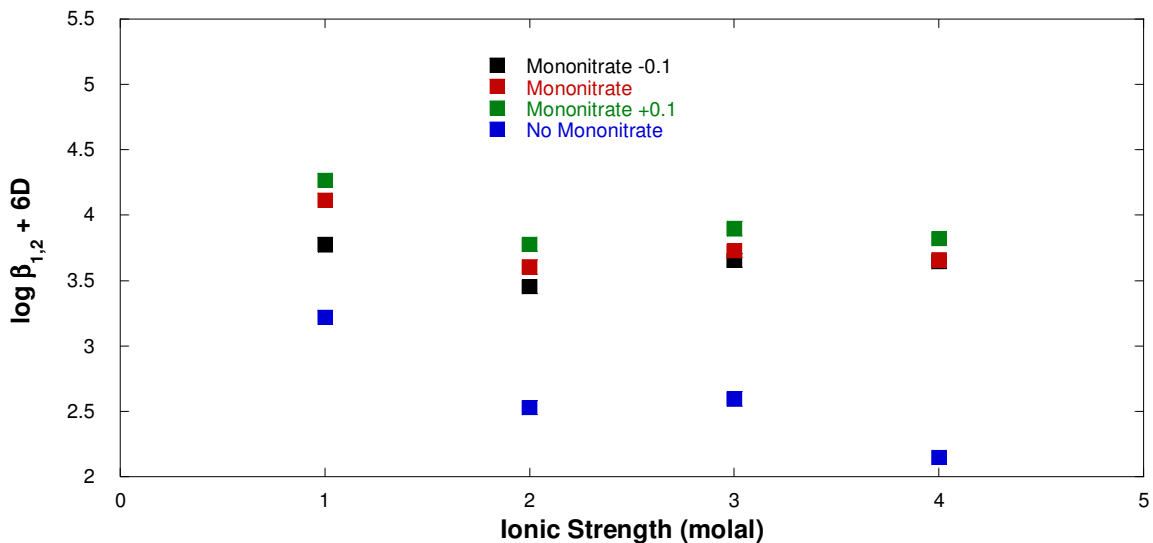


Figure 52 – Linearization of the uranyl dinitrate stability constants refined with a standard uranyl spectrum included.

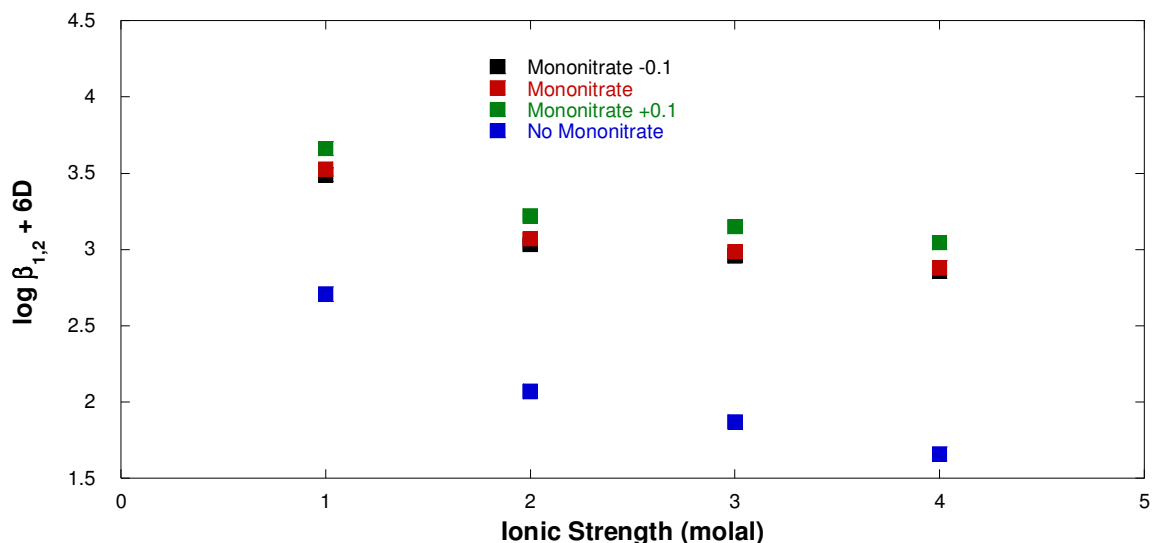


Figure 53 - Linearization of the uranyl dinitrate stability constants with free refinement of all spectra.

hypothesis may be realistic as the uranyl hydroxide system forms dimers and multiple hydroxide species rather than the 1:1 uranyl hydroxide at concentrations above 0.1 mmol/L. In addition, there is a debate as to if the UO_2OH^+ species exists in solution at all [66].

One of the few weak ligands in the literature to which comparisons can be drawn is the uranyl chloride system. The monochloro and dichloro complexes have been reviewed by the authors in [66] and two studies were found to be reliable. These were used to extrapolate the zero ionic strength stability constants, $\log \beta_1^0 = 0.17 \pm 0.02$ and $\log \beta_2^0 = 1.1 \pm 0.4$. These values are similar to those found in the current uranyl nitrate system. However, this does not necessarily conflict with the proposed theory. Indeed, if the uranyl chloride system is reevaluated with a dichloro-centric model it may show similar results.

Table 21 - Zero Ionic Strength Stability Constants and Specific Ion Interaction parameters for the uranyl dinitrate species

Refinement Scenario	Thermodynamic Parameters		
	$\Delta(\log \beta_{1,1})$	$\log \beta^0$	$\epsilon_{\text{UO}_2(\text{NO}_3)_2}$
Uranyl Standard Spectrum	-0.1	3.67 ± 0.02	0.61 ± 0.09
	0.0	3.80 ± 0.02	0.60 ± 0.09
	0.1	3.95 ± 0.02	0.60 ± 0.09
	Not Used	3.14 ± 0.02	0.79 ± 0.09
Free Refine	-0.1	3.27 ± 0.02	0.68 ± 0.09
	0.0	3.37 ± 0.02	0.67 ± 0.09
	0.1	3.48 ± 0.02	0.66 ± 0.09
	Not Used	2.66 ± 0.02	0.77 ± 0.09

The inclusion of the $\log \beta_{1,1}$ in the refinement scenario has the effect of raising the $\log \beta_{2,1}$ value by ~ 1 log unit. While the amount of mononitrate in the solution remains negligible ($<5\%$), the dinitrate becomes dominant far quicker than without the mononitrate. However, the model which includes the uranyl mononitrate may match physical observations of the uranyl-nitrate system better than without (Section 6.3.7.4).

6.3.6 Plutonium Factor Analysis

The plutonium(IV) nitrate system was also processed through the Factor Analysis program of HypSpec. The number of species present was calculated for progressively fewer samples to determine rough speciation information, though not enough data was generated to produce a full speciation diagram. The results of the factor analysis are compiled in Table 22.

Table 22 – Number of significant factors in the plutonium nitrate system in the specified total nitrate ranges.

Nitrate Range (mol/L)	2-10	3-10	4-10	2-7	3-7	4-7
Significant Factors	5	4	3	4	3	2

A total of 5 spectroscopically significant (>10% fraction) species were found between 2 and 10 mol/L nitrate. Based on the work of Viers and Ryan (43,62) the last species is most likely the hexanitrate species. The remaining 4 species cannot be assigned with any certainty from this data. However, where species appear and disappear from the system can be determined giving focus to future studies. The total number of species drops at 3 and 4 mol/L nitrate and increases at 7 mol/L. The factor analysis shown graphically in Figure 54 gives enough information to tailor future experiments. Specifically, the 4-7 mol/L nitrate range should only have 2 major species. Once these are determined, the remaining two species, one of which may be the plutonium-aquo compound, can be investigated.

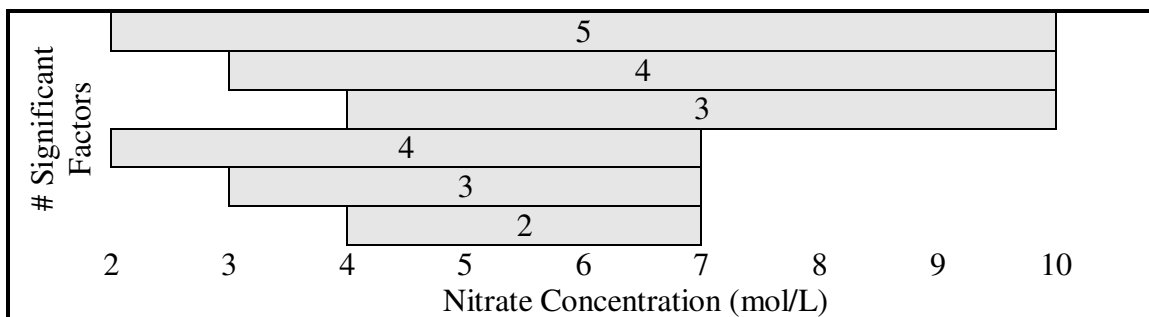


Figure 54 - Graphical representation of plutonium nitrate Factor Analysis results. The number of significant factors drop at 3 and 4 mol/L total nitrate and increase at 7 mol/L nitrate. The species that adds to the system above 7 mol/L nitrate is likely the $\text{Pu}(\text{NO}_3)_6^{2-}$ species.

6.3.7 Influences of symmetry on speciation

Several observations have been made that call into question the current uranyl nitrate speciation model. Specifically, the failure of the speciation model to explain solvent

extraction (Section 2.6) and ion exchange data [68]. These have led to a hypothesis that the symmetry of these species has a direct effect on their thermodynamic stability. If valid, this hypothesis could be extended to help explain inconsistencies in the plutonium(IV) nitrate system as well.

6.3.7.1 Solvent Extraction

The speciation diagram formed using the uranyl nitrate stability constants in the literature (Figure 6) do not adequately explain the extraction behavior observed in the TBP-Dodecane extraction system as the neutral dinitrate species is not dominant up to 8 mol/L nitrate. This is at odds with the extraction of uranyl into the organic phase (Figure 9). For comparison, this extraction has a distribution coefficient of nearly 30 by 3 mol/L total nitrate while the uranyl dinitrate fraction is only 10-15% at 3 mol/L. It could be argued that the extraction is removing the uranyl dinitrate from the system which would in turn cause the aqueous phase to re-equilibrate. However, the reaction is fast and easily reversible by decreasing the nitrate concentration [81] which indicates that there is no mechanism removing the dinitrate from the equilibrium. If the uranyl dinitrate was truly removed from the equilibrium, changing the aqueous chemistry would have no effect. Finally, Marcus and Kertes state that the degree of extraction into an organic solvent is directly proportional to the degree of formation of the extractable species in aqueous solution [162].

6.3.7.2 Anionic species

The existence of anionic uranyl nitrates would seem to be unlikely with the standard model. The best estimates in the literature place $\log \beta_{3,1}$ at between -1.7 and 0.5. The uranyl trinitrate has been thought to have been observed in organic solvents and there is

anecdotal evidence for them in concentrated nitric solutions (Section 2.2.2.1). Anionic exchange resins have also been used to separate uranium from nitric acid solutions with a high efficiency; the adsorption maxima occurs at 8 mol/L HNO₃ with a distribution coefficient of ~10 [68]. This agrees with the results of the peak ratio studies. Since the peak ratio is an indirect measurement of the speciation and the dinitrate dominates by ~1 mol/L, the increase in the peak ratio could be ascribed to the formation of the trinitrate.

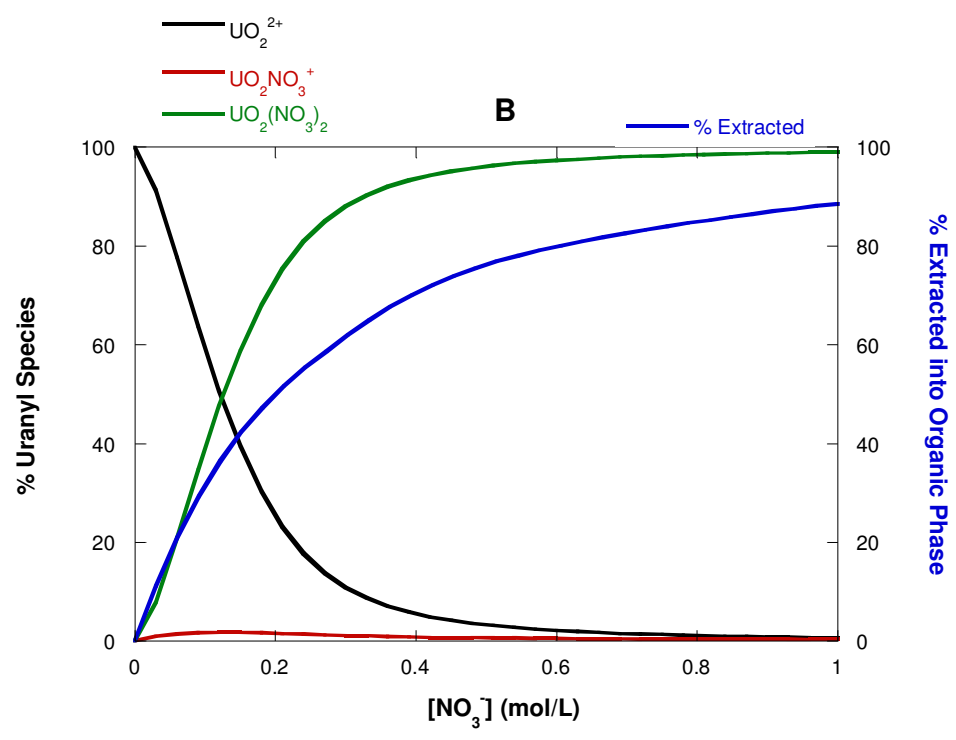
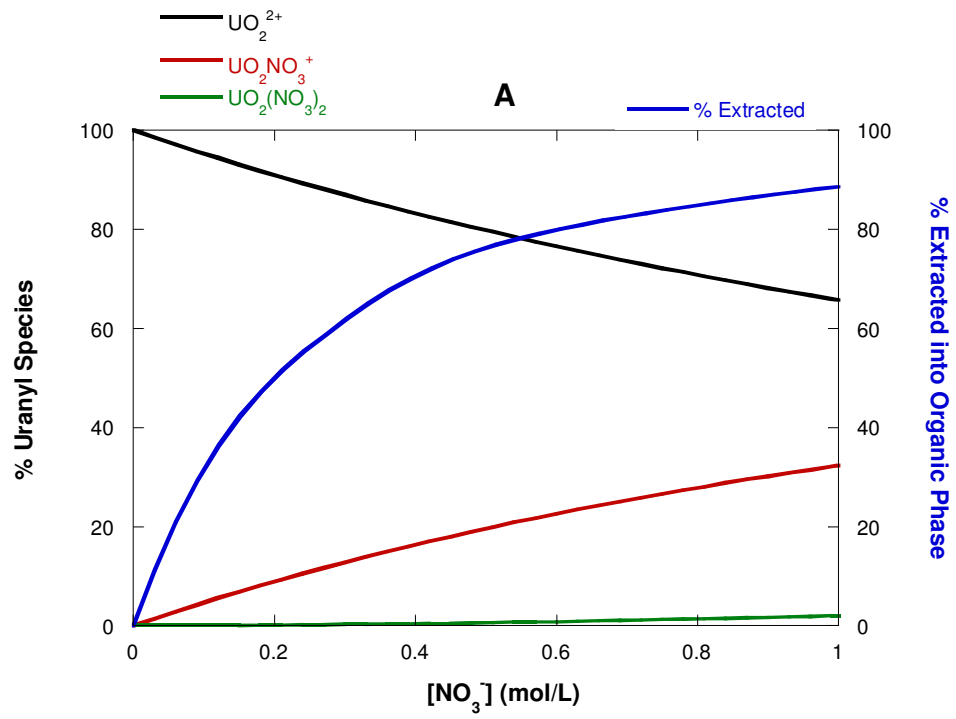
6.3.7.3 Tetravalent plutonium Nitrate Speciation

The speciation of the plutonium(IV) nitrate system does not seem to follow the usual progression of nitrates. The major species have been identified as the mononitrate, dinitrate, tetranitrate, and hexanitrate [43]. The reasons for the exclusion of the tri- and pentanitrates have not been adequately explained.

6.3.7.4 Hypothesis

These inconsistencies can be explained if the symmetry of the species is considered as a factor in their speciation. It is hypothesized here that for weakly interacting systems, in the absence of external factors such as steric hindrance, that the symmetry of the present species will directly influence the speciation of the system. This implies that the stability of a given complex is proportional to its symmetry. This would be applicable to weak systems such as the uranyl or plutonium(IV) nitrates.

For the uranyl nitrate system, the low symmetry mononitrate becomes de-emphasized while the higher symmetry dinitrate and trinitrate species are much stronger than previously thought. This is corroborated by the relative chemical stability of these species represented by the HOMO-LUMO gap in Table 19.



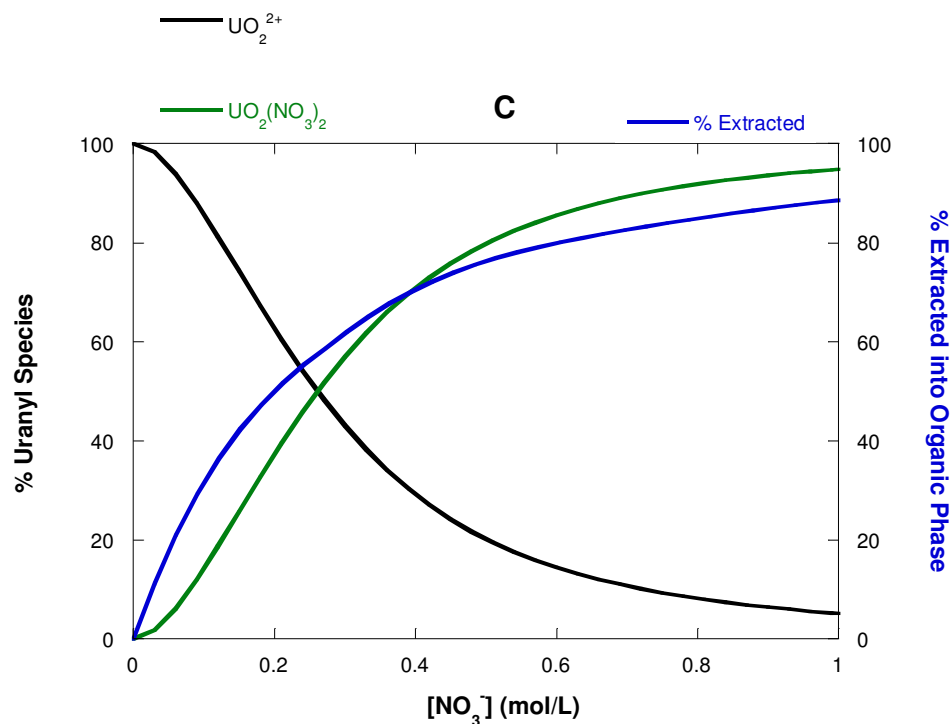


Figure 55 – Speciation diagrams for scenarios A, B, and C found in at $[\text{UO}_2^{2+}] = 50$ mmol/L. The best correlation to the experimental data is found with the data set refined including the mononitrate species. That dataset shows an excess of extractable species compared to the extraction data.

Table 23 – Stability constants used in Figure 55 A, B, and C. Values from this work can be found in Table 20. ^a from [19]. ^b from [112].

Figure	log $\beta_{1,1}$	log $\beta_{2,1}$
A	-0.3 ^a	-1.5 ^b
B	-0.315	2.26
C	N/A	1.35

When the symmetry is taken into account, it explains the need for the revised uranyl-nitrate speciation model used in this work as suggested by the DFT calculations (Section 6.3.3). Furthermore, when this model is used, the stability constants derived from the spectrophotometric titrations (Section 6.3.4) are hundreds of times larger than those

found in the literature. When the speciation diagram generated with the constants in this work is compared to solvent extraction data, there is better agreement than with the current model. Specifically, Figure 55B shows a realistic scenario where there is an excess of extractable species with respect to the extraction efficiency which will occur when the extraction does not proceed completely. Table 23 gives the relevant parameters for Figure 55 (A-C) which show the comparison of the various speciation models to the solvent extraction data in [67]; the “% Extracted” is derived from the distribution coefficient data assuming equal volumes in both phases.

The plutonium speciation diagram can also be justified if high symmetry species are emphasized over low. If the di-, tetra-, and hexanitrate species are expected to have high symmetry and the mono-, tri- and pentantrate have lower symmetries, then the hypothesis would explain the results. The plutonium factor analysis in this work shows five species in solution between 2 and 10 mol/L nitrate. These factors can be explained by the free plutonium, mono-, di-, tetra-, and hexanitrates as proposed in [43]. However, further work will need to be done to confirm this, including modeling of the Pu(IV)-nitrate-water system by DFT.

6.4 Conclusions

This work has shown the potential and use of visible spectroscopy, specifically UV-Visible and Time Resolved Laser induced Fluorescence, for the monitoring of nuclear fuel reprocessing streams. Both uranium and plutonium concentrations can be measured directly by UV-Visible spectroscopy if enough information is known about the solution composition. The total plutonium(IV) concentration can also be determined in the

absence of process chemistry information by using one of the isobestic points present in the absorbance spectrum. Finally, in select process streams, TRLFS monitoring can be used to detect millimolar concentrations of uranium.

A multiple wavelength monitor for determining the nitrate concentration of a process stream from the uranium absorbance signal was derived. The technique uses a ratio of the uranyl absorbance peaks at 426 and 403 nm to predict the nitrate concentration. This indirect monitor can also be applied as a process monitor to detect changes in process chemistry that may be indicative of a process upset or chemistry based diversion attempt. The method operates independent of metal concentration or the determination pathlength which gives this technique added flexibility.

The thermodynamics of the uranyl-nitrate system was investigated with potentiometric and spectrophotometric titrations. Due to the proposed influence of molecular symmetry, a new model was used for the spectrophotometric method that included the mononitrate as a non-absorbing species or as a non-existent species and the dinitrate as the predominant species. The dinitrate stability constants were refined at multiple ionic strengths and extrapolated to zero ionic strength using the Specific Ion Interaction Theory. This new data and model explains observations of solvent extraction data more accurately than the currently accepted data set. The dinitrate species becomes dominant at low nitrate concentrations, ~ 0.5 mol/L, which is where solvent extraction studies show a distribution coefficient greater than 1. By moderate nitrate concentrations, ~ 3 mol/L, the dinitrate exists as greater than 95% of the uranyl species. Additionally, the best fit is found when the uranyl mononitrate is excluded from the model.

The speciation of the plutonium(IV) nitrate system was investigated using a Factor Analysis approach. Five plutonium species are expected to exist between 2 and 10 mol/L nitrate. General inferences have been made as to where species add or drop from the system which will allow future studies to focus their efforts. The symmetry of the various plutonium(IV) nitrate compounds may influence the spectroscopy as well.

REFERENCES

- 1 Safely Managing Used Nuclear Fuel.
<http://www.nei.org/keyissues/nuclearwastedisposal/factsheets/safelymanagingusednuclearfuel/> (accessed August 2, 2010)
- 2 Processing of Used Nuclear Fuel. <http://www.world-nuclear.org/info/inf69.html>,
(accessed May 3, 2010)
- 3 Radioactive Waste Management. <http://world-nuclear.org/info/inf04.html>
(accessed August, 1, 2010)
- 4 Wigeland, R.A.; Criteria Derived for Geologic Disposal Concepts. Presented at OECD/NEA 9th Information Exchange Meeting on Actinide and Fission Product Partitioning and Transmutation, Nimes, France September 2006
- 5 Richter, B.; Hoffman, D.C.; Mtingwa, S.K.; Omberg, R.P.; Rempe, J.L.; Warin, D. *Report of Advanced Nuclear Transformation Technology Subcommittee*; ANTT Report; US Department of Energy, October 7, 2006
- 6 World Nuclear Association, "Safeguards to Prevent Nuclear Proliferation", <http://world-nuclear.org/info/inf12.html>, May 2010, accessed August, 1, 2010
- 7 Fuel Cycle R&D: 2011 Fact Sheet.
http://www.ne.doe.gov/pdfFiles/factSheets/2011_FCRD_Factsheet.pdf (accessed May 4, 2010)
- 8 Miller, M.; Advanced Fuel Cycle Safeguards. Presented at DOE NRC Seminar Series, June 10, 2008.
- 9 Silva, R.J.; Netsche, H. *Radiochim. Acta* **1995**, 70/71, 377-396
- 10 Meinrath, G. et al. *J. Radioanal. Nucl. Chem.* **1993**, 174 (2), 299-314

- 11 Palmer, D.A.; Nguyen-Trung, C. *J. Solution Chem.* **1995**, 24 (12), 1281-91
- 12 Meinrath, G. *J. Radioanal. Nucl. Chem.* **1997**, 224 (1-2), 119-126
- 13 Meinrath, G. *J. Alloys Compd.* **1998**, 275/277, 777-781
- 14 Meinrath, G. *J. Radioanal. Nucl. Chem.* **1998**, 232 (1-2), 179-188
- 15 Moll, H. et al. *Radiochim. Acta* **2003**, 91 (1), 11-20
- 16 Glorius, M. et al. *Radiochim. Acta* **2007**, 95 (3), 151-157
- 17 Ahrland, S.; *Acta Chem. Scand.* **1949**, 3, 374-400
- 18 Betts, R.H.; Michels, R.K. *J. Chem. Soc.* **1949**, 2, S286-S294
- 19 Ahrland, S. *Acta Chem. Scand.* **1951**, 5, 1271-82
- 20 Klygin, A.E. et al. *Zh. Neorg. Khim.* **1970**, 15, 1719-1721
- 21 Rao, L.; Tian, G. *J. of Chem. Thermodyn.* **2008**, 40, 1001-1006
- 22 Suleimenov, O.M. et al. *J. Solution Chem.* **2007**, 36, 1093-1102
- 23 Bell, J.T; Biggers, R.E. *J. Mol. Spectrosc.* **1965**, 18 (3), 247-75
- 24 Bell, J.T; Biggers, R.E. *J. Mol. Spectrosc.* **1967**, 22 (3), 262-71
- 25 Bell, J.T; Biggers, R.E. *J. Mol. Spectrosc.* **1968**, 25 (3), 312-29
- 26 Kaplan, L. et al. *J. Inorg. Nucl. Chem.* **1956**, 2, 153-63
- 27 Bostick, D.T. *Simultaneous Analysis of Uranium and Nitrate*; Report TM-6292;
Oak Ridge National Laboratory: Oak Ridge, TN, 1978
- 28 Billard, I. et al. *Chem. Phys.* **2001**, 270 (2), 345-354
- 29 Brachmann, A. et al. *Radiochim. Acta* **2002**, 90 (3), 147-153
- 30 Walter, M. et al. *J. Colloid Interface Sci.* **2005**, 282 (2), 293-305
- 31 Wang, Z., et al. *Geochim. Cosmochim. Acta* **2005**, 69 (6), 1391-1403
- 32 Guenther, A. et al. *Polyhedron* **2007**, 26 (1), 59-65

- 33 Moulin, C. et al. *Appl. Spectrosc.* **1991**, 45, 116-118
- 34 Moulin, C. et al. *Anal. Chim. Acta* **1996**, 321, 121-126
- 35 Moulin, C. et al. *Radiochim. Acta* **1991**, 52/53, 119-125
- 36 Moulin, V. et al. *Radiochim. Acta* **1992**, 58/59, 121-128
- 37 Reiller, P. et al. *J. Colloid Interface Sci.* **1994**, 163, 81-86
- 38 Moulin, C. et al. *Anal. Chem.* **1995**, 67, 348-353
- 39 Moulin, C. et al. *Anal. Chem.* **1996**, 68 (18), 3204-3209
- 40 Meinrath, G. et al. *J. Alloys Compd.* **2000**, 300-301, 107-112
- 41 Geipel, G. et al. *Radiochim. Acta* **2000**, 88 (9-11), 757-762
- 42 Geipel, G. et al. *Radiochim. Acta* **1996**, 75 (4), 199-204
- 43 Veirs, D.K. et al. *J. Alloys Compd.* **1994**, 328-332
- 44 Lee, M.H. et al. *J. Radioanal. Nucl. Chem.* **2007**, 273 (2), 375-382
- 45 Wilson, R.E. et al. *Radiochim. Acta* **2005**, 93, 203-206
- 46 Deniau, H. et al. *Radiochim. Acta* **1993**, 61 (1), 23-8
- 47 Lascola, R. et al. *J. Process Anal. Chem.* **2002**, 7 (1), 14-20
- 48 Day, R.A.; Powers, R.M. *J. Am. Chem. Soc.* **1954**, 76, 3895-3897
- 49 Banerjea, D.; Tripathi, K.K. *J. Inorg. Nucl. Chem.* **1961**, 18, 199-206
- 50 Lahr, H.; Knoch, W. *Radiochim. Acta* **1970**, 13, 1-5
- 51 Ahrland, S. *Acta Chem. Scand.* **1949**, 3, 783-808
- 52 Ahrland, S. *Acta Chem. Scand.* **1951**, 5, 199-219
- 53 Ahrland, S. *Acta Chem. Scand.* **1951**, 5, 1151-67
- 54 Hindman, J.C. In *The transuranium elements*; Seaborg, G.T., Katz, J.J., Manning, W.M., Eds.; McGraw-Hill: New York, 1949; 388-404

- 55 Rabideau, S.W.; Lemons, J.F. *J. Am. Chem. Soc.* **1951**, 73, 2895-2899
- 56 Grenthe, I.; Norén, B. *Acta Chem. Scand.* **1960**, 14, 2216-2229
- 57 Danesi, P.R. et al. *J. Inorg. Nucl. Chem.* **1966**, 28, 1047-1054
- 58 Wain, A.G., *The potential of the Pu(III)-Pu(IV) couple in nitric acid solution and equilibrium constants for the nitrate complexes of Pu(IV)*; Report AERE-R5320; UK Atomic Energy Research Establishment, 1966
- 59 Bagawde, S.V. et al. *J. Inorg. Nucl. Chem.* **1976**, 38, 1339-1345
- 60 Golub, A.M.; Golodets, G.I. *Ukr. Khim. Zh.* **1961**, 27, 141-146
- 61 Brothers, J.A. et al. *J. Inorg. Nucl. Chem.* **1958**, 7, 85-93
- 62 Ryan, J.L. *J. Phys. Chem.* **1960**, 64, 1375-1385
- 63 Veirs, D.K.; Smith, C.A.; Zwick, B.D.; Marsh, S.F.; Conradson, S.D. *Characterization of the Nitrate Complexes of Pu(IV) using Absorption Spectroscopy, ¹⁵N NMR, and EXAFS*; Report LA-UR-93-3281; Los Alamos National Laboratory, Los Alamos, NM, September, 1993
- 64 Berg, J.M. et al. *J. Radioanal. Nucl. Chem.* **1998**, 235 (1-2), 25-29
- 65 Bagawde, S.V. et al. *Radiochem. Radioanal. Lett.* **1977**, 31, 65-74
- 66 Grenthe, I.; Fuger, J.; Konings, R.J.M.; Lemire, R.J.; Muller, A.B.; Ngyuen-Trung Cregu, C.; Wanner, H. *Chemical Thermodynamics of Uranium*. Wanner, H., I. Forest, Eds.; Chemical Thermodynamics Series. Elsevier Science Publishers: New York, NY, 1992
- 67 Nash, K.; Madic, C.; Mathur, J.N.; Lacquement, J. In *The Chemistry of the Actinide and Transactinide Elements*, Morss, L.R., Edelstein, N.M., Fuger, J., Eds.; Springer Link: Netherlands, 2006; 2622-2798

- 68 Gindler, J.E. *The Radiochemistry of Uranium*, Nuclear Science Series Report NAS-NA-3050; US Atomic Energy Commission: Oak Ridge, TN, March 1962
- 69 Lemire, R.J.; Fuger, J.; Nitsche, H.; Potter, P.; Rand, M.H.; Rydberg, J.; Spahiu, K.; Sullivan, J.C.; Ullman, W.J.; Vitorge, P.; Wanner, H. *Chemical Thermodynamics of Neptunium and Plutonium*, OECD, Eds.; Chemical Thermodynamics Series. Elsevier Science Publishers; New York, NY, 2001
- 70 Atkins, P.; de Paula, J. *Physical Chemistry*, 7th Ed.; W.H. Freeman and Company: New York, NY, 2002
- 71 Harris, D.C. *Quantitative Chemical Analysis*, 6th Ed.; W.H. Freeman and Company, New York, NY, 2003
- 72 Yu, Y.X. et al. *J. Radioanal. Nucl. Chem.* **2003**, 245 (3), 581-587
- 73 Beyer, R.; Steiger, M. *J. Chem. Thermodyn.* **2002**, 34, 1057-1071
- 74 Hamer, W.J.; Wu, Y. *J. Phys. Chem. Ref. Data* **1972**, 1 (4), 1047-1100
- 75 Fanghänel, T. et al. *J. of Solution Chem.* **1996**, 25 (4), 327-343
- 76 Rossotti, F.J.C.; Rossotti, H. *The determination of stability constants, and other equilibrium constants in solution*; McGraw-Hill: New York, NY, 1961
- 77 Ciavatta, L. *Ann. Chim. (Rome, Italy)* **1980**, 70, 551-567
- 78 Grenthe, I.; Ots, H. *Acta Chem. Scand.* **1972**, 26, 1229-1242
- 79 Strong, F.C. *Anal. Chem.* **1952**, 24, 338-42
- 80 IUPAC. Compendium of Chemical Terminology, 2nd ed. (the "Gold Book"). Compiled by A. D. McNaught and A. Wilkinson. Blackwell Scientific Publications, Oxford (1997). XML on-line corrected version: <http://goldbook.iupac.org> (2006-)

created by M. Nic, J. Jirat, B. Kosata; updates compiled by A. Jenkins. ISBN 0-9678550-9-8. doi:10.1351/goldbook.

- 81 Vandegrift, G.F.; Regalbuto, M.C.; Aase, S.; Bakel, A.; Battisti, T.J.; Bowers, D.; Byrnes, J.P.; Clark, M.A.; Emery, J.W.; Falkenberg, J.R.; Guelis, A.V.; Pereira, C.; Hafenrichter, L.; Tsai, Y; Quigley, K.J.; Vader Pol, M.H. Designing and Demonstration of the UREX+ Process Using Spent Nuclear Fuel. Presented at ATATLANTE 2004 - Advances for Future Nuclear Fuel Cycles, Nimes, France, June 21-24, 2004; 012-01
- 82 May, I. et al. *J. Alloys Compd.* **1998**, 275-277, 769-772
- 83 Thompson, M.C.; Norato, M.A.; Kessinger, G.F.; Pierce, R.A.; Rudisill, T.S.; Johnson, J.D. *Demonstration of the UREX Solvent Extraction Process with Dresden Reactor Fuel Solution*; Report WSRC-TR-2002-00444; Westinghouse Savannah River Company; Aiken, SC September, 2002
- 84 Marcus, Y.; Kolarik, Z. *J. Chem. Eng. Data* **1973**, 18 (2), 155-63
- 86 Matsika, S. et al. *J. Phys. Chem. A* **2001**, 105 (15), 3825-3828
- 87 Ryzhkov, M.V.; Gubanov, V.A. *J. Radioanal. Nucl. Chem.* **1990**, 143 (1), 85-92
- 89 Wolsey, W.C. *J. Chem. Educ.* **1973**, 50 (6), A335-A344
- 90 Ikeda, A. et al. *Anal. Chem.* **2008**, 80, 1102-1110
- 91 Servaes, K. et al. *Eur. J. Inorg. Chem.* **2007**, 5120-5126
- 94 Denecke, M.A. *Coord. Chem. Rev.* **2006**, 250, 730-754
- 95 Ikeda-Ohno, A. et al. *Inorg. Chem.* **2009**, 48, 7201-7210
- 96 Cleveland, J.M. *Coord. Chem. Rev.* **1970**, 5, 101-137
- 97 Spahiu, K.; Puigdomenech, I. *Radiochim. Acta* **1998**, 82, 413-419

- 98 Choppin, G.R. *Radiochim. Acta* **1983**, 32, 43-53
- 99 Marsh, S.F.; Gallegos, T.D. *Chemical Treatment of Plutonium with Hydrogen Peroxide Before Nitrate Anion Exchange Processing*; Report LA-10907; Los Alamos National Lab: Las Alamos, NM, 1987
- 101 Tkac, P. et al. *J. Chem. Eng. Data* **2009**, 54, 1967-74
- 102 Allen, P.G. et al. *Inorg. Chem.* **1996**, 35, 2841-2845
- 103 Grenthe, I.; Wanner, H.; *Guidelines for the Extrapolation to Zero Ionic Strength*; Report TB-2; OECD Nuclear Energy Agency: Issy-les-Moulineaux, France, 2000
- 104 Pereira, C.; UREX+ Process Overview. Presented at DOE NRC Seminar Series, March 26, 2008.
- 105 Lanham, W.B.; Runion, T.C. *Purex process for plutonium and uranium recovery*; Report ORNL-749; Oak Ridge National Laboratory: Oak Ridge, TN, 1949
- 106 Anderson, H.H.; Asprey, L.B. Solvent extraction process for plutonium. Patent US2924506 (A), 1960-02-09
- 107 International Atomic Energy Agency. *Treaty on the Non-Proliferation of Nuclear Weapons*, IAEA Information Circular, INFCIRC/140, 22 April 1970
- 108 *Nuclear Safeguards, Security, and Nonproliferation*; Doyle, J.E., Ed.; Butterworth-Heinemann Homeland Security Series; Butterworth-Heinemann: Burlington, MA, 2008.
- 109 Nuclear Materials Management & Safeguards System Homepage.
<http://www.hss.energy.gov/nmmss/> (accessed August 28, 2010)
- 110 Zanonato, P. et al. *J. of Solution Chemistry* **2001**, 30 (1), 1-18
- 111 Rao, L. et al. *Radiochim. Acta* **2002**, 90 (9-11), 581-588

- 112 Jiang, J. et al. *J. Chem. Soc., Dalton Trans.* **2002** 8, 1832-1838
- 113 Gans, P. Protonic Software Home Page. <http://www.hyperquad.co.uk>
- 114 Cary 50 Spectrometer.
<http://www.varianinc.com.cn/products/spectr/uv/brochure/1942.pdf> (accessed August 5, 2010)
- 115 Cary 4000/5000/6000 Spectrometers.
<http://www.varianinc.com/image/vimage/docs/products/spectr/uv/brochure/si-0137.pdf> (accessed August 5, 2010)
- 116 USB 2000+ Miniature Fiber Optic Spectrometer.
<http://www.oceanoptics.com/Products/usb2000+.asp> (accessed August 5, 2010)
- 117 General Purpose Transmission Dip Probes.
<http://www.oceanoptics.com/products/t300t200transdipprobes.asp> (accessed August 5, 2010)
- 122 Lakowicz, J.R. "Principles of Fluorescence Spectroscopy" **1999**, Kluwer Academic/Plenum, New York, NY
- 123 "epi-Fluorescence with the microscope. <http://web.uvic.ca/ail/techniques/epi-fluorescence.html> (accessed August 4, 2010)
- 125 UPAC. Compendium of Chemical Terminology, 2nd ed. (the "Gold Book").
Compiled by A. D. McNaught and A. Wilkinson. Blackwell Scientific Publications, Oxford (1997). XML on-line corrected version: <http://goldbook.iupac.org> (2006-) created by M. Nic, J. Jirat, B. Kosata; updates compiled by A. Jenkins. ISBN 0-9678550-9-8. doi:10.1351/goldbook.

- 126 Jameson, D.; Basic Fluorescence Principles II: Lifetimes, Quenching and FRET.
Presented at Principles of Fluorescence Techniques, Genova Italy, June 2004.
- 127 Newville, M. et al. *Phys. Rev.* **1993**, B47, 14126
- 128 Ressler, T. *J. Synchrotron Radiat.* **1998**, 5, 118
- 129 Rehr, J.J.; Albers, R.C. *Rev. Mod. Phys.* **2000**, 72, 621
- 130 Ravel, B. *J. Synchrotron Radiat.* **2001**, 8, 314
- 131 Knoll, G. *Radiation Detection and Measurement, 3rd Ed.*; John Wiley and Sons:
New York, NY, 2000
- 132 Tri-Carb 3110TR Low Activity Liquid Scintillation Analyzer.
<http://las.perkinelmer.com/Catalog/ProductInfoPage.htm?ProductID=B311000>
(accessed August 2, 2010)
- 133 Rodríguez, L. et al. *Nucl. Instrum. Methods Phys. Res., Sect. A* **1992**, 312 (1-2),
124-131
- 134 Tri-Carb 3110TR Liquid Scintillation Analyzer.
<http://las.perkinelmer.com/Catalog/ProductInfoPage.htm?ProductID=B311000>
(accessed August 5, 2010)
- 136 Stock, S.A. Quantitative comparison of sample preparation methods for low-level
alpha spectrometry. Master's Thesis, University of Nevada, Las Vegas, Las Vegas,
Nevada, 2007
- 137 Pettit, L.D.; Puigdomenech, I.; Wanner, H. *Aqueous Solutions*, Version 2; IUPAC,
2004 (Solubility limits under “Molarity/Molality” tab.)
- 138 K. Czerwinski, University of Nevada, Las Vegas, Las Vegas, NV. Personal
communication, 3/2010.

- 139 Clark, D.L. *Los Alamos Science* **2000**, 26
- 140 Sill, C.W. *Nucl. Chem. Waste Manage.* **1987**, 7 (3-4), 201-215
- 141 Gans, P. et al. *Talanta* **1996**, 43(10), 1739-1753.
- 142 Sabatini, A. et al. *Coord. Chem. Rev.* **1992**, 120, 389-405
- 143 Schlens, J. A Tutorial on Principal Component Analysis.
<http://www.sn1.salk.edu/~shlens/pca.pdf> (accessed August 12, 2010)
- 144 Alderighi, L. et al; *Coord. Chem. Rev.* **1999**, 184, 311-318
- 146 Brønsted, J. N. *J. Am. Chem. Soc.* **1922**, 44, 938-948
- 147 Brønsted, J. N. *J. Am. Chem. Soc.* **1922**, 44, 877-898
- 148 Scatchard, G. *Chem. Rev.* **1936**, 19, 309-327
- 149 Guggenheim, E. A. *Philos. Mag.* **1935**, 19, 588-643
- 150 Sukhno, I.; Buzko, V.; Pettit, L.D. *The Adjustment, Estimation and Uses of Equilibrium Reaction Constants in Aqueous Solution*; Report 2006-010-1-500; IUPAC Analytical Chemistry Division, 2006
- 151 Kohn, W. et al. *J. Phys. Chem.* **1996**, 100, 12974-12980
- 152 Weck, P.F.; University of Nevada, Las Vegas, Las Vegas, Nevada. Personal communication, July 28, 2010
- 153 Delley, B. *J. Chem. Phys.* **2000**, 113, 7756-7764
- 154 Perdew, J.P.; Wang, Y. *Phys. Rev. B* **1992**, 45, 13244-13249
- 155 Hehre, W.J.; Radom, L.; Schleyer, P.vR.; Pople, J.A. *Ab Initio Molecular Orbital Theory*; John Wiley & Sons: New York, NY, 1986
- 156 Weck, P.F. et al. *Inorg. Chem.* **2010**, 49, 1465
- 157 De Jong, W.A. et al. *Theor. Chem. Acc.* **2001**, 107, 22-26

- 158 Buehl, M. et al. *Inorg. Chem.* **2007**, 46, 5196-5206
- 161 Gans, P. *HypSpec*, Version 1.1.16; Protonic Software, 2008 (Help file entry - The Mathematics of Factor Analysis)
- 162 Marcus, Y.; Kertes, S. *Ion Exchange and Solvent Extraction of Metal Complexes*; John Wiley & Sons: New York, NY, 1969

VITA
Graduate College
University of Nevada, Las Vegas

Nicholas Alexander Smith

Degrees:

Bachelor of Science, Chemistry 2005
Lake Superior State University

Special Honors and Awards:

Magna Cum Laude, LSSU

Publications:

Warburton, J.; **Smith, N.**; Czerwinski, K. "Method for Online Process Monitoring for Use in Solvent Extraction and Actinide Separations" *Separation Science and Technology* (2010) 45 (12-13), 1763-1768

Poineau, F.; Du Mazaubrun, J.; Ford, D.; Fortner, J.; Kropf, J.; Silva, G. W. C.; **Smith, N.**; Long, K.; Jarvinen, G.; Czerwinski, K. "Uranium/technetium separation for the UREX process - synthesis and characterization of solid reprocessing forms" *Radiochimica Acta* (2008) 96 (9-11), 527-533

Smith, N.A.; Cerefice, G.S.; Czerwinski, K. "Reduction of measurement uncertainty in the spectroscopic determination of uranium" Annual Meeting Proceedings of the Institute of Nuclear Materials Management (2008), 49th 212/1-212/7

Smith, N.A.; Cerefice, G.S.; Czerwinski, K. "Application of optical techniques for on-line materials accountability in the UREX solvent extraction process" Annual Meeting Proceedings of the Institute of Nuclear Materials Management (2006), 47th 530/1-530/8

Dissertation Title: Speciation and Spectroscopy of the Uranyl and Tetravalent Plutonium Nitrate systems: Fundamental Studies and Applications to Used Fuel Reprocessing

Dissertation Examination Committee:

Chairperson, Kenneth Czerwinski, Ph.D.
Committee Member, Alfred Sattelberger, Ph.D.
Committee Member, Gary Cerefice, Ph.D.
Graduate Faculty Representative, Ralf Sudowe, Ph.D.